

The author(s) shown below used Federal funds provided by the U.S. Department of Justice and prepared the following final report:

Document Title: A Forensic Pathology Tool to Predict Pediatric Skull Fracture Patterns

Author(s): Brian J. Powell, Timothy G. Baumer, Nicholas V. Passalacqua, Christina D. Wagner, Roger C. Haut, Todd W. Fenton, King H. Yang

Document No.: 240683

Date Received: December 2012

Award Number: 2007-DN-BX-K196

This report has not been published by the U.S. Department of Justice. To provide better customer service, NCJRS has made this Federally-funded grant report available electronically.

Opinions or points of view expressed are those of the author(s) and do not necessarily reflect the official position or policies of the U.S. Department of Justice.

A FORENSIC PATHOLOGY TOOL TO PREDICT PEDIATRIC SKULL FRACTURE PATTERNS – FINAL TECHNICAL REPORT

Award No. 2007-DN-BX-K196

Brian J. Powell¹, Timothy G. Baumer¹, Nicholas V. Passalacqua², Christina D. Wagner³, Roger C. Haut¹, Todd W. Fenton², King H. Yang³

¹Orthopaedic Biomechanics Laboratories, College of Osteopathic Medicine, Michigan State University, East Lansing, MI 48824

²Department of Anthropology, College of Social Sciences, Michigan State University, East Lansing, MI, 48824

³Department of Biomedical Engineering, Wayne State University, Detroit, MI, 48202

ABSTRACT

Introduction

In cases of violence against infants and young children that result in death, the victims are voiceless and incapable of telling their own stories. It is the job of the forensic pathologist to determine the cause and manner of death in these cases. The ability to establish the circumstances of death in these cases is severely hampered by the lack of skull fracture standards for infants and young children. Namely, it is difficult to determine if the observed pediatric cranial trauma is consistent with inflicted trauma or with an accidental fall from a short distance. The lack of baseline data represents a major “gap in best practice” in the forensic death investigation. The current research is a collaborative effort between forensic anthropologists and biomechanical engineers focused on generating baseline data on pediatric cranial fracture initiation, propagation, and patterning using a porcine animal model.

Research goals and objectives

This research had four primary aims. The first aim was to conduct impact experiments at high and low impact energy on developing porcine skulls of varying age using rigid and compliant interfaces to show characteristic fracture patterns. The second aim was to perform tests to determine the elastic and failure properties of the developing porcine bone and suture. The third aim was to develop a computational tool to predict fracture patterns on the porcine skull. And, the fourth aim was to develop a mathematically based model of the pediatric human skull.

Materials and Methods

The first two sets of experiments focused on low and high energy impacts on entrapped porcine heads with the goal of establishing baseline data on fracture initiation and propagation.

Porcine specimens aged from 2 to 28 days (n=76 in the low energy impacts and n=57 in the high energy impacts) were placed in a bed of air-hardening epoxy. Each specimen was subjected to a single impact with a gravity-accelerated mass (GAM). Two interchangeable impact interfaces were created for the GAM to represent rigid and compliant impact interfaces.

A computational tool was developed based initially on the porcine anatomy. The anatomy of the skull was discretized for a Finite Element Analysis (FEA) model to predict fracture patterns based on the assumption these defects progress along lines of maximum principal tensile stresses. A subcontract research team attempted to more specifically study the mechanisms of fracture initiation and propagation using more sophisticated theories.

A few cases of crush injury to the human pediatric skull were modeled and fracture patterns on the basal skull were compared to the directions of maximum principal tensile stresses using the simplified fracture mechanism theory.

Results

A number of findings were evident in the research on the porcine animal model: (1) With increased impact energy there were more sites of fracture initiation and propagation into adjacent bones; (2) Fracture initiation occurred away from the impact site; (3) One impact frequently produced two or more linear fractures away from the impact site; (5) Rigid and compliant interfaces generated different fracture patterns; (6) Developmental changes in the material properties of porcine skulls from 2-24 days paralleled those of the human skull from 2-24 months; and (7) Equivalent energies of impact to an entrapped head generated more fractures than a free falling head onto a rigid interface.

Some of the current studies on finite-element modeling indicated that a simplified model of fracture prediction based on principal stress and strain theory could predict general patterns of

skull fracture. However, more sophisticated models of fracture initiation and propagation were found to be too sensitive to subject-specific characteristics and model assumptions to limit the utility of current computational tools to predict fracture patterns for general use in forensic cases.

TABLE OF CONTENTS

Executive Summary	6
Introduction.....	22
Statement of Problem.....	22
Literature Review: Pediatric Cranial Trauma.....	22
Literature Review: Finite Element Models.....	25
Statement of Hypothesis or Rationale for Research	42
Materials and Methods.....	43
Low Energy Entrapped Head Impacts	43
High Energy Entrapped Head Impacts	47
Porcine Skull Material Property Study	48
Free Fall Head Drops	53
Porcine Head Model Computational Modeling (MSU).....	57
Porcine Computational Modeling (WSU)	59
Human Pediatric Crush Scenario Computational Modeling (MSU)	70
Results.....	72
Low Energy Entrapped Head Impacts	72
High Energy Entrapped Head Impacts	76
Porcine Skull Material Property Study	81
Free Fall Head Drops	87
Porcine Head Model Computational Modeling (MSU).....	92
Porcine Computational Modeling (WSU)	94
Human Pediatric Crush Scenario Computational Modeling (MSU)	108
Conclusions.....	113
Discussion of Findings.....	113
Implications for Policy and Practice	117
Implications for Further Research	118
References.....	121
Publications, Presentations, and Awards	126

EXECUTIVE SUMMARY

Problem

Pediatric deaths involving head injury with associated cranial fractures represent one of the greatest challenges to forensic professionals. The ability of the forensic investigator to establish the circumstances of death in these cases is severely hampered by the lack of skull fracture standards for infants and young children. This lack of baseline data means that forensic pathologists and anthropologists have great difficulty in interpreting the circumstances surrounding the trauma. Namely, it is difficult to determine if the observed pediatric cranial trauma is consistent with inflicted trauma (e.g., a blow with an implement) or with an accidental fall from a short distance (such as from a diaper-changing table). This lack of baseline data on pediatric cranial fracture represents a clear “gap in best practice” in the forensic death investigation. This is clearly an issue of justice for the children who have died, as well as for those who go to trial accused of child abuse and/or murder. This “gap in best practice” is the impetus for this research that focuses on generating baseline data on how pediatric cranial fractures initiate and propagate. Unfortunately, the ability to produce experimental human skull fracture data is limited by ethical considerations surrounding experimentation on pediatric cadavers, even if available tissue were to exist. Thus, the developing porcine head is being used as an animal model to generate experimental baseline data on skull fracture initiation and propagation as a function of age, impact energy, and interface condition. These data are then used in an attempt to develop a computer-based technology that may ultimately help predict various skull fracture patterns in human infants and young children.

Purpose of the research

The initial goal of this experimental blunt force research was to understand the basic principles of cranial fracture initiation and propagation using the developing porcine skull under known conditions of specimen age, energy of impact, and impact interface, which can ultimately be used to guide later human pediatric research. The ultimate goal was to develop a computational tool to predict fracture patterns on the porcine skull, and eventually to develop a mathematically based model of the pediatric human skull.

Research Design

Aim #1

The first aim was to conduct impact experiments on developing porcine skulls of varying age using rigid and compliant interfaces to show characteristic fracture patterns. Several sets of experiments were performed, including: A. low energy impacts on entrapped skulls; B. high-energy impacts on entrapped skulls; and C. head drop impact experiments.

A. This first set of experiments focused on low energy impacts to the entrapped porcine head with the goal of establishing baseline data on fracture initiation. Porcine specimens aged 2 to 28 days (n=76) were placed in a bed of air-hardening epoxy. Each specimen was subjected to a single impact with a gravity-accelerated mass (GAM). Two interchangeable impact interfaces were created for the GAM to represent rigid and compliant impact interfaces. The rigid interface was a solid aluminum cylinder with approximately 16 cm² of impact surface. The compliant interface was a deformable aluminum material (1.10 MPa crush strength Hexcel, Hexcel Corp., Stamford, CT), approximately 3 cm thick with a 16 cm² impact surface, fastened to the rigid interface. Both interfaces had greater surface area than the resulting contact area on the skull.

After each impact the scalp and periosteum was removed in order to inspect for skull fracture and suture damage. Each specimen was then cleaned via standard anthropological procedures, removing all remaining soft tissue. Complete fracture diagrams and measurements were made for each specimen. Total length of the skull fractures was measured to the nearest millimeter with a flexible measuring tape, which conformed to the curvature of the skull.

B. The second set of experiments under Aim #1 involved high-energy impacts of entrapped porcine heads with the goal of generating baseline data on fracture propagation. A total of 57 specimens (aged 2 to 28 days) were used for this part of the study. Again, impact energy was established by varying the drop height of a 1.67 kg GAM. A slightly larger mass (1.92 kg) was used to generate fracture in specimens aged twenty-one days and older. Energy levels for each age were double those of previous low energy impacts. The input energy for the compliant and rigid interfaces was equal at each age, however, the impact energy had to be increased with specimen age.

In order to compare the patterns of fracture between specimens and interfaces, a Geographic Information System (GIS) method was utilized in the study. The pattern of fracture from each skull was constructed using a projected view of the porcine cranium which best highlighted the right side of the skull with fracture configurations superimposed on it for each specimen. A second view of the posterior aspect of the cranium was also included, as many high-energy cases involved the occipital bone. Porcine specimens were separated into two different age groups (2-9 and 19-28 days) for both the rigid and compliant interfaces, and at low and high energy levels to better demonstrate fracture pattern changes in relation to porcine growth and development, impact interface, and input energy. These age groups were chosen based on general observations of gross fracture and material property changes for the skull and suture

tissues documented during the material property experiments (see below). The fracture pattern for each porcine cranium was traced into individual shape files. The GIS model then counted overlaid fracture patterns, generating a map of where fractures appeared most frequently. After each map was constructed, the GIS model was used to discuss the differences in fracture patterns between specimens of different age, impact energy, and interface.

C. The third set of experiments on the porcine animal model under Aim #1 involved free fall head drops. A total of 31 porcine specimens ranging from 2-17 days old were utilized here. Each isolated head was dropped from a custom designed drop tower utilizing an electromagnetic solenoid to hold a gravity-accelerated trolley at a given height. A second solenoid was used to catch the trolley after the first impact. The trolley base impacted a soft padded surface while the skull was free to impact an aluminum interface. The skull was allowed to impact only once by using an operational amplifier comparator circuit to monitor the impact. A load cell (2.22 kN capacity, model 1010AF-500, Interface, Scottsdale, AZ) mounted immediately behind the impact interface recorded impact force, duration, and energy. Energy values were matched in this study to those of the previous high energy, entrapped head experiments. Due to the differences in mass of the head with age, each specimen mass was measured and given a respective drop height to match impact energies.

After impact, the scalp and periosteum were removed and each skull was visually inspected for fractures and these were recorded. The periosteum and remaining soft tissues were then removed and the length of skull fracture was measured to the nearest millimeter using a soft, flexible measuring tape, which contoured to the curvature of the skull. Complete fracture diagrams were manually constructed for each specimen. The Geographic Information System (GIS) method was again used to project a view of the fracture pattern on the porcine cranium.

The porcine specimens were again separated into two different age groups (2-9 and 10-17 days) to demonstrate fracture pattern changes in relation to porcine growth and development, as well as the impact scenario. The fracture pattern data from these free fall experiments were then compared to the fracture patterns generated in the entrapped head impacts.

Aim # 2

The second aim of this research was to perform material property tests to determine the elastic and failure properties of the developing porcine bone and suture as a function of specimen age, and anatomical orientation of the bone from the skull. Porcine specimens aged 3 days (n=5), 7 days (n=8), 10 days (n=7), 14 days (n=5), 18 days (n=5), and 21 days (n=4) were used here. Three beam specimens were cut from each skull: one across the coronal suture and two from the parietal bone, one parallel to and one perpendicular to the coronal suture. Potted specimens were mounted in a custom-designed 4-point bending fixture attached to a servo-hydraulic testing machine (Model 1331, Instron Corp., Canton, OH). The force and actuator displacement were recorded during each experiment. From these values, initial specimen stiffness, ultimate stress, ultimate strain, bending modulus, and strain energy to failure were determined.

Aim #3

The third aim of this research was to develop and validate a finite element model of the immature porcine skull to study the magnitude and distribution patterns of stress and strain, and to predict the experimentally produced cranial fracture patterns.

The Michigan State University team created a simplified model of a porcine cranium in a finite element package (Abaqus v.6.3, Hibbitt, Karlsson & Sorensen, Inc., Pawtucket, RI, USA)

using dimensions from a typical CT scans. Finite Element (FE) analysis was utilized in an effort to produce and examine the expected stresses and strains developed on the cranium and to compare these stresses and strains to experimentally observed fracture patterns with respect to both age and interface. The thickness of the cranium and the material properties of the bone and suture were altered in the model to represent changes in age. Age related changes in the elastic moduli of bone and suture were taken from Aim #1 experimental results. The average impact force and contact area data needed for boundary conditions were also taken from Aim #1 experiments. Numerous trials were run within the elastic range of the bone to develop a representative and clearly characterized pattern of principal stresses and strains. Initially it was assumed that the patterns of fracture may follow the patterns of maximum principal tensile stresses and strains generated within the cranium from the boundary impact loads.

The goal of the Wayne State team was to develop a complex finite-element model of the porcine skull. Several finite element models developed to study infant skull biomechanics have been published in the literature. To date, no immature animal FE models of the cranium have been found in the literature, and none of the published pediatric head models utilize techniques to represent lines of fracture propagation, as opposed to general fracture location. Through experimental analysis, it has been seen that fracture lines occur in areas of high transparency, and anecdotal evidence suggests that fracture lines follow the bony spiculae radiating from ossification centers of the infant skull bone plates. Based on the consistent fracture patterns produced in drop tests, it was clear that any proposed injury mechanism should take into account that the fracture initiation occurred remotely from the impact center, and fracture propagation follow a perpendicular path to the suture lines. This implies that there is some mechanical phenomenon at play. Several possibilities were considered. The parietal bone grows radially

from a central ossification point, which may indicate that, in this case, the impacted area has higher strength than the periphery. A combined compressive loading plus internal pressure from the incompressible brain leading to bone rupture may also explain the observed fracture patterns. A final injury mechanism is hypothesized: That the fracture mechanism was related to tensile strain. During a bending event such as that produced in the impacted skull, part of the parietal bone may be in compression and other areas in tension. Furthermore, it is hypothesized that the sutures play a role in allowing rotation at the parietal bone borders.

Aim #4

The fourth aim of this research was to develop a mathematically based model of the pediatric human skull.

The Michigan State University team utilized four clinical cases of fatal crush injuries to young children between 1.5 and 6 years of age under known conditions as a baseline for applied forces and resulting fracture patterns. In each case the skull was trapped between a vehicle tire and the ground. These cases were quasi-static in nature and presented as a good way to initiate studies on developing a computational tool. A simplified model of a skull was created in a finite element package (Abaqus v.6.3, Hibbitt, Karlsson & Sorensen, Inc., Pawtucket, RI). The model was subjected to quasi-static pressures corresponding to the specific exterior injury locations noted by the forensic pathologist for each case. The magnitude of the pressure applied to the cranial model was the same for each case and scaled to be sure no stresses were generated that would exceed the failure tolerance of the cranial bones. By restricting the analyses to the elastic region, the exact material properties were not required for this simple analysis. FE analysis was

utilized in an effort to reproduce and examine possible relationships between the theoretical pre-failure stresses developed on the modeled crania and the fracture patterns observed clinically.

The goal of the Wayne State team was to develop a mathematically based model of the pediatric human skull and perform theoretical impact loading experiments on the models for cases where the input conditions are well established from the forensic literature, and compare the predicted fracture patterns with case reports.

Once the porcine head computational models were developed and validated, the goal was to use the same techniques to develop several template human pediatric models at WSU using CT data available at the Children's Hospital of Michigan, an integral part of the WSU Medical School. Burdi et al (1969) stated that the pediatric skull changes not only in size but also in shape during development. In this effort, the WSU planned to generate as much information as possible on various ages of pediatric skulls to decide which age groups can be clustered into one template model, so that development of victim-specific head models from CT information could be achieved.

Forensic case studies were then to be utilized to further judge the robustness of the human infant model based on techniques developed while validating porcine models. Using fracture pattern information from well-documented cases, as well as available specific witness-derived testimony, the modeling tool was to be exercised to validate its efficacy in the prediction of actual fracture patterns in forensic cases.

Findings

Findings Aim #1 – Low-energy

For both rigid and compliant impact interfaces, linear regression analyses showed a significant increase in impact force with age that was required to produce a fracture ($p < 0.001$).

Linear regression analyses showed a significant increase (0.0516 mm/day) in average parietal bone thickness with age ($p < 0.001$). The area of contact for the compliant interface significantly increased with age ($p < 0.001$), but no significant change was noted for the rigid interface. Bone fractures for all ages, and for both interfaces, occurred at sites away from the point of impact. These bone fractures initiated at a suture-bone interface. A two-factor (age, interface) ANOVA performed on the total fracture length (bone and diastatic combined) revealed significantly more damage caused by the compliant interface than by the rigid interface on pig skulls less than seventeen days of age, similar amounts of damage were shown by the interfaces between 17 and 22 days of age, and significantly more damage was caused by the rigid interface than by the compliant interface for specimens aged 24 to 28 days ($p < 0.05$).

Findings Aim #1 – High-energy

The length of fracturing (in bone and along sutures) versus age plot showed, on average, a significantly larger ($p = 0.034$) amount of fracturing for the rigid than the compliant interfaces. The GIS fracture maps confirmed that the length of fractures was greater for rigid than compliant interface impacts for the younger age group in the current study. For the compliant interface experiments the pattern maps showed fractures primarily initiating at 4 sites adjacent to sutures along the perimeter of the parietal bone. This compared to 3 sites in the low energy experiments. For the rigid interface, however, there were even more sites of fracture initiation along the bone-suture boundary in the high energy experiments. There were many specimens in both high-energy groups where fractures also appeared in the occipital region. These fractures were not present in the low energy study.

Findings Aim #1 – Free fall head drops

In the younger age group (2-9 days old), fractures tended to initiate in the anterior parietal at the coronal suture. There were no documented initiation sites along the posterior or superior edges of the parietal bone. Extensive diastatic fracture was documented along the coronal suture in these experiments. Additionally, several bi-lateral bone fractures extended across the coronal suture into the frontal and parietal bones. In the older age group (10-17 days old), several fracture initiations were documented at the lambdoidal and squamosal suture intersection. However, fracture initiation was documented more frequently along the anterior parietal bone as in the younger age group. There were no documented occipital fractures in the free fall head impacts of both age groups contrasting with the extensive occipital fracture noted in the high energy, entrapped, rigid impacts.

Findings Aim #2 – Mechanical property testing

For each orientation of parietal bone from the skull, there was a significant increase in bending stiffness with age. Interestingly, there was no significant change in bending stiffness in the bone-suture-bone specimens up to 14 days of porcine age, but between 14 and 18 days there was a significant increase. The stiffness of the suture was lower than that of the bone up to 14 days, but it became statistically greater than the parallel bone specimens at 18 days. There was no change with age in the bending modulus of the bone (6.01 ± 1.73 GPa) and bone-suture-bone (2.73 ± 0.84 GPa) specimens. The bending modulus of the bone-suture-bone specimens was significantly lower than that of the bone specimens up to 14 days.

The morphological characteristics of the skull bone from the infant porcine specimens changed during the aging process. It was found that two distinct layers, one that was visually quite compact and another more porous layer, were present as early as 3 days.

Using bending modulus data from Coats and Margulies, 2006 and thickness values obtained during the Li et al, 2007 study, bending rigidity of human infant parietal bone versus age in months was compared to that of the porcine specimens versus age in days. The slopes of parietal bone bending rigidity versus age were $0.505 \text{ GPa}\cdot\text{m}^4/\text{month}$ for humans and $0.596 \text{ GPa}\cdot\text{m}^4/\text{day}$ for the porcine specimens.

Findings Aim #3 – Porcine head computational model

Michigan State University Team

Using a simplistic model, the Michigan State team focused on the analysis of maximum principal tensile stress. It was found that maximum principal stress directions revealed a concentration at the impact site for all age-interface combinations. Larger regions of high tensile stresses were located nearer the suture-bone boundary for compliant interface impacts than for rigid interface impacts. Furthermore, tensile stresses developed in the sutures of the young specimens were significantly greater for compliant interface impacts than for rigid interface impacts. The older specimens had similar levels of stress in the sutures for both interfaces.

The orientation of maximum principal tensile strain revealed high strains at or near bone-suture boundaries, with lower levels of strain at the impact site for all age-interface combinations. The rigid interface impact produced higher levels of strain closer to the impact site than the compliant interface impact, however, the highest strains were still located away from the impact site. Furthermore, the magnitude of the tensile strains developed in the sutures of the

young specimens from compliant interface impacts was considerably greater than those from rigid interface impacts.

The Wayne State University Subcontract

A number of important results were documented in the more detailed studies of fracture initiation and propagation. Basic sensitivity studies on defined geometries indicated that the degree of model smoothness will significantly affect the pattern of fracture. It was also anticipated that the suture boundary characteristics will play an important role in the generated patterns of cranial bone fracture. These patterns will also be controlled by the degree of element refinement in the models and the orientation of the impact against the skull.

The development of a computational model for the 21 day-old piglet has shown some important results. While a purely elastic material model for the cranial bone showed fracture at the impact site, an elastic-plastic model was able to show fracture lines along the margins of the impacted parietal bone, as well as near the impact site. When the material model incorporated tension-compression non-linearity into the bone's failure properties, a central impact on the parietal bone produced radial fractures that were perpendicular to frontal and lambdoidal suture lines. This pattern compared with the experimental results from MSU. Furthermore, when the tangent modulus (stiffness) of the plastic response was increased, these fractures were limited to the peripheral areas of the parietal bone, as shown in the experimental data of MSU. Importantly, stiffening of the suture properties resulted in a diffuse pattern of cranial fractures along the boundary of the parietal bone, as expected from the earlier sensitivity studies.

The Wayne State team focused on developing a computational-based tool that could be used to determine the input required to generate a specific pattern of fracture on the developing porcine skull. While the model was developed, it proved to be too sensitive and dependent on

minute geometry and material properties of the cranial vault, resulting in the lack of functional utility. While the studies on a computational-based modeling effort showed that some of the general characteristics of cranial fracturing can be predicted with rather simplified models, the advanced studies that sought to better understand the physics of cranial fracture showed that these mathematical-predicted fractures are quite sensitive and dependent on local geometry and material properties of the cranial vault, making them very subject specific. The sensitivity of the model to even very small changes in curvature and other geometry shows that more biomechanical FE models need to be developed from high-resolution medical imaging and meshed finely in order to facilitate adequate numerical approximation. Currently, there are insufficient methods available that could precisely determine these properties for each case to make the modeling efficient enough for current forensic practice.

Findings Aim #4 – Human head computational model

The Michigan State University Team

The Michigan State team modeled four clinical cases with a simplified FE model revealing that locations of high tensile stress and high tensile strain were located on the basicranium. It was found that the path of these stresses run parallel with the fractures in these cases. In Case 1, an overlay of the directions of maximum principal tensile stresses revealed a linear concentration on the right side of the cranial base which correlated well with sections of the observed fracture. In Cases 2 and 3, the overlay of the directions of maximum principal tensile stresses was identical in both cases due to the similarity of loading patterns. There was correlation between the stress and the fracture for both cases, especially along the line of similar fracture, although each had areas of high stress where fracture did not occur.

The Wayne State University Subcontract

The ultimate goal of the Wayne State University team was to develop a human computational model, and test it. However, due to problems with the functionality of the porcine model, this could not happen. It is recommended that further work on the piglet FE model should be carried out before translation into human subjects.

Conclusions: Implications for Policy and Practice

There are several important conclusions from this research on the immature porcine animal model: 1. The study showed that with increased impact energy came increased fracturing and longer fractures. 2. All major fractures on the cranium initiated away from the point of impact at the parietal suture margins, and radiated back toward the point of impact in the center of the parietal. This phenomenon occurred with regularity regardless of the type of interface (rigid or compliant). 3. With increasing energy of impact, fractures begin to cross sutures and propagate into adjacent bones of the skull. 4. It was typical in our experiments for a single impact to cause multiple cranial fractures in the impacted and adjacent bones of the skull. This result can have critical implications in abuse cases where multiple sites of cranial fracture are often associated with multiple sites of blunt force trauma to the pediatric victim. 5. Fracture initiation occurred at consistent locations, including: on the parietal bone at, and perpendicular to, the coronal suture; on the parietal bone at, and perpendicular to, the lambdoidal suture; on the frontal bone at, and perpendicular to, the coronal suture; and on the frontal bone at the superior orbit and parallel to the coronal suture. 6. Fracture patterns caused by the different interfaces (rigid and compliant) were different and varied with animal age. On the skulls of animals aged less than seven days, there was significantly more fracture caused by the compliant interface than

by the rigid interface. In contrast, impacts with rigid objects cause relatively more fracture than with compliant objects in the more mature individuals. 7. The beam studies on individualized sections of bone, as well as bone-suture, showed that while sutures were quite compliant in the very young specimen, in older specimens the suture rigidity and strength approached that of skull bone itself. This result helps to explain the nature of diastatic (suture) fracturing in the very young pediatric specimen, versus more bone fracture in the more matured pediatric specimen. Secondly, the results of the study showed a parallel pattern of bone stiffness (rigidity) change with age between the porcine skull and human data from a recent reference in the literature. This result helps to validate the developing porcine model as a surrogate of the human pediatric skull. 8. Another important aspect of the current study was the initial work on the development of computational tools that could ultimately be used to predict cranial fracture patterns based on known input boundary loading conditions.

While simplified modeling of the cranial vault and assuming that patterns of maximum principal stresses generated in an impacted skull may correlate with patterns of skeletal fracture, relatively good correlations were established in computational models of the porcine and human skulls. However, more complex, detailed models of the cranial vault and more sophisticated models of the mechanisms of fracture initiation and propagation indicated that these more complex models will be difficult to utilize as a generalized tool for the investigation of forensic cases. Refinements of a computational model, while shown to yield quite reasonable fracture line predictions in the current studies involve a significant level of subject-specific anatomical and material property information that is needed, making the tool less than currently adequate as a general use tool in forensic cases. Other computer-based methodologies need to be investigated in the near future. Still, the goal of this multiphase, interdisciplinary research team is to develop

a computer-based tool that could be used to predict expected cranial fracture patterns from human pediatric victims for a variety of typical scenarios documented in the current forensic case files. Such a tool would ultimately help provide an important link that might help close a current and major “gap in best practice” for forensic death investigations.

INTRODUCTION

1a. Statement of Problem: Pediatric Cranial Fracture

Traumatic injury to the head is a common cause of death in infant humans. Often, children sustain skull fractures due to accidental falls during the development of walking motor skills (Zimmerman and Bilaniuk, 1994) and death resulting from falls is the third leading cause of death in infants aged 1-4 years of age (Hall et al., 1989). However, distinguishing an accidental fall from inflicted abuse is difficult due to both scenarios producing similar types of injury (Billmire and Myers, 1985). In a study of 89 children under the age of 2 years, 19 of the 20 fatalities were due to abuse (Hobb, 1984). In contrast, short falls rarely cause serious injury or death in young children (Reiber, 1993). A study of 1,881 falls from bed height reported no deaths (Belechri et al., 2002). However, short falls (less than 3 feet) can still produce skull fracture in infants less than 12 months of age (Gruskin and Schutzman, 1999). Further, linear, complex, and depressed fractures can be seen in cases of both accidental falls and in abuse (Reece and Sege, 2000; Wheeler and Shope, 1997). Due to a lack of pediatric cranial trauma data, diagnosing skull fracture due to abuse or from an accidental fall poses a significant challenge to forensic pathologists and anthropologists and the call is often made based on the presence of soft tissue damage or antemortem skeletal fractures. Justice in these cases would be much better served if baseline biomechanical data existed on skull fracture patterns in infants and young children.

1b. Literature Citations and Review: Pediatric Cranial Fracture

Skeletal fractures are diagnosed in nearly 1 of 3 children investigated for physical abuse (Belfer et al., 2001); and 80 % of all fractures from abuse are seen in children less than 18

months of age. Furthermore, in a study of 64 falls from 3 meters or more of subjects ranging from 0-18 years, 48% of the subjects with head injuries were under 5 years of age and 50% of these head injuries involved skull fracture (Lallier et al., 1999). The most commonly fractured cranial bone in both accidental injury and abuse cases is the parietal (Hobb, 1984; Meservy et al., 1987; Leventhal et al., 1993), and linear, complex, and depressed fractures can be seen in both types of cases (Reece and Sege, 2000; Wheeler and Shope, 1997). The risk of injury is also dependent on the contacting surface and fall height (Bertocci et al., 2003; Chalmers et al., 1996). Other variables, such as the area struck, thickness of the skull, thickness of scalp and hair, and impact direction can also affect the fracture pattern (Knight, 1991; Cooperman and Merten, 2001).

While several studies have documented important information regarding the response of the infant skull and brain to blunt force impact, these data are limited to one or two age groups. And because of ethical considerations, experimentation on human pediatric specimens is very limited. While scaling of the adult skull has met with some success in predicting impact response of the pediatric skull (Prange et al., 2004), the head of an infant is smaller and geometrically unlike that of an adult (Schneider et al., 1986) and the validity of predicting skull fracture patterns in infants from adult data has not been investigated. Using adult data to predict skull fracture patterns in the pediatric skull may also be problematic due to the different structural (ease of deformation and decreased threshold to fracture) and mechanical properties of the infant skull (Thibault and Margulies, 1998; Prange et al., 2000; Prange and Margulies, 2002). Thus, while injury biomechanics are used in case-based investigations of suspected child abuse (Bertocci and Pierce, 2006) animal models are often used in these cases to correlate data to

humans. From these correlations, one animal model of the human infant has begun to emerge regularly in the current literature.

A study by Dickerson and Dobbing (1967) shows a similarity in development of the central nervous system when correlating months of the human to weeks of the pig. Other studies have used porcine models to predict fracture loads for the infant human femur (Pierce et al., 2000) and strain in the braincase and sutures (Herring and Teng, 2000). More recently, age-related rates of change in the bending rigidity of the infant human and infant porcine skulls has been found to be similar for a correlation based on months in humans to days in pigs (Baumer et al., 2009).

Recently, Margulies and Thibault (2000) have attempted to correlate the mechanical behavior of human infant cranial bone to porcine infant cranial bone. While the ages and number of specimens tested were limited, the data shows a linear increase in mechanical properties with age, but the data includes prenatal and postnatal aged specimens. Other studies have shown that growth of the human skull involves large increases in size over the first two years of life, with decreasing growth rates into adulthood (Mertz, 1984). Since questions of abuse in the pediatric patient typically involve subjects up to 18 months of age, the documentation of the biomechanical properties of developing porcine skulls and sutures over a longer period of developmental time is necessary.

Additionally, Margulies and colleagues have documented the biomechanical properties of infant porcine parietal bone using beam specimens oriented perpendicular to and across the coronal suture, but case-based investigations show linear skull fractures in infants typically initiate at an ossification center and run parallel to and perpendicular to developmental spiculae in the parietal bone (Holck, 2005). It has also been demonstrated that the mechanical properties

of prenatal human infant parietal bone is non-isotropic (McPherson and Kriewall, 1980). Therefore the data from the current study will provide information on the age factor for developing parietal bone and coronal suture in the porcine infant model, as it may relate to the human pediatric victim.

1c. Literature Review: Finite Element Models of the Developing Porcine Head

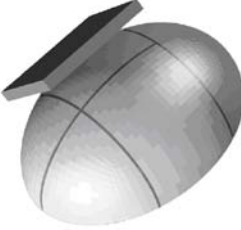
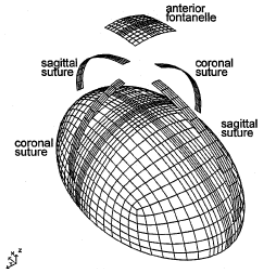
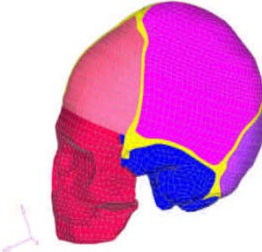
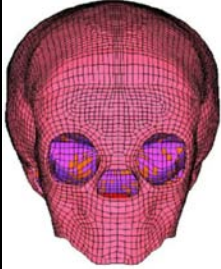
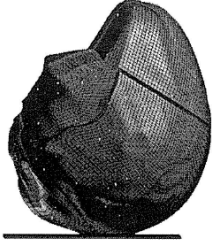
In addition to animal models, Finite Element Analysis (FEA) is a powerful and commonly used tool used in biomechanics studies. While fracture simulations have extremely high computational costs, it has been noted in the literature that principal stress or strain directions found in finite element simulations correlate well with experimentally and clinically observed fractures (Bozic et al., 1994; Silva et al., 1998). Frank and Lawn (1967) propose that fracture propagates perpendicular to the direction of the greatest principal tensile stress as a method of dissipating the maximum amount of energy in a system. Thus, it is assumed that the maximum principal stress directions may be used as a predictor of fracture in a finite element simulation.

Several finite element models developed to study infant skull biomechanics have been published in the literature. A majority of these are impact models, although there are also some models used to study fetal head molding during birth. The published details of each model and results are described below to highlight the modeling techniques and material behavior that have been employed by other researchers. Biomechanically-related conclusions that may be drawn from these models contribute to the background of the current piglet modeling study. To date, no immature animal FE models of the cranium are found in the literature, and none of the

published pediatric head models utilize techniques to represent lines of fracture propagation as opposed to general fracture location.

Table 1 summarizes the construction of various models in the current literature. Note that the bone itself is generally modeled as isotropic or orthotropic elastic. Plasticity is not considered, although many studies of the adult skull and some of the pediatric skull have reported material property values for such behavior. Many of the material properties are derived from porcine specimens or scaled from human adult values, so some degree of estimation is evident. In order to ensure biofidelity, validation studies are necessary, but none of these FE models have undergone rigorous validation for lack of an appropriate dataset. While this does not mean that the models are meaningless, it does mean that critical evaluation of the findings should be exercised. In addition, the mesh densities are relatively coarse in relation to the size of the head. While this decreases the required computational time for solution, it also limits anatomical accuracy and the resolution of local mechanical response predictions needed in the current piglet head modeling study. Applications and findings of each model, as well as additional statically loaded models, are described in the following paragraphs.

Table 1 Technical details of FE models presented in the literature

Author	Kurtz, et al. (1998)	Margulies and Thibault (2000)	Klinich, et al. (2001)	Roth, et al. (2007, 2008)	Coats, et al. (2008)
Figure					
Software	LS-DYNA3D	ANSYS/LS-DYNA3D	LS-DYNA		ABAQUS/Explicit
Geometry	Idealized	Idealized	CT from 27 week subject; facial geometry from Zygote model	CT from 6 month subject	CT and MRI from 5 week old subject; suture geometry idealized
Age	3 months	1 month	6 months	6 months	1.5 months

<p style="text-align: center;">Elements</p>	<ul style="list-style-type: none"> • 25,279 eight-node hexagonal solids for the indenter, brain, and CSF • 5,514 four-node quadrilateral shells for the bone, foramen magnum, and dura • 137 two-node, 1D springs 	<p>12,772 total elements</p>	<ul style="list-style-type: none"> • Shell: scalp • Solid: CSF, dura, and brain • Thick shell: skull and suture 	<p>69,324 bricks 9,187 shells</p>	<ul style="list-style-type: none"> • 11,066 ten-node tetrahedral solids for brain • 18,706 8-node hexagonal continuum shells for skull • 2,485 4-node membrane elements for sutures • 624 8-node
---	--	------------------------------	--	---------------------------------------	--

					hexagonal solids for scalp 1
Author	Kurtz, et al. (1998)	Margulies and Thibault (2000)	Klinich, et al. (2001)	Roth, et al. (2007, 2008)	Coats, et al. (2008)
Materials	Elasto-plastic bone: E = 880 MPa $\sigma_y = 12$ MPa $\sigma_t = 47$ MPa $\nu = 0.28$ Suture (springs): K = 189 N/mm Linear	Bone: E = 1300 MPa $\rho = 2150$ kg/m ³ $\nu = 0.28$ Suture: E = 200 MPa $\rho = 1130$ kg/m ³ $\nu = 0.28$ Linear viscoelastic brain	Skull (from porcine): $\rho = 2150$ kg/m ³ E = 3.0 GPa $\nu = 0.22$ Suture (from porcine): $\rho = 2150$ kg/m ³ E = 1.95 GPa $\nu = 0.22$	Skull: $\rho = 2150$ kg/m ³ E = 2.5 GPa $\nu = 0.22$ Suture: $\rho = 2150$ kg/m ³ E = 1.5 GPa $\nu = 0.22$	Nonlinear isotropic viscoelastic hyperelastic (Odgen) brain (μ and α scaled from adult, using porcine ratios): $\mu = 559$ Pa

	<p>viscoelastic</p> <p>brain (from porcine):</p> <p>$G_0 = 5.99e-3$ MPa</p> <p>$G = 2.32e-3$ MPa</p> <p>$G_0 = 5.99e-3$ MPa</p> <p>$G = 2.32e-3$ MPa</p> <p>$\beta = 9.43e-2$ s</p> <p>$K = 2110$ MPa</p> <p>Dura and foramen magnum:</p> <p>$E = 100$ MPa</p>	<p>(from porcine):</p> <p>$G_0 = 5.99e-3$ MPa</p> <p>$G = 2.32e-3$ MPa</p> <p>$\beta = 9.43e-2$ s</p> <p>$K = 2110$ MPa</p> <p>Dura and foramen magnum:</p> <p>$E = 100$ MPa</p>	<p>Brain (from porcine):</p> <p>$G_0 = 5.99$ kPa</p> <p>$G = 2.32$ kPa</p> <p>$\beta = 9.43e-2$ s</p> <p>$K = 2110$ MPa</p> <p>CSF (from adult):</p> <p>$\rho = 1040$ kg/m³</p> <p>$E = 70$ kPa</p> <p>$\nu = 0.499$</p> <p>Dura (from adult):</p> <p>$\rho = 1133$ kg/m³</p> <p>$E = 31.5$ MPa</p> <p>$\nu = 0.45$</p> <p>Scalp (from adult):</p>	<p>Brain (from porcine):</p> <p>$G_0 = 5.99$ kPa</p> <p>$G = 2.32$ kPa</p> <p>$\beta = 9.43e-2$ s</p> <p>$K = 2110$ MPa</p> <p>CSF (from adult):</p> <p>$\rho = 1040$ kg/m³</p> <p>$E = 12$ kPa</p> <p>$\nu = 0.49$</p> <p>Dura (from adult):</p> <p>$\rho = 1040$ kg/m³</p>	<p>$\alpha = 0.00845$</p> <p>$\rho = 1040$ kg/m³</p> <p>$\nu = 0.499$</p> <p>Orthotropic linear elastic bone:</p> <p>$\rho = 2090$ kg/m³</p> <p>$\nu_{12} = 0.19$</p> <p>Parietal:</p> <p>$E1 = 453$ MPa</p> <p>$E2 = 1810$ MPa</p> <p>$G = 662$ MPa</p> <p>Occipital:</p> <p>$E1 = 300$ MPa</p> <p>$E2 = 1200$ MPa</p> <p>$G = 503$ MPa</p>
--	--	---	--	---	---

			$\rho = 1200 \text{ kg/m}^3$ $E = 17 \text{ MPa}$ $\nu = 0.42$ Face (estimated): $\rho = 9000 \text{ kg/m}^3$ $E = 30 \text{ kPa}$ $\nu = 0.22$	$E = 31.5 \text{ GPa}$ $\nu = 0.45$ Scalp (from adult): $\rho = 1200 \text{ kg/m}^3$ $E = 16.7 \text{ MPa}$ $\nu = 0.42$	Linear elastic suture (ρ and ν from adult primate): $\rho = 1130 \text{ kg/m}^3$ $\nu = 0.49$ $E = 8.1 \text{ MPa}$ Linear elastic scalp (from adult primate): $\rho = 1200 \text{ kg/m}^3$ $\nu = 0.42$ $E = 16.7 \text{ MPa}$
--	--	--	--	--	---

Idealized 3-month-old: skull deformation

To study the deformations of the immature skull, Kurtz et al. (1998) created an idealized partial infant head model representing a 3-month-old. Bone was modeled using shell elements, but the sutures were modeled as linear springs, supporting tension and not bending. Given that sutures function mechanically as hinges allowing rotation, the use of springs may be inappropriate. The idealized brain included a separate dura (shells) and continuum cerebral spinal fluid (CSF)/brain (solids). Frictionless contact was used at the skull-brain interface. The authors cited the theory proposed by Hughes (1984) and modeled the bone using an isotropic, deviatoric rate-independent plasticity with von Mises yield criterion. This theory allows compressibility during elastic deformations, but no volume change during plastic deformations. The brain was modeled as a linear viscoelastic solid. Material properties for the bone and suture were derived from a single 3-month-old subject (Runge et al. 1998). Elastic properties of the dura and foramen magnum were chosen to be comparatively small to account for the mechanical impedance of the spinal cord. A flat impactor was modeled to simulate lateral and posterior impacts of 1 kN at 45 degrees. The lateral load produced plastic deformations of the parietal region and strains up to 7%. An occipital impact predicted strains of 12.6%, which is higher than the maximum effective strain for infant bone, according to their material property study. However, the boundary conditions for this model were relatively artificial and may have enhanced the severity of the impact.

Idealized 1-month-old infant and adult: influence of skull material on brain response

Another simplified model was created by Margulies and Thibault (2000) to compare biomechanical response using infant and adult material properties of the skull and suture. The

adult model had an elastic modulus of 10 GPa, while the infant model had moduli of 1.3 GPa for bone and 200 MPa for suture. A homogenous brain mass was included, but the brain tissue properties were not varied between the adult and infant. A half-sine load of 10 ms duration was applied to the parietal region at a 45-degree angle using a flat impactor at 1000 and 5000 N amplitudes, as shown in Figure 1. Skull deformations and the accompanying intracranial strains affecting the brain were noticeably affected by the change in elastic modulus from adult to infant. Peak intrusion was more than double for the infant as compared to the adult, and the response of the brain showed diffuse bilateral strain distribution in the infant and focal unilateral distribution in the adult. This may indicate that impacts causing focal brain injuries in adults may yield diffuse injuries in children, due to the more compliant braincase.

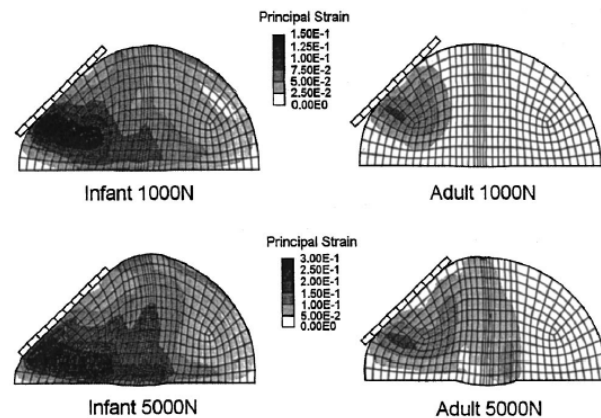


Figure 1. Strain distributions in adult and infant braincase models (Image: Margulies and Thibault, 2000)

Detailed 6-month-old: comparison with CRABI dummy

DeSantis-Klinich et al. (2002) created an infant head model to study automotive impact and compare results with those obtained from a 6-month-old CRABI dummy. The geometry for this model was based on manual processing of the CT scan of a 27-week-old subject. The skull

and sutures were modeled using thick shells, and the average skull thickness measured from each CT slice was used to determine the inner skull surface for projection. Other components, including a homogeneous brain, were composed of solid elements. The elements of the skull were projected 0.5 mm inward to create a dural layer, and a second projection created the 1.5-mm CSF layer, with solid elements occupying the remainder of the cranial cavity to represent the brain. The face was modeled as rigid, using geometry from the Zygote infant model (Zygote Media Group, Inc., Linden, Utah). Immature porcine data (Thibault and Margulies 1998; Margulies and Thibault 2000) were used for material properties whenever possible. A series of parametric studies were performed to quantify the effects of using adult and/or estimated properties for the brain, CSF, dura, and scalp, and the effects were found to be minimal on the magnitude and pattern of stress distributions. Decreasing the bulk modulus of the brain increased the predicted stresses by >15% and increased head acceleration. Increasing the long-term shear modulus (G_{∞} of the brain or Young's modulus (E) of the skull) also increased head acceleration. The suture stiffness, however, did not have a significant effect on stress distributions.

Loading was applied using a rigid, flat impactor with a velocity equal to that measured on the child restraint system (CRS) during CRABI tests replicating real-world crashes. Symmetric loading to back of head, which approximates real-world loading conditions during frontal impact, was used as an initial input. The results indicated high stresses in the occiput. Off-center loading conditions, representing three real-world cases, were then modeled. In automotive accidents, parietal fractures may be seen, and it was hypothesized that loading to the occipital caused outbending of the parietals, resulting in fracture. However, areas of highest stress occurred at the occiput, and it was suggested that the most severe fracture would occur at the site of loading, while other remote fractures were possible. Logistic regression was performed to

estimate tolerance values from the model and the injuries from the few real-world cases (Figure 2). Whether von Mises stress is an appropriate criterion for skull fracture given the overlap in binary evaluation of injury, especially since the location of fracture could not be predicted accurately by the FE model. Drop tests were also simulated for comparison of acceleration time histories and deformation with experimental data using the CRABI dummy as the test subject. In this comparison, it was seen that the model predicted shorter duration, greater acceleration impacts for the same test conditions. However, the deformations predicted by the model were smaller than those measured from the dummy. Whether the dummy or the model are more biofidelic remains to be determined.

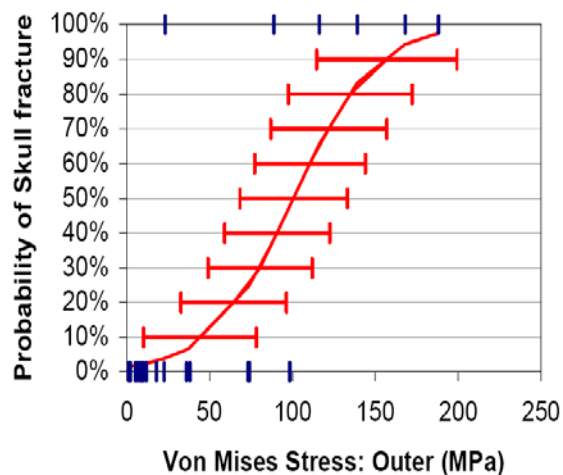


Figure 2. Probability of skull fracture predicted by the Klinich model (Image: DeSantis-Klinich et al., 2002)

Detailed 6-month-old: investigation of SBS and comparison with scaled model

Roth et al. (2007) created a complete head model from CT data of a 6-month-old child to study Shaken Baby Syndrome (SBS). This model is the most detailed of all currently published infant head models, including anatomical structures such as the skull, sutures and fontanelles, the scalp, and a layer of CSF between the skull and brain. The brain was not an idealized homogenous model (like many of the other pediatric head impact models), instead consisting of the tentorium, falx, cerebrum, and cerebellum. The skull, sutures, fontanelles, falx, and tentorium were modeled using shell elements, while the cerebrum, cerebellum, CSF, and scalp were modeled with brick elements. Springs were added to represent the bridging veins, which may be of importance in SBS.

Both shaking and an impact to the occiput were simulated separately. Although direct nodal connectivity and brick layers of CSF fluid are generally accepted as appropriate for blunt impact, oscillatory loading may require a different technique. In this case, the shaking pulse was a 400 ms sinusoid at 30 rad/s, for one cycle duration. Relative displacement in the sagittal plane was used to evaluate bridging vein strain during shaking. The impact was modeled using a 3 m/s initial velocity onto a rigid wall. The results showed that brain pressure and shear stress were lower during shaking than during impact, but bridging vein strain was equal for both cases. However, the maximum strain was reached late in the shaking event compared with immediately upon impact. Although no validation study was published for this model, the peak strain predicted for bridging vein strain was not dependent on loading mode and agreed with data reported by other researchers (Lee and Haut 1989), according to the authors.

In a different publication in 2008, Roth et al. compared this infant head finite element model (Roth et al. 2007) directly to a scaled adult head model. The scale factor used was 0.775 in all directions, and the mass of the scaled model was 2.1 kg compared with 2.2 kg for the infant

model. Differences in inertial values were most prominent in the x-axis (anterior-posterior plane). Frontal, lateral, and occipital impacts against a rigid wall at 1 m/s were simulated. Comparisons between the scaled adult model and the infant model showed differing pressure and stress distributions and time histories for all cases. “Fracture prediction” from stress criteria showed differing locations in each simulation, with the child model showing a more reasonable prediction, based on one real-world case shown in Figure 3. However, this part of the study was particularly poorly described, and although the results seem promising, one case is not sufficient to determine if this technique is accurate for skull fracture prediction. Additionally, note that the mesh density of the child head is much greater than that of the adult head, which would affect both local and global responses.

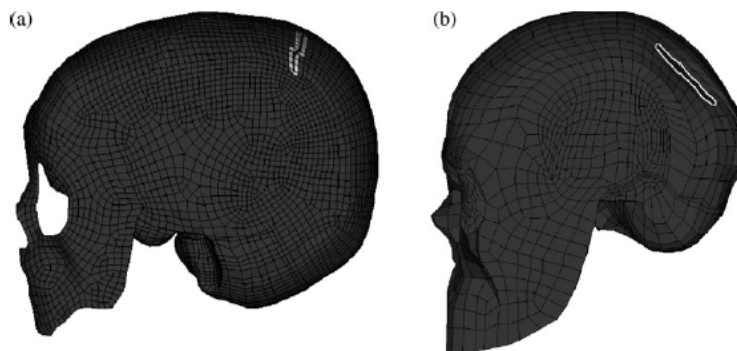
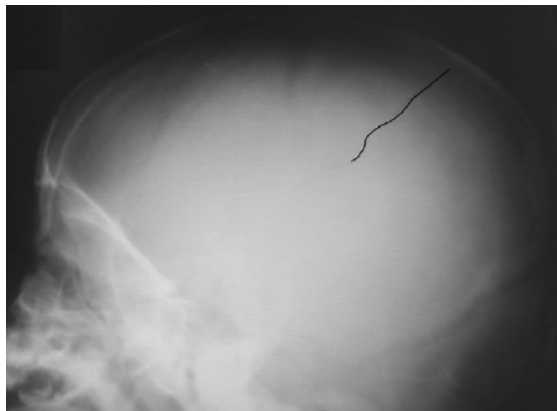


Figure 3. Fracture prediction from a real-world case (upper), showing better agreement with the infant model (lower, a) than with the scaled adult model (lower, b) (Image: Roth et al. 2007)

Detailed 6-week-old infant: skull biomechanics

Another detailed infant head model by Coats et al. was published in 2007. The geometry for this model was based on MRI and CT images of a 5-week-old, which were used to create closed boundary contours for the outer skull surface. The thickness of each skull plate was measured from CT, and the outer surface projected inward accordingly to create internal cranial structures. It is not clear whether each skull plate had a uniform thickness or if random samples were taken and applied for inhomogeneity, although the skull was modeled using shell elements. The brain was modeled as homogenous and isotropic, due to purpose of the model being developed for investigation of skull injury. A scalp was created using solid elements with a thickness of 3.5 mm, a value found in the literature.

The material properties for this model were based mostly on experimental studies performed on piglets and humans. For the skull, the parietal bone was found to be stiffer than the occiput and was modeled accordingly. Based on the findings of McPherson and Kriewall (1980), a ratio of 4:1 was used to find the elastic modulus in the direction parallel to the bone fiber orientation, allowing for an orthotropic constitutive model to be employed. Frictional contact was used, with the suture represented by membrane elements whose nodes were tied to the skull element nodes. The foramen magnum was left open and allowed brain motion through its boundary.

A series of parametric studies were performed to investigate the effects of changing five parameters (brain stiffness, brain compressibility, suture thickness, suture width, and scalp inclusion) at two or three levels. Note that the levels did not correspond to normal anatomic ranges. The model used in the parametric studies simulated a fall from a height of 0.3 m with the occiput impacting a rigid surface. For input, an initial velocity was calculated as 2.44 m/s using

energy conservation, and the model outputs examined were peak contact force, contact duration, peak principal stress, and maximum contact area. The parametric study results showed that increasing brain stiffness or altering brain incompressibility had an effect on peak stress and contact force parameters, as well as an effect on contact duration when incompressibility was changed. Although suture thickness did not affect the results significantly, abnormally large suture width did affect peak principal stress in the skull, peak contact force, and contact duration. The authors note that this indicates need for prudence when assigning brain properties, even for a skull fracture model. Eliminating the sutures entirely did not significantly affect the maximum stress in the parietal region.

Validation for this model was attempted by simulating of Weber's infant cadaver study (Weber 1984). Weber dropped infant cadavers from a height of 82 cm onto different rigid surfaces, and the fracture lines observed. Coat's model, when given this input, predicted high stresses in the parietal-lambdoidal suture region where some of Weber's fractures occurred, but the length of the fracture was not considered. As Weber's study did not provide quantitative data for validation, this must be considered a subjective validation. Validation of the braincase material properties was performed quantitatively through modeling of 3-point bending tests.

The model was used to investigate fracture tolerance, based on material failure values found in the material property study. Fracture in the model was assigned through a 3x3 element array calculation of average stress to avoid localized peak values in an isolated element. Fracture was defined in those arrays exceeding the ultimate stress obtained from material failure tests using 0.5-2.5 month old subjects. The mean ultimate stress values of 9.4 MPa for occipital and 27 MPa for parietal bones were considered to be 50% risk of fracture (Figure 4). The left parietal bone had higher fracture risk because of natural anatomic convexity in the region of the

parietal-occipital impact simulated to emulate the Weber experiments. However, the model does not predict severity or type of fracture, as crack propagation algorithms are not included.

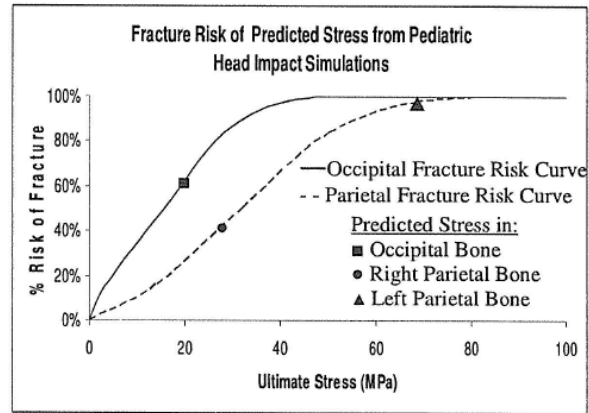


Figure 4. Probability of fracture predicted by the Coats model (Image: Coats et al. 2007)

Simplified newborn parietal bone: birth deformation

McPherson and Kriewall (1980) used rudimentary finite element techniques to study fetal head molding during birth. In this process, the parietal bone undergoes most of the deformation, and a quantitative understanding of biomechanics of fetal molding was desired. Given that this model was developed nearly thirty years ago, it is expectedly limited by finite element and computing technology of the time, but the small strains and stresses justify the use of finite element theory, even at this elementary stage in its development.

The geometry for this model was taken from three orthogonal radiographs, and using orthographic projection, a rough 3D model of the left parietal bone was constructed (Figure 5). This model included 63 thin shell elements, with nodes chosen from anatomically relevant landmark points. The radial mesh mirrors radial bone fibers seen in fetal parietal bone, and bone thickness decreased in three concentric rings from eminence to margins (element thickness =

0.89, 0.74, and 0.61 mm). Boundary conditions attempted to eliminate possibility of overlapping parietals, as this does not occur during birth. Material properties $E_1 = 3860$ MPa and $E_2 = 965$ MPa were taken from a previous study. Describe which direction is 1 and 2. Because the material was considered orthotropic but thin, plane stress was assumed, yielding $\nu_{12} = 0.08$ calculated from constitutive equations and a reported adult value of $\nu_{21} = 0.28$. The loading profile was based on pressure transducer data during birth. Results showed bone deformation, as opposed to rigid body motion, with strains from -0.0133 to 0.01 at 50 % dilation. The maximum membrane stress was predicted to be less than 5.5 MPa and bending moment less than 0.1 MPa. Validation was subjective, using kinematic trends, and the boundary conditions were not chosen properly, so parietal overlapping did occur during simulation.

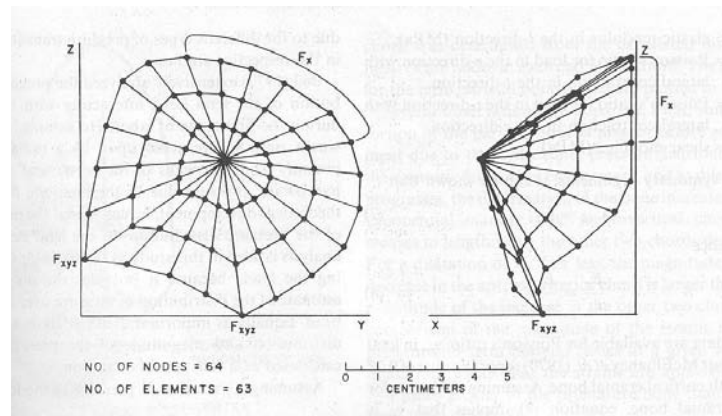


Figure 5. McPherson and Kriewall's infant parietal bone model (Image: McPherson and Kriewall 1980)

Detailed newborn: skull biomechanics during birth

Lapeer and Prager (2001) used a static model to investigate pressure distribution on the fetal skull during the first stage of labor. Geometry for this model was obtained through laser scanning of an infant skull replica, although an earlier paper by the same authors showed a

method for creating 3D geometry of the infant skull using a master and slave warping technique (Lapeer and Prager 2000). The resulting nonlinear model was meshed with 63,413 first-order triangular shell elements (Figure 6). Variable skull thickness was employed, using the same values and contours as McPherson and Kriewall, with 2 mm at the skull base and maxilla and 0.57 mm for suture and fontanelle. A slightly modified version of McPherson and Kriewall's material behavior profile was used, in which the Poisson's ratio was defined as 0.22, leading to slightly different parameter values in the in-plane orthotropic constitutive model. The suture material was based on fetal dura mater properties (Bylski et al. 1986): homogenous, isotropic, non-linear elastic, and incompressible hyperelastic. The Mooney Rivlin constitutive model was used with constants of $c_1 = 1.18$ MPa and $c_2 = 0.295$ MPa. Anisotropic and viscoelastic behavior was ignored, based on the findings of Melvin et al. (1970) that anatomical variation overshadows these effects. Adult properties were assumed for the skull base and maxilla.

Static radial pressures were applied based on measured normal birth pressures. The base of the skull and some facial nodes were constrained to prevent rigid body translation and rotation. Diametral strains of -2.84% to 1.63% compared favorably to published clinical experiments and global deformation shape was considered reasonable.

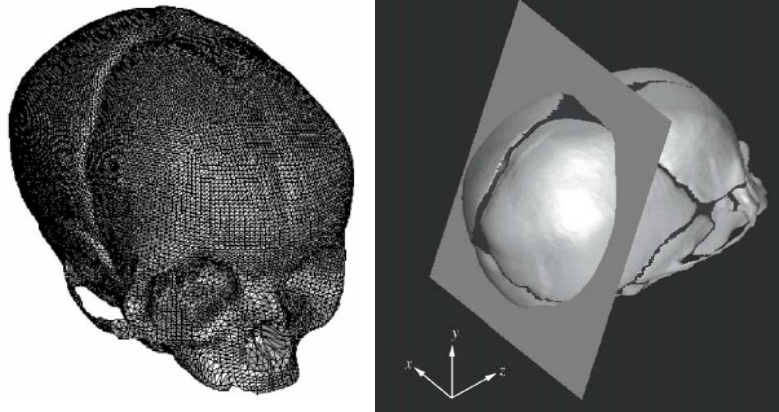


Figure 6. *Lapeer's birth model (Image: Lapeer and Prager, 2001)*

Summary

Infant skull biomechanics, in particular, the influence of sutures on skull fracture, is not clearly understood. Although the infant head is undeniably more compliant than the adult head, due to the nature of the birth process, the role of this compliance and possible viscoelastic response warrants further study in regard to impact biomechanics. It has been postulated that outbending plays a significant role in infant skull fracture, although this has not been confirmed with physical experiments. Skull fracture patterns have rarely been investigated experimentally to elucidate further information on the biomechanics of fracture, and the fracture locations relative to the impact location are unknown, as are fracture initiation and termination locations. Through experimental analysis, it has been seen that fracture lines occur in areas of high transparency, and anecdotal evidence suggests that fracture lines follow the bony spiculae radiating from ossification centers of the infant skull bone plates.

Although finite element models of the infant head have been developed, analysis of skull fracture has been limited to stress tolerance criteria, and no attempts have been made to account for crack propagation or non-uniform skull thickness. Material models used in these models may

simplify the mechanics of the biological material behavior (e.g., using a linear material model to represent nonlinear behavior). Based on this review, it is evident that further pediatric FE cranium models should incorporate some consideration for bone morphology and more accurate material models, as well as crack propagation algorithms.

Statement of Hypothesis or Rationale for the Research

Hypotheses of the MSU Studies

The hypotheses generated for the blunt force impact experiments on the developing porcine skulls are as follows:

1. The porcine model will have some characteristics similar to the human pediatric skull.
2. Impact interface will play a significant role in the production of fracture patterns.
3. Energy of impact will play a significant role in the production of fracture patterns.
4. Individual age will play a significant role in the production of fracture patterns.
5. The level of constraint of the head will play a significant role in the production of fracture patterns.
6. The fracture patterns will correlate well with the patterns of maximum principal tensile stresses theoretically generated during impact to the cranium.

Rationale for the Finite Element Model of the Developing Porcine Head (WSU)

Based on the consistent fracture patterns produced in drop tests, it was clear that any proposed injury mechanism should take into account that the fracture initiation occurred remotely from the impact center, and fracture propagation followed a perpendicular path to the

suture lines. This implies that there is some mechanical phenomenon at play. Several possibilities were considered. The parietal bone grows radially from a central ossification point, which may indicate that, in this case, the impacted area has higher strength than the periphery. A combined compressive loading plus internal pressure from the incompressible brain leading to bone rupture may also have explained the observed fracture patterns. However, preliminary modeling results were not promising. A final injury mechanism was hypothesized, that the fracture mechanism was related to tensile strain. In long bones, it is well understood that the strain tolerance is significantly higher in compression than in tension. This may be true of skull bone plates as well. During a bending event such as that produced in this study, part of the impacted parietal bone will be in compression while other sections will be in tension. Furthermore, it is hypothesized that the sutures play a role in allowing rotation at the parietal bone borders, complicating the boundary conditions.

MATERIALS AND METHODS

Low Energy Entrapped Head Impacts

Porcine specimens aged from 2 to 28 days (n=76) were obtained from a local supplier and stored at -20°C . All animals died of natural causes. The specimens were frozen within 12 hours of death. None of the specimens had outward signs of head injury, which was later confirmed during specimen preparation.

Each specimen was thawed at room temperature for 24 hours prior to testing. All soft tissue was removed from the left side of the skull, leaving the periosteum to help prevent drying of the bones and sutures. This side of each skull was placed in a bed of air-hardening epoxy (Fibre Strand, Martin Senour Corp., Cleveland, OH). Capturing the skull in this manner allowed

deformation of the skull bones and sutures, but eliminated gross motions (translations and rotations) of the skull as a whole. After the potting material had hardened, the skull was bathed in phosphate-buffered saline (PBS) solution in regular intervals until the experimental impact. Each skull, with the scalp in place, was impacted in the center of the right parietal bone. The impact location was controlled by a custom-made, four degree-of-freedom, lockable fixture that was built to hold the potted skull (Figure 7). The skull was oriented so that the impact was normal to the bone surface.

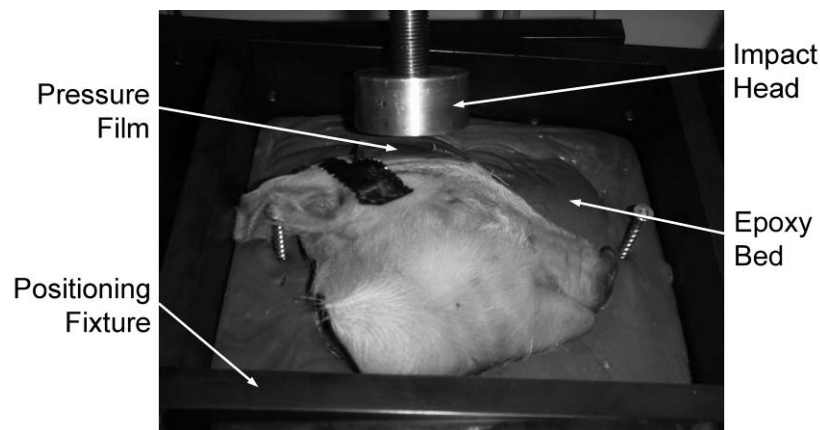


Figure 7. Skull positioning and set-up showing rigid impact head.

Each specimen was subjected to a single impact with a gravity-accelerated mass (GAM) (Figure 8). A load transducer (4.45 kN capacity, model AL311CV, Sensotec, Columbus, OH) was mounted on the GAM behind the impact interface to record forces. A single impact was assured by using an operational amplifier comparator circuit to monitor the impact forces and energize an electromagnetic solenoid to catch the impactor immediately after the load returned to zero. Two interchangeable impact interfaces were created for the GAM to represent rigid and compliant impact interfaces. The rigid interface was a solid aluminum cylinder with approximately 16 cm² of impact surface. The compliant interface was a deformable aluminum material (1.10 MPa crush strength Hexcel, Hexcel Corp., Stamford, CT), approximately 3 cm

thick with a 16 cm² impact surface, fastened to the rigid interface. Both interfaces had greater surface area than the resulting contact area on the skull.

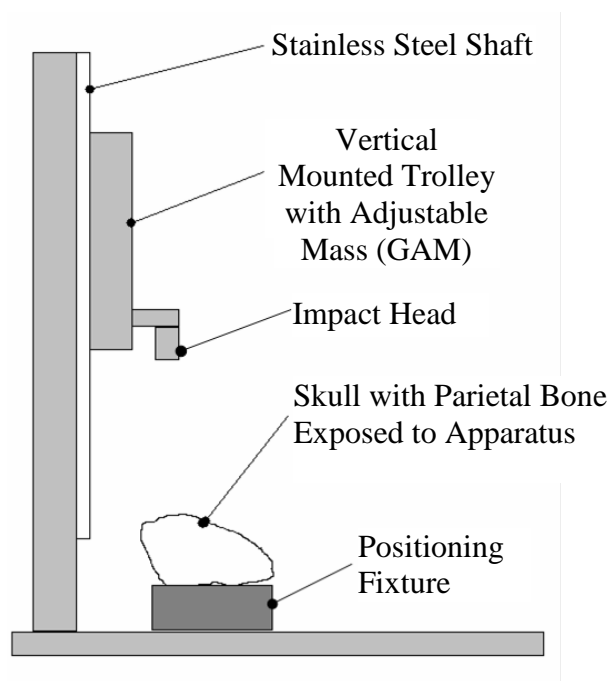


Figure 8. Drop test fixture set-up.

Input energy was adjusted by changing the drop height of the 1.67 kg GAM. A second mass of 1.92 kg was necessary for specimens twenty-one days and older, as the drop height was limited in the laboratory. The mass of the impact interface for each impact was included in the total mass of the GAM, and the force data was checked for inertial effects. Preliminary data collected at several ages was used to estimate the input energy needed to initiate a fracture using the rigid interface for each specimen age. In a few cases (n=7), the first impact with a rigid interface did not cause a fracture, so a second, higher energy impact was performed. Impacts were always conducted in pairs. All skulls impacted with the compliant interface were impacted at the same energy that caused fracture in the paired rigid impact on another skull of the same age. While the input energy was the same for rigid and compliant impacts at each age, the energy

of impact required to cause fracture initiation had to be increased with specimen age. The forces and impact durations were recorded at 10,000 Hz.

Pressure sensitive film packets (Prescale, Fuji Film Ltd., Tokyo, Japan) were attached with tape to the skull at the impact site to measure contact area and pressures generated during impact. Low (0-10 MPa) and medium (10-50 MPa) range pressure films were stacked together and sealed between two sheets of polyethylene (0.04 mm thick) to prevent exposure to fluids during the impact (Atkinson et al, 1998). Using the previously documented procedure, the film was scanned and converted to pressure using a dynamically calibrated density-to-pressure scale. Only the low pressure film was analyzed in these experiments as the pressures were not high enough to record on the medium pressure film.

Computed tomography (CT) scans were conducted for each skull after impact (625 μ m-thick coronal slices). The width of the skull vault and average thickness of the parietal bone were obtained from these scans using reconstruction software (Osirix version 3.0, Open Source General Public License). The width of the vault was measured at its widest point from parietal bone to parietal bone. Average parietal bone thickness was determined from a slice near the center of the parietal bone.

Visual inspection was conducted on each skull after the soft tissue and periosteum were removed from the impacted side. All suture damage and any visible bone fractures were recorded. Each specimen was then cleaned via standard anthropological procedures, removing all remaining soft tissue. Complete fracture diagrams and measurements were made for each specimen. Total length of the skull fractures was measured to the nearest millimeter with a flexible measuring tape, which conformed to the curvature of the skull.

The impact and pressure data were analyzed for age effects using linear regression analyses. Comparisons between the interfaces were performed using a two-factor (age, interface) ANOVA. Statistically significant effects were reported for $p < 0.05$.

Materials and Methods: High Energy Entrapped Head Impacts

All materials were stored and prepared in the same process as the low energy impacts, however, a total of 57 specimens (aged 2 to 28 days) were used for this study. Again, impact energy was controlled by varying the drop height of a 1.67 kg GAM. A slightly larger, 1.92 kg mass, was used to generate fracture in specimens aged twenty-one days and older. The mass of the impact interface was included in the GAM. Energy levels for each age were double those of a previous low energy impacts. The impact energy was doubled by raising the height of the GAM to twice the height of the previous study. The input energy for the compliant and rigid interfaces was equal at each age, however, the impact energy was increased with specimen age. For cases in which the first impact did not cause fracture of the skull ($n=5$ in the current study), the skull was impacted a second time at a slightly higher energy. The force data was sampled at 10,000 Hz.

Pressure sensitive film packets (Prescale, Fuji Film Ltd., Tokyo, Japan) were attached to the impact site of each specimen to capture contact area. Two sheets of polyethylene were used to protect low (0-10 MPa) and medium (10-50 MPa) range pressure films stacked on top of one other from fluids (Atkinson et al., 1998). The medium pressure film was not used in the current study as the impact pressures were too low to record on the film.

In order to compare the patterns of fracture between specimens and interfaces, a Geographic Information System (GIS) method was utilized in the study. The pattern of fracture

from each skull was constructed using a projected view of the porcine cranium which best highlighted the right side of the skull with fracture configurations superimposed on it for each specimen. A second view of the posterior aspect of the cranium was also included as many high energy fractures involved the occipital bone. Fracture data from the low energy impacts was also revisited to compare low energy rigid and compliant fracture configurations to the current study. Porcine specimens were separated into two different age groups (2-9 and 19-28 days) for both the rigid and compliant impact interfaces and at low and high energy levels to better demonstrate fracture pattern changes in relation to porcine growth and development, impact interface, and input energy. These age groups were chosen based on general observations of gross fracture and material property changes for the skull and suture tissues documented during the beam bending experiments (see below). The fracture pattern for each porcine cranium was traced into individual shape files (Marean et al., 2001). The GIS model then counted overlaid fracture patterns on each cranium, generating a map of where fractures appeared most frequently. After each map was constructed, the GIS model was used to discuss the differences in fracture patterns between specimens of different age, impact energy, and interface.

The impact data were analyzed for age effects using linear regression analyses. Comparisons between the interfaces were performed using a two-factor (age, interface) ANOVA. Statistically significant effects were reported for $p < 0.05$.

Materials and Methods: Porcine Skull Bone and Suture Study

Porcine specimens aged 3 days (n=5), 7 days (n=8), 10 days (n=7), 14 days (n=5), 18 days (n=5), and 21 days (n=4) were obtained from a local supplier and stored at -20°C until testing. All animals died of natural causes and the specimens were frozen within 12 hrs of death.

None of the specimens had outward signs of head injury, which was later confirmed during specimen preparation.

Each specimen was thawed at room temperature for 24 hours prior to testing. The scalp was removed, but the periosteum was left intact to help prevent drying of the bone and sutures. The top palette of the skull was removed using a surgical saw (Autopsy Saw, Stryker, Kalamazoo, MI). Cuts were made at the lambdoid suture, along the lateral aspect of the parietal bone, and diagonally across the frontal bone from the lateral aspect of the coronal suture to an anterior location along the sagittal suture.

Three beam specimens were cut from each skull: one across the coronal suture and two from the parietal bone, one parallel to and one perpendicular to the coronal suture (Figure 9). The specimens were cut with a bone saw (Isomet 1000, Buehler, Lake Bluff, IL), while bathed in phosphate buffered saline (PBS). The specimen width varied from 4.5 to 5.5 mm wide. Due to the non-uniform thickness of the beam specimens, three thickness measurements were taken from each specimen at equally spaced intervals along the beam. These measurements were used to calculate an average thickness of each specimen. The length of the beam specimens was fixed at 15 mm to yield a length to thickness ratio of approximately 8:1. The cut specimens were stored in room-temperature PBS for less than 1 hour before testing.

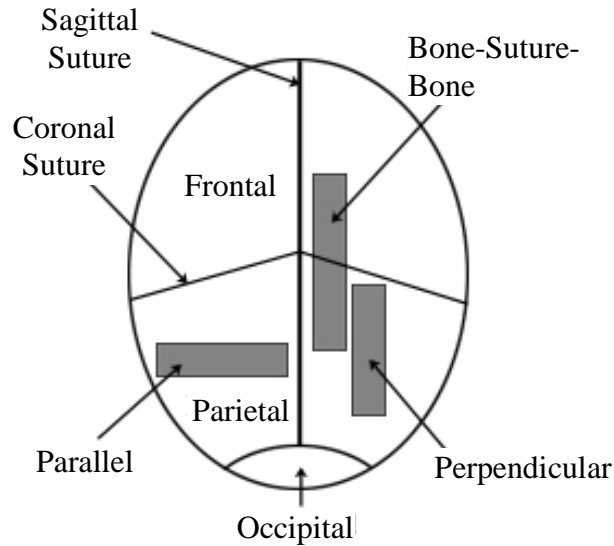


Figure 9. Top view of cranium with locations of the beam specimens.

The beam specimens were loaded to failure in 4-point bending. Each specimen was mounted between two aluminum sleeves using air-hardening cement (Technovit, Jorgensen Laboratories Inc., Loveland, CO). The fixed testing length of 15 mm was maintained with a thin aluminum bar fastened between the sleeves. This bar also served to prevent damage to the specimen during preparation and mounting in the test fixture.

The potted specimens were mounted in a custom-designed 4-point bending fixture (Figure 10) attached to a servo-hydraulic testing machine (Model 1331, Instron Corp., Canton, OH). One end of the fixture was mounted on linear bearings to allow displacement along the specimen axis. An actuator-mounted probe was located on each of the two sleeves to apply 4-point bending. A 111.2-N load-cell (Model #JP25, Data Instruments Inc., Acton, MA) was mounted between the probe and actuator. The experiments were run with the machine in displacement control at 25 mm/sec to generate the bending moment on the beam specimens.

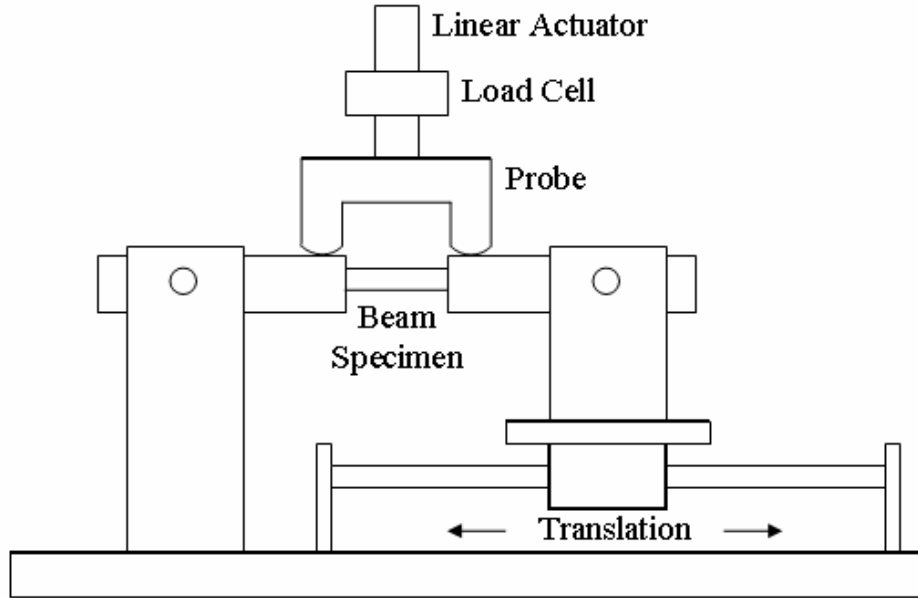


Figure 10. Diagram of testing fixture.

The force and actuator displacement were recorded to failure during each experiment. From these values, initial specimen stiffness, ultimate stress (s_{ult}), ultimate strain (e_{ult}), bending modulus (E), and strain energy to failure (U) were determined using the following information. Initial stiffness was calculated from the initial linear portion of the force-actuator displacement plot. Ultimate stress at the endocranial surface was determined from simple beam theory using

$$\sigma_{ult} = \frac{M^* y}{I_f}$$

where M^* was the bending moment at failure, y was the distance from the inner surface of the specimen to the centroidal axis, and I_f was the second moment of the rectangular area measured at the fracture location. Ultimate strain at the fracture location was calculated from

$$\varepsilon = \frac{2y\alpha}{L}$$

where y was the distance from the inner surface of the specimen to the centroidal axis, α was the angular rotation of the beam under the probes at failure, and L was the length of the specimen.

The elastic modulus was also determined from simple beam theory using

$$E = \frac{M}{\alpha} \frac{L}{2I_{\text{avg}}}$$

where M/α was the moment-angular rotation ratio during the initial linear region of the force-displacement trace, and I_{avg} was the second moment of area determined using the average thickness over the length of the beam specimen. The failure strain energy was then computed with the following integral equation

$$U = \int_0^L \frac{(M^*)^2}{2EI_{\text{avg}}} dx$$

where 'x' was the distance along the beam from the stationary aluminum cylinder.

The gross morphological features of the beams were documented by staining the length-wise cross-section of the failed specimens with India ink (Figure 11). Each test specimen was photographed with a digital camera mounted to a dissecting microscope at 50x magnification (Wild M5A, Wild Heerbrugg, Switzerland). A representative section of bone was cropped from the exocranium to the endocranium that included an equal distance along the length of the beam. This image was always taken in an area between characteristic undulations in the specimen thickness, as this was the area of failure during the experiments. The image was imported to an image analysis program (Sigma Scan, Jandel Scientific, San Rafael, CA) and converted to grayscale. The porosity was determined as the area of the stain (voids) per total area.

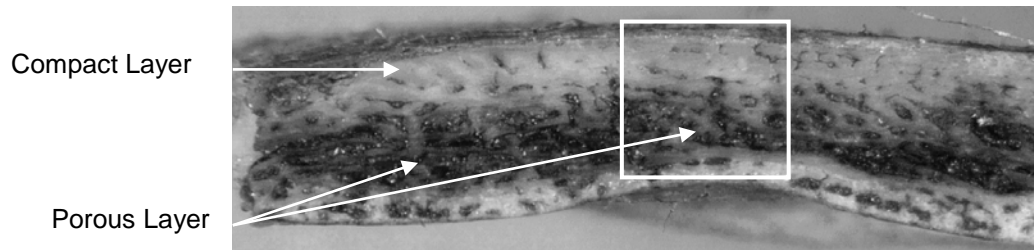


Figure 11. Representative stained cross-section of a beam from a 14 day specimen showing separation of compact and porous layers. Voids in the bone matrix were colored black. The box represents the analyzed area of a test specimen.

Each material property data set was analyzed for age effects using linear regression analyses. Comparisons between the three specimen types were performed using a two-factor (age, type) ANOVA. A Pearson Product Moment correlation was used to analyze the effect of porosity on ultimate stress. Statistically significant effects were reported for $p < 0.05$.

Materials and Methods: Free Fall Head Drops

A total of 31 porcine specimens were received from a local supplier and stored at a temperature of -20°C . All animals had died of natural causes and were frozen within 12 hours of death. The specimens ranged from 2-17 days of age. Each animal was inspected for initial head injury by palpating the parietal bone prior to experimentation.

Each specimen was fastened to a mounting plate using Velcro straps. A four degree-of-freedom clamp directly attached to the mounting plate was used to orient the parietal bone normal to the impact interface (Figure 12). The mounting plate was fastened to a hollow aluminum rod, supported by two linear bearings.



Figure 12. Picture of pig attached to mounting rod with straps.

A custom designed drop tower utilized an electromagnetic solenoid to hold a gravity-accelerated trolley at a given height (Figure 13). A second solenoid was used to hold the mounting plate and rod. During the experiment, both solenoids disengaged, allowing the drop trolley and mounting rod to fall freely. The trolley base impacted a soft padded surface while the skull impacted an aluminum interface with an approximate surface area of 324 cm^2 . The skull was allowed to impact only once by using an operational amplifier comparator circuit to monitor the impact and reenergize the electromagnetic solenoid to catch the mounting rod immediately after the impact force returned to zero. A load cell (2.22 kN capacity, model 1010AF-500, Interface, Scottsdale, AZ) mounted immediately behind the impact interface recorded impact force, duration, and energy. The force data was sampled at 10,000 Hz.

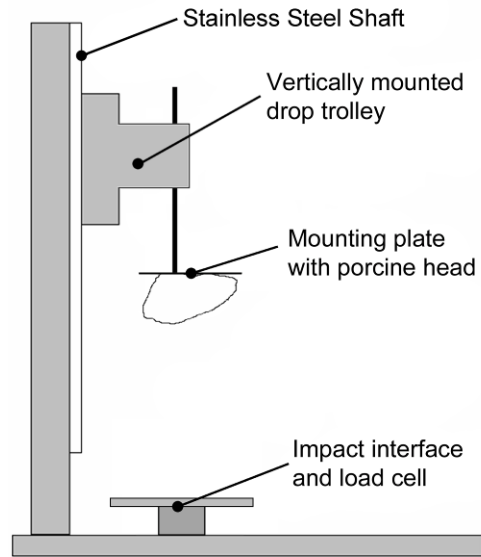


Figure 13. Schematic of free-fall drop tower.

Energy values were matched in the current study to those used in our previous head impacts by varying the drop height of each specimen. Due to the differences in mass of the head with age, each specimen mass was measured and given a respective drop height to match impact energies using

$$U = m * g * h$$

where m was the mass of the specimen, g was the gravitational acceleration, and h was the respective drop height.

After impact, the scalp and soft tissues of the skull were removed using standard anthropological procedures. Each skull was visually inspected for fractures and was recorded with photo documentation. The periosteum and remaining soft tissues were then removed via standard anthropological procedures. The length of skull fracture was measured to the nearest millimeter using a soft, flexible measuring tape, which contoured to the curvature of the skull. Complete fracture diagrams were manually constructed for each specimen.

The Geographic Information System (GIS) method was again used in this chapter to map the frequency of fractures. The pattern of fracture from each skull was constructed using a projected view of the porcine cranium which best highlighted the right side of the skull with superimposed fracture configurations for each specimen. A second view of the posterior aspect of the cranium was also included to display fractures of the occipital bone. The porcine specimens were again separated into two different age groups (2-9 and 10-17 days) to demonstrate fracture pattern changes in relation to porcine growth and development, as well as the impact scenario. Fracture pattern data from the entrapped impacts were revisited to compare the fracture patterns of the 2-9 day old and 10-17 day old age groups from high energy, rigid interface, entrapped impacts to the free fall experiments. The age groups were chosen based on the available specimens, as well as general observations of gross fracture and material property changes for the skull and suture tissues documented in the literature (Baumer et al., in press; Baumer et al., 2009). The pattern of fracture for each porcine cranium was traced into individual shape files (Marean et al., 2001). The GIS software then counted overlaid fracture patterns on each cranium, generating a map of where fractures appeared most frequently. After each map was constructed, the GIS maps were used to compare the patterns of fracture produced from free falls and entrapped impacts using the same energy.

Impact force, impact duration, contact area, and total fracture length were analyzed for age effects using linear regression analyses. Data from our previous head impacts was revisited to compare the two impact scenarios. Statistically significant effects were reported for a p-value of less than 0.05.

Materials and Methods: Porcine Head Model Computational Modeling (MSU study)

A simplified model of a porcine cranium was created in a finite element package (Abaqus v.6.3, Hibbitt, Karlsson & Sorensen, Inc., Pawtucket, RI, USA) using dimensions from CT scans of impacted crania. Most elements of the cranial geometry were accounted for, although some regions were simplified due to the distance from the area of interest and complexity of meshing (Figure 14). The curvature of the parietal bone was determined from CT scans and a 5-point spline was used to simulate the measured curvature. The average bone thickness of the parietal bone was taken from specimens tested in 4-point bending (Baumer et al., 2009) and was altered with age, but the modeled bone was assumed to have a uniform thickness. The sutures were given a more pronounced width than observed on the actual cranium since the material properties used in the model were not directly obtained from sutures, but involved the bone on both sides of the sutures as well. The primary landmarks in the basal region were included, but the specific undulations were removed and replaced by a flat plate with the same thickness as the rest of the cranium. A region of the frontal bones was modeled, but the snout and orbits were removed. The model consisted of symmetry about the sagittal plane, but not about the coronal or transverse planes. Each bone and suture of the cranium was modeled separately and constrained at the bone-suture interfaces to form the full cranial model.

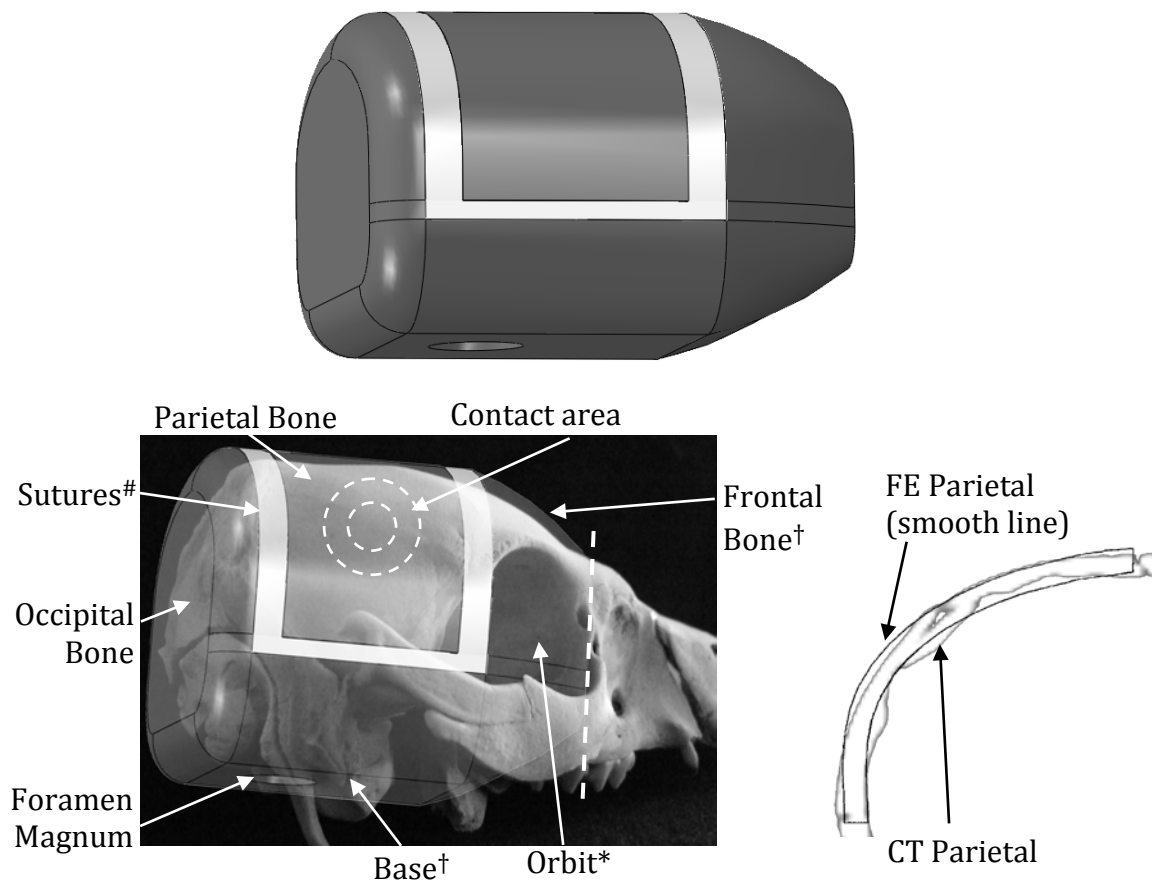


Figure 14. Simplified cranial model with overlays of modeled structures on true structures. Coronal cut of CT used for thickness comparison. *Feature not modeled. †Feature simplified. #Suture width altered for consistency with material property data obtained previously. Dotted line represents location of frontal bone removal.

Finite Element (FE) analysis was utilized in an effort to produce and examine the expected stresses and strains developed on the cranium and to compare these stresses and strains to experimentally observed fracture patterns with respect to both age and interface. The thickness of the cranium and the material properties of the bone and suture were altered in the model to represent changes in age. Age related changes in the elastic moduli of bone and suture were taken from experimental results of a previous study (Baumer et al., 2009), and average impact force and contact area data from another study were used to simulate the difference between a rigid and a compliant interface (Baumer et al., in press) (see Table 2). Briefly, the rigid interface

was constrained to produce smaller contact areas than the compliant interface with both interfaces producing the same magnitude of impact force. Numerous trials were run within the elastic range of bone to develop a representative and clearly characterized pattern of principal stress and strain directions.

Table 2. (Average) properties used in development of the FE model and impact conditions.

Specimen Age	Elastic Modulus		Impact Force		Contact Area	
	E_{sut}	E_{bone}	Rigid	Compliant	Rigid	Compliant
Young (3-7 days)	3.38	7.21	561	508	94	119
Old (18-21 days)	3.37	5.29	930	860	176	322

The magnitude of principal stress and strain directions were filtered to remove the lowest 20%. The remaining stresses and strains were compared to the experimentally produced fracture patterns. A representative cranium from young and old specimens impacted by each interface was selected. Each chosen cranium displayed all the common fracture sites from the age/interface and no instances of uncommon sites. A photo-editing program (Adobe Photoshop 5.5, Adobe Systems Incorporated, San Jose, CA) was used to overlay the modeled stresses and strains onto a photograph of the chosen, experimentally fractured cranium.

Materials and Methods Porcine Model: Material constitutive model equations and behavior (Wayne State Study)

The Hughes-Liu shell element formulation was used in this study to represent a single layer of bone. The immature skull morphs from a single layer at birth into the three-layered diploë structure later in development. Shell elements were chosen because they can support both bending and transverse shear, related to the hypothesized mechanism of injury in this case. Both

fully and reduced integration schemes were investigated, but they were not found to show significant differences in fracture pattern. One concern with using thin shells is the ratio of thickness to length (i.e. how thick can thin shell be?). To investigate the applicability of thin shell formulation to this model, a convergence study was performed on a simply supported square plate. A 10 x 10 cm plate was modeled and assigned elastic material properties ($E= 6$ GPa) with 2 mm thickness. A static 10 N load was applied the model solved implicitly. Each element of the mesh was perfectly ideal, but five different mesh densities were chosen, with element size ranging from 5 to 0.3125 mm. The physical solution to the peak deflection of the plate, based on the following equation, is 2.74 mm.

From the convergence plot shown in Figure 15, a thickness to length ratio of 0.15 still yields reasonable deformation results for this type of bending problem. In the piglet model, the average ratio is approximately 0.125.

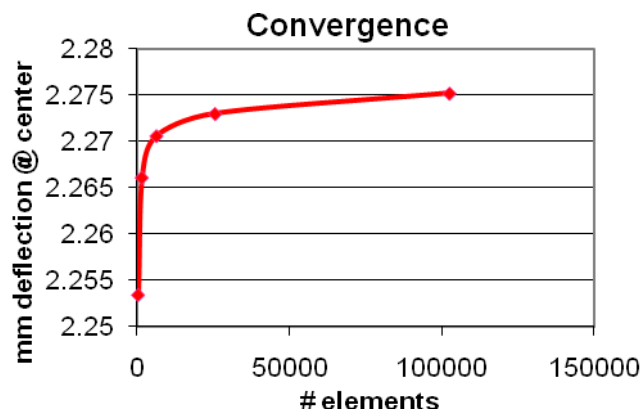


Figure 15. Convergence study to investigate thickness to length ratio in shell elements

Based on a pediatric material property literature review conducted prior to this study (Franklyn et al. 2007) and the proposed injury mechanism, several constitutive models were considered. The material property tests conducted for this study showed no evidence of a plastic behavior. However, based on published studies regarding the biomechanics of bone fracture, evidence of yielding and plastic behavior, as well as rate dependence, should be expected. It is unclear if the lack of a plastic region is an artifact of test methodology or a consequence of pediatric growth and development.

Bone consists only partially of mineral components. Especially in a developing skull, there is a significant contribution to material response from collagen. If one makes the assumption that both of these major components display purely elastic behavior, but with different moduli and ultimate stress/strain, Figure 16 shows what the shape of a typical stress-strain curve would be expected to look like. After failure of the mineralized bone, the collagen matrix would be expected to support some loading before failure (Burstein et al. 1975). As this is not what happens, it should be understood that bone itself is not a purely elastic, brittle material.

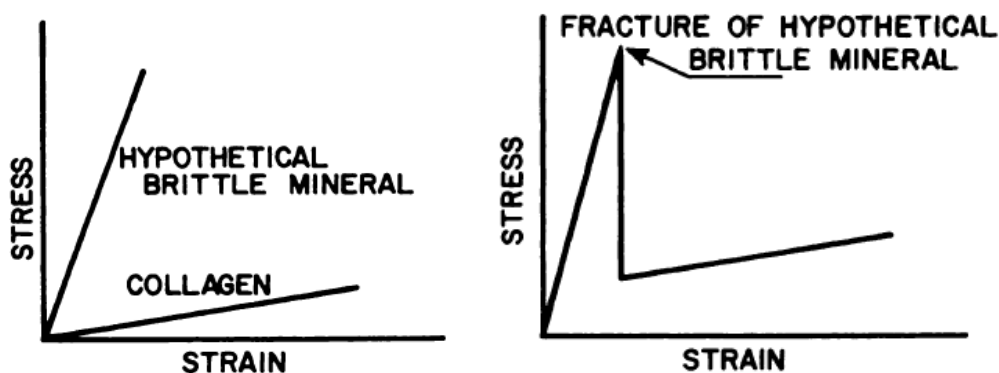


Figure 16. Hypothetical bone failure response [Reproduced from Burstein et al. 1975]

The mineral content of the piglet bones was not measured in the MSU tests, but it can be assumed that the growth of the skull plates at these ages indicates some level of mineralization. In Burstein et al. (1975), as well as other published literature, cortical bone was shown to exhibit elastic-plastic properties, with failure occurring in the plastic region. Partial demineralization of the bone did not affect the general shape of the curve, but rather only the elastic modulus and yield stress. Even the ultimate strain remained unchanged until complete demineralization, at which point it increased significantly.

A constitutive model was chosen based on the above information and the availability and compatibility of material models in LS-DYNA v971. Of the available material failure models that were compatible with thin shells, originally MAT24 was chosen to represent the elastic-plastic behavior of the bone without orthotropic effects. For the pilot model, the elastic modulus was taken from age-matched MSU data. The other plastic material parameters were estimated based on (Currey 1999) from data averaged from multiple species and presented as a function of known elastic properties. A yield stress of 100 MPa and a tangent modulus of 2 MPa were assigned. Although this constitutive model allows for rate dependent effects, only one loading rate was tested at MSU.

Based on well-established published literature on bone fracture, it is clear that a strain-based failure criterion is the most appropriate. However, it must be noted that the numerical basis of element elimination to represent fracture in finite element modeling makes it challenging to translate experimentally measured ultimate strains to an appropriate strain threshold for computational simulations. In the constitutive model chosen, effective plastic strain is defined as the failure criterion. When a certain strain parameter is reached, the element is deleted from the

simulation, with the mass retained at the nodes. The ε_p of each element at each timestep is calculated based on the following:

$$E_p = \frac{E_t E}{E - E_t} \qquad \Delta \varepsilon^p = \frac{(s^* - \sigma_y^n)}{(3G + E^p)}$$

It can be seen that the selection of tangent modulus and yield stress contribute greatly to the numerical development of plastic strain within the shell elements due to mesh density. One reason that the numerically defined failure strain may differ from the experiments is that microcracks and other incomplete fractures are not considered in a mm-scale model. Additionally, while crack propagation is determined by strain energy vectors, these may not be well-defined in the context of MAT24. Numerical failure strain was therefore determined parametrically.

The failure algorithms in LS-DYNA do not allow for a separate tensile and compressive strain failure threshold (and effective plastic strain is an inherently positive value). However, an extension of the elastic-plastic model with failure is MAT124, which allows separate plastic stress-strain curves to be defined for tension and compression. Although only one failure criterion value can be defined, changing the yield stress and/or tangent modulus can delay or prevent element elimination in areas experiencing compressive mean stress (e.g., in direct contact areas). Reverse engineering based on literature-reported yield strains were used to define the plastic regions, as no appropriate data was generated as a part of the current study. The curves shown in Figure 17 are an example and were used as baseline values for a simplified geometry sensitive study to exercise the failure behavior of this material model.

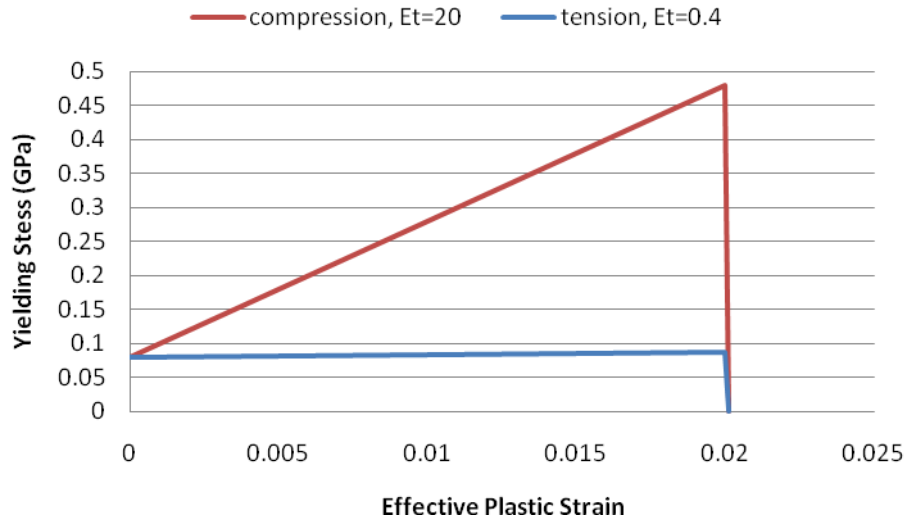


Figure 17. Example of plastic region behavior assigned in MAT124 for sensitivity studies. Based on the MSU data and the collagen data from Burstein et al. (1975), an elastic material model was chosen for the sutures, since sutural membranes are collagenous connective tissue. Failure of these elements was not necessary, as a vast majority of the fractures reported affected only the bone plates themselves. However, the inclusion of sutural representation for total head compliance is critical to the hypothesized injury mechanism in this study.

Materials and Methods: Piglet head finite element model development (Wayne State Team)

Based on data supplied by MSU, it was determined that biomechanical response shifted at approximately fourteen days old in the age range of piglets tested. Because this is obviously not an instantaneous occurrence, due in part to anatomical and developmental variation in piglet specimens, two models were developed representing piglets with a buffer of seven days from this cutoff point (7 and 21 days of age).

The geometry necessary for FE model development was obtained through CT imaging and 3D reconstruction. A 0.5 mm spiral CT scan (GE Medical Systems) with 0.293 mm in-plane

resolution was performed axially on a 21-day-old intact piglet head and exported in DICOM format. This resolution was not sufficient for accurate depiction of the thinner 7-day-old piglet head, microCT (Henry Ford Hospital, Detroit, Michigan) was employed for the second scan in order to ensure multiple voxels through the thickness for accurate reconstruction. In one region of interest (ROI), a cross-section of the parietal bone, Figure 18 shows that the skull thickness in this ROI ranged from 1.6 to 3.4 mm at 21 days but 0.5 to 1.3 mm at 7 days. However, the 90 μm resolution scan could not be performed on the entire piglet head, due to bore size and field-of-view deficiencies. Instead, a post-impact dried skull was imaged and will be reconstructed through post-processing.

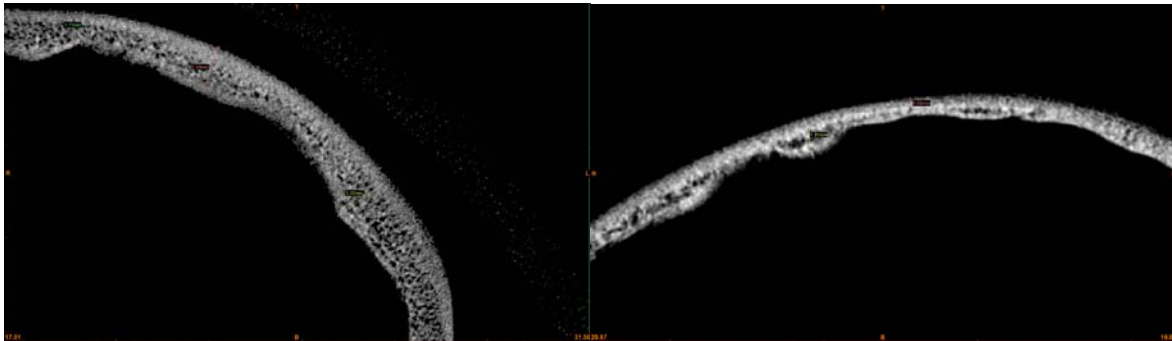


Figure 18. 90 μm resolution cross-sections of the parietal bone (left = 21 days, right = 7 days)

For 3D reconstruction, the images were imported into Mimics 13 (Materialise, Leuven, Belgium). Thresholding, region-growing, and other segmentation techniques were applied to reconstruct the skull bones (see Figure 19). The inner and outer surfaces of the skull were converted to STL format, in which the surface is represented by connected 2D triangles in 3D space. The inner and outer surfaces were separated, and the foramen magnum and all other

anatomical orifices were filled to preserve intracranial pressure in simulation. Manual smoothing algorithms were utilized to prepare the outer skull surface for meshing, balancing

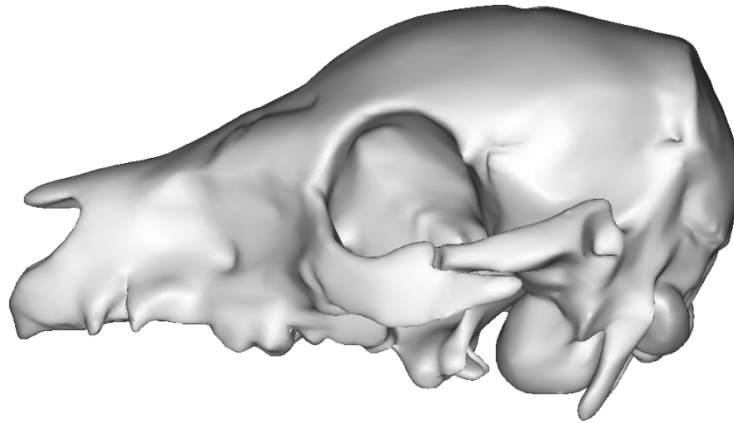


Figure 19. 21-day-old piglet skull 3D reconstructions, partially smoothed

anatomical accuracy with curvatures suitable to minimizing warpage during meshing. The final outer skull STL was exported to Hypermesh 9.0 (Altair, Troy, Michigan), where the triangular surface mesh was manually converted into 4-node quadrilateral shell elements on the parietal bone, with care taken to preserve element quality. The rest of the skull bones were meshed using automated optimization and mixed elements in Hypermesh. Through convergence testing, a mesh size of 0.5 mm was chosen. Elements were selected to represent the areas of sutural interdigitation with approximately 1 mm total width, and the edges of these lines smoothed manually. The meshed model, with 94,923 shell elements, is shown in Figure 20. In the skull and suture elements, only 6% of the total number of elements had warpage greater than 10%, mostly in elements on the inferior aspect of the cranial vault. The Jacobians were at least 0.6 for 98% of elements.

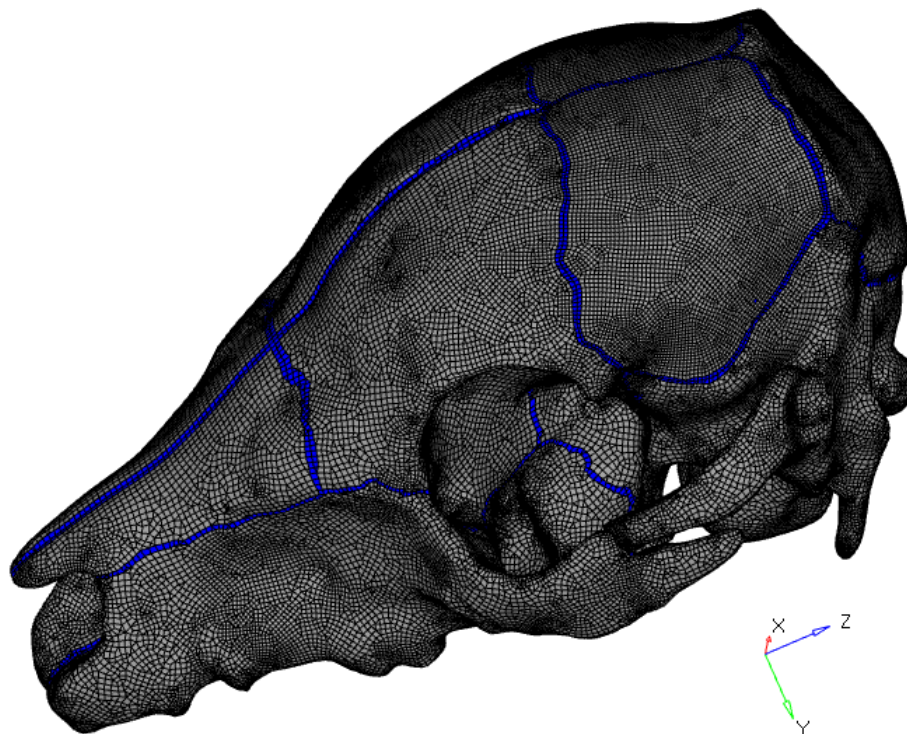


Figure 20. 21-day-old piglet skull and suture mesh

The thickness of each cranial bone was calculated through an in-house program coded in Python 2.4, which projected the quadrilateral mesh for each bone plate onto the unsmoothed inner surface STL, in a direction normal to the elemental surface, graphically describes the procedure. Histograms were produced to determine an appropriate thickness value for each bone, generally based on either the median or the mean (Figure 22). For the parietal bone, variable thickness assignment was considered, but preliminary results with MAT124 were satisfactory. Additionally, since stress concentrations can occur at the border of differing element properties, the inclusion of this possible artifact was avoided.

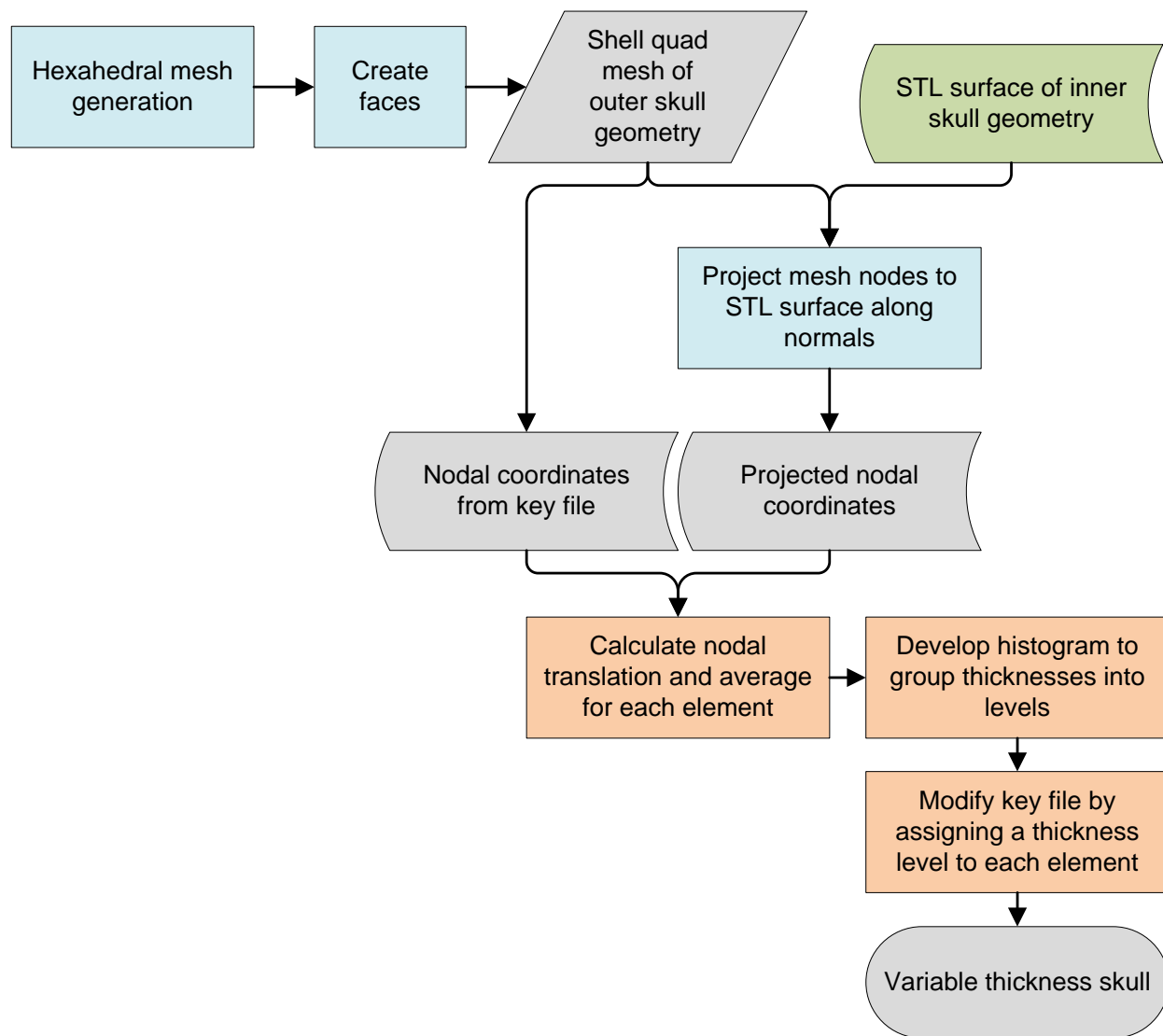


Figure 21. Flowchart describing Python algorithm (blue boxes are performed in Hexmorpher, green in Mimics, gray in Hypermesh, orange in Python scripting)

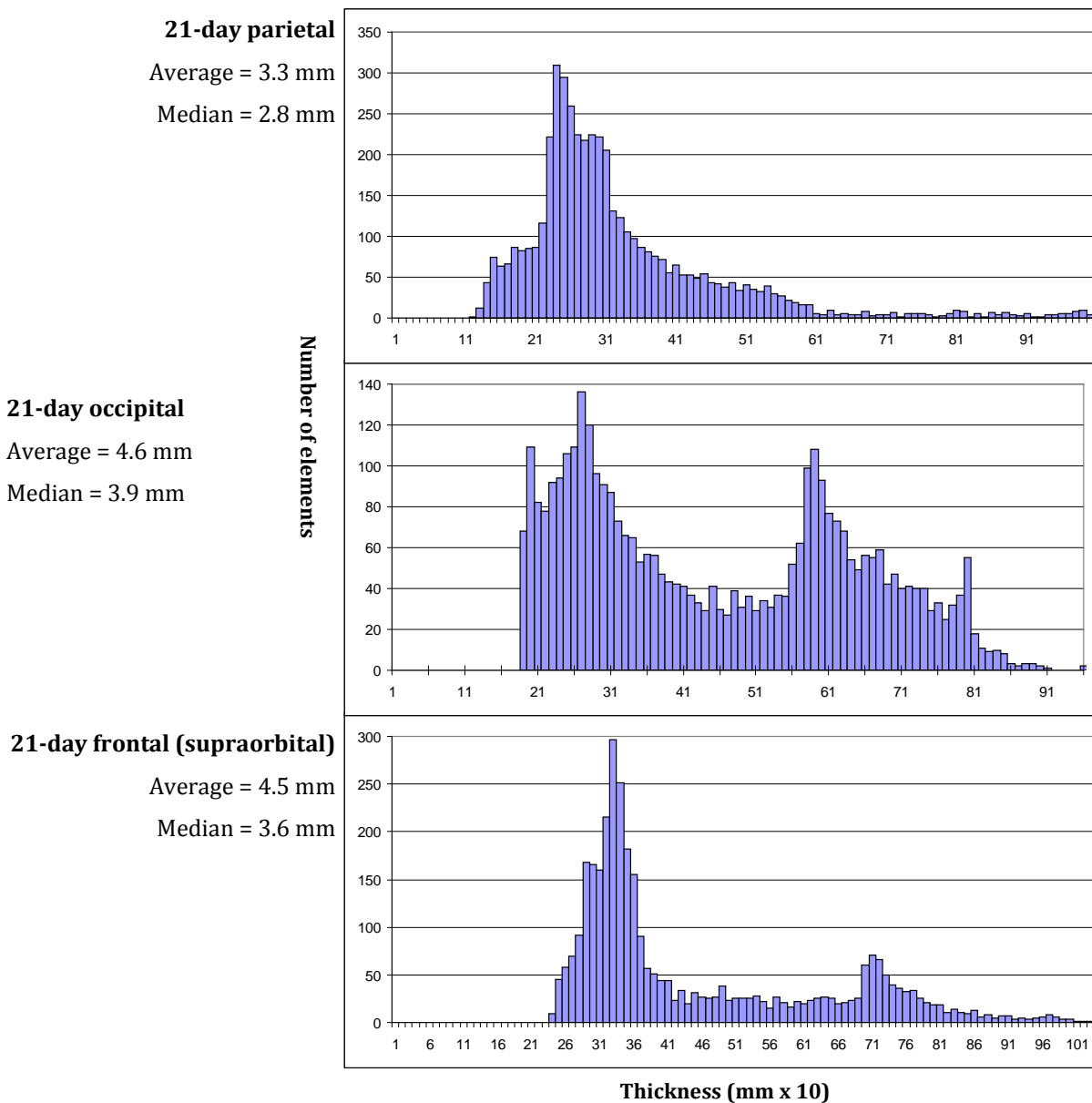


Figure 22. Bone thickness histograms for the 21-day-old piglet head

A similar procedure was employed for the 7-day-old model, however, the scanned sample was a post-impacted skull hence fracture lines had to be removed manually during the segmentation process. Given the nature of the physical reconstruction of the post-impacted dried skulls, glue introduced into the sutural space will make the sutures appear wider than they are in reality.

Observation of fresh, intact pig skulls indicates that the suture width in a 7-day-old piglet does not seem to be significantly different from the 21-day-old.

The skin of the piglet may play an important role in impact biomechanics in these simulations; however, this only pertains to the skin underneath the impactor. Therefore, a 2 mm thick layer of brick elements were modeled on the impactor surface to represent the skin of the pig. Using this technique simplifies numerical contact interfaces that must be utilized in FEM. Because these techniques are inherently approximations, some degree of validation will be required to ensure a reasonable model. An elastic material law was applied to the skin using values found in the literature and used in other pediatric head models ($E = 17 \text{ MPa}$, $\nu = 0.45$).

Materials and Methods: Human Pediatric Crush Scenario Computational Modeling (MSU Study)

Four clinical cases of fatal crush injuries to young children between 1.5 and 6 years of age under known conditions were used as a baseline for applied forces and resulting fracture patterns. In all cases the skull was trapped between a vehicle tire and the ground. The contact sites and skull fractures were identified and diagramed during autopsy by the investigating forensic pathologist (M.N.). Biomechanical modeling was then conducted in an attempt to recreate and explain the similarities exhibited in the fracture patterns of these cases.

A simplified model of a skull was created in a finite element package (Abaqus v.6.3, Hibbitt, Karlsson & Sorensen, Inc., Pawtucket, RI) (Figure 23). This model consisted of symmetry about the sagittal plane, but not about the coronal or transverse planes. Each major bone of the vault was modeled separately, assumed to have a uniform thickness, and constrained at the suture joints to form the full cranial model. The base of the cranium was modeled as a flat surface with the same thickness as the vault. The primary landmarks in the basal region were

modeled: a hole was added to simulate the foramen magnum, dense oblong extrusions lateral to the foramen magnum were generated to represent the petrous portions, and anterior to the foramen magnum the thickness was reduced to represent the region of the spheno-occipital synchondrosis.

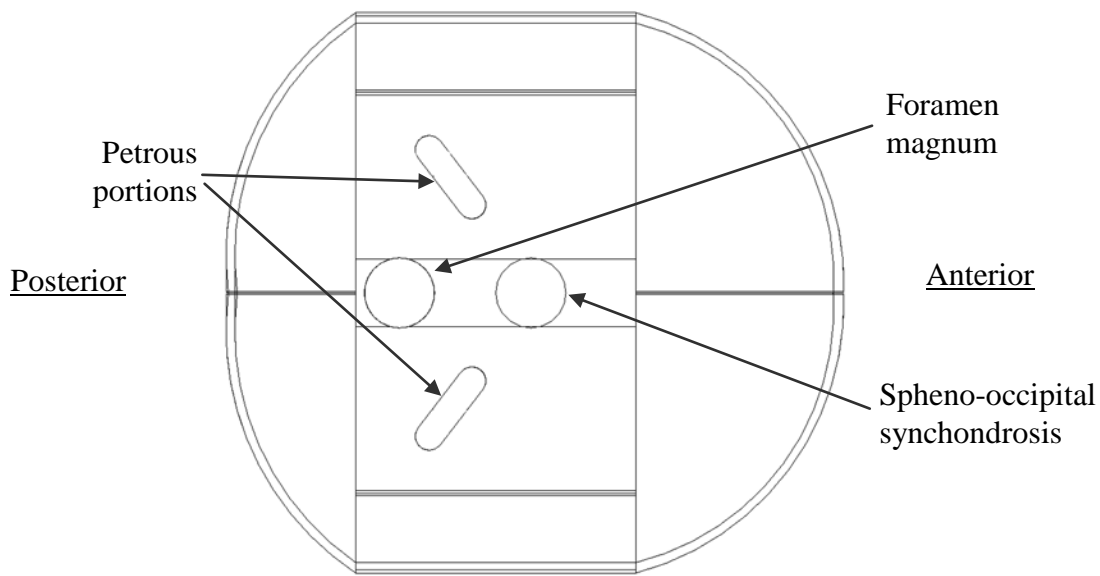


Figure 23. Simplified cranial model showing modeled landmarks of the basicranium. View of endocranial surface with vault removed.

This model did not utilize specific, age-dependent material properties for the crania and consisted of simplified, although generally accurate, geometry.

The model was subjected to quasi-static pressures corresponding to the specific exterior injury locations for each case. The magnitude of the pressure applied to the cranial model was the same in each case and was scaled down such that the generated stresses would not cause material failure. By restricting the analyses to the elastic region, the exact material properties were not required for this simple analysis. FE analysis was utilized in an effort to reproduce and examine possible relationships between the theoretical pre-failure stresses developed on the modeled crania and the fracture patterns observed clinically. Using some basic stress transformation principles at many pre-defined locations on the skull (finite elements), the

direction and magnitude of tensile and compressive stresses at each location were determined. The full-field map was then filtered to remove all regions of low stress. Areas of tensile (principal) stress were assumed to be the most likely location(s) of potential fracture (Frank and Lawn, 1967) and the general trends produced by the model were examined in comparison with the clinical cases. Numerous trials were run within the elastic (non-failure) range of bone to develop a representative and clearly characterized pattern of principal stress and strain directions.

RESULTS

Low Energy Entrapped Head Impacts

Linear regression analyses showed a significant increase (0.0516 mm/day) in average parietal bone thickness with age ($p < 0.001$), but no change in skull vault width with age.

The input energy required to cause fracture increased from 1.5 J at two days of age to 11.5 J at twenty-eight days of age. A characteristic rapid drop in force appeared in the force-time plot for all rigid interface impacts that were associated with fracture (Figure 24). In rigid interface impacts that did not cause fracture, a more pronounced peak was observed. Rapid drops in force during compliant interface impacts could not always be associated with fractures due to the deformation of the interface.

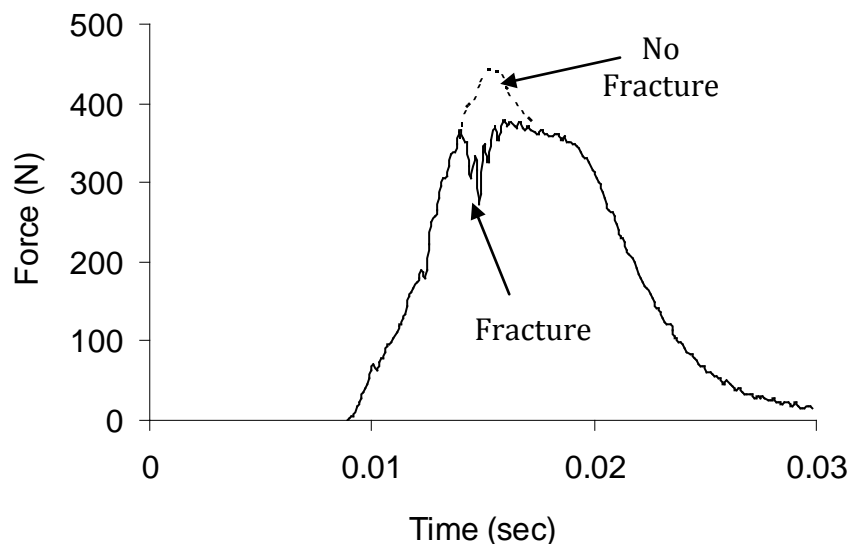


Figure 24. Overlay of force-time plots showing typical characteristics of an impact that caused fracture and one that did not.

For both impact interfaces, linear regression analyses showed a significant increase in impact force with age that was required to produce a fracture ($p < 0.001$) (Figure 25). The slopes and intercepts of impact forces versus age were not different based on interface.

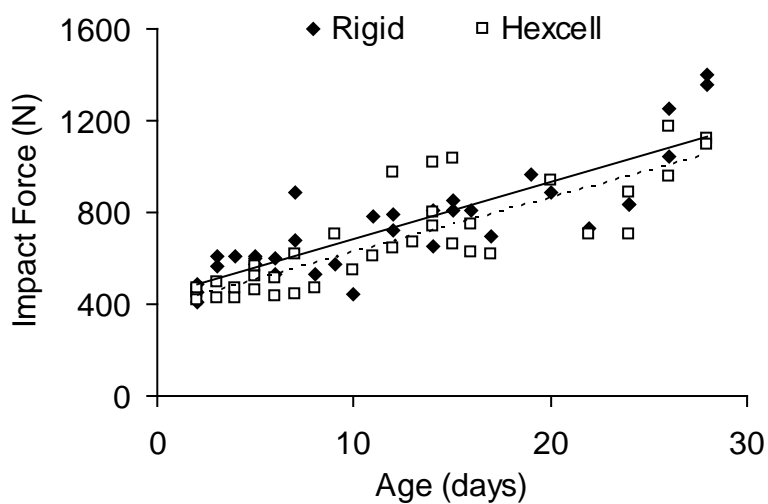


Figure 25. Peak force during impact for rigid and compliant interfaces.

The area of contact for the compliant interface significantly increased with age ($p < 0.001$), but no significant change was noted for the rigid interface (Figure 26).

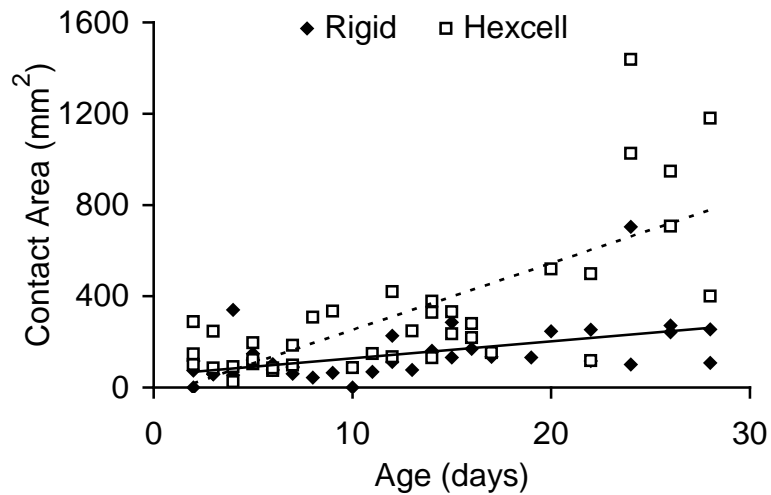


Figure 26. Contact area recorded on pressure sensitive film during impacts for rigid and compliant interfaces.

Bone fractures for all ages, and for both interfaces, occurred at sites away from the point of impact (Figure 27). These bone fractures initiated at a suture-bone interface. Frequently, bone fractures were accompanied by diastatic fractures that were generally located near the fracture tip at the bone-suture interface. Diastatic fractures caused by a rigid interface impact were not present until specimens were ten days of age, while diastatic fractures caused by a compliant interface were present as early as four days of age (Figure 28). Diastatic fractures were common for both interfaces between ten and seventeen days. Neither interface showed suture damage after seventeen days.

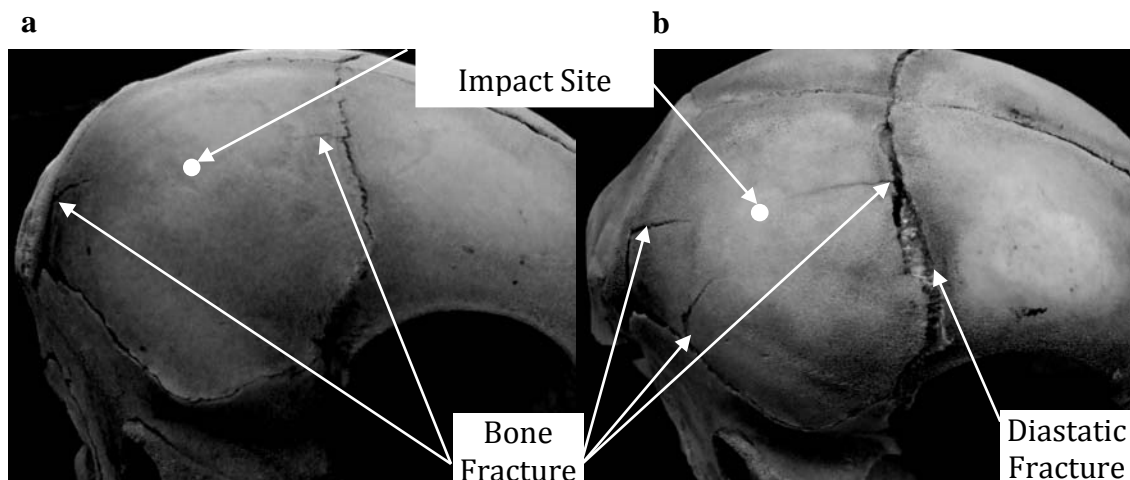


Figure 27. Representative fracture sites for (a) rigid and (b) compliant interface impacts (five-day-old specimens shown). Fracture sites initiated at bone-suture boundaries. Compliant interface impact showed increased fracture lengths at similar initiation sites as the rigid interface impacts as well as diastatic fracture of coronal suture.

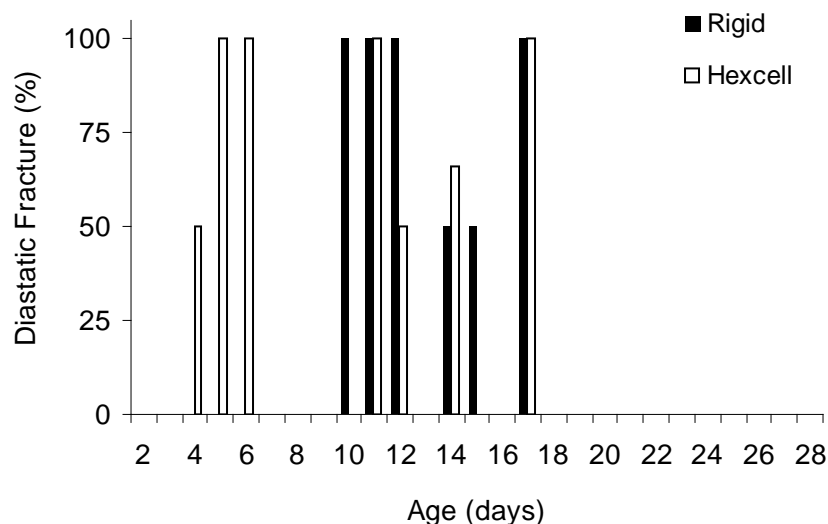


Figure 28. Frequency of diastatic fractures caused by both rigid and compliant interfaces versus age.

A two-factor (age, interface) ANOVA performed on the total fracture length (bone and diastatic combined) revealed significantly more damage caused by the compliant interface than by the rigid interface on pig skulls less than seventeen days of age, similar amounts of damage from both interfaces between seventeen and twenty-two days of age, and significantly more

damage caused by the rigid interface than by the compliant interface for specimens aged twenty-four to twenty-eight days ($p < 0.05$) (Figure 29).

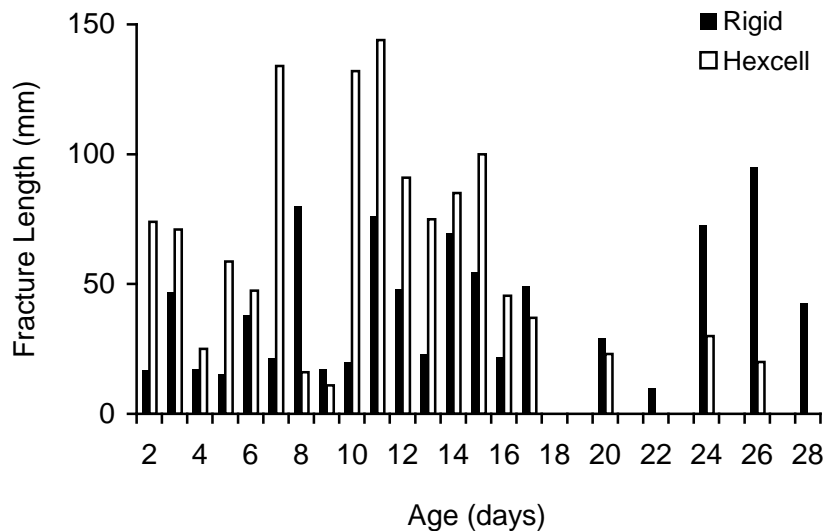


Figure 29. (Average) Fracture length generated by rigid and compliant impacts at the same impact energy.

Results: High Energy Entrapped Head Impacts

Impact energies were doubled from those used by Baumer et al. (in press) by doubling the drop height at each age. The drop heights ranged from 0.2 m for a 2 day-old specimen to 1.2 m for a 28 day-old specimen. The values of impact energy ranged from 3.1 J to 22.6 J, respectively.

The impact force on the skulls increased with age for both interfaces, and there was little difference in the peak impact force (within 100 N at a given age) between the two interfaces (Figure 30). Linear regression analysis indicated a significant increase in impact force with age for the compliant ($p < 0.001$) and the rigid interfaces ($p = 0.006$).

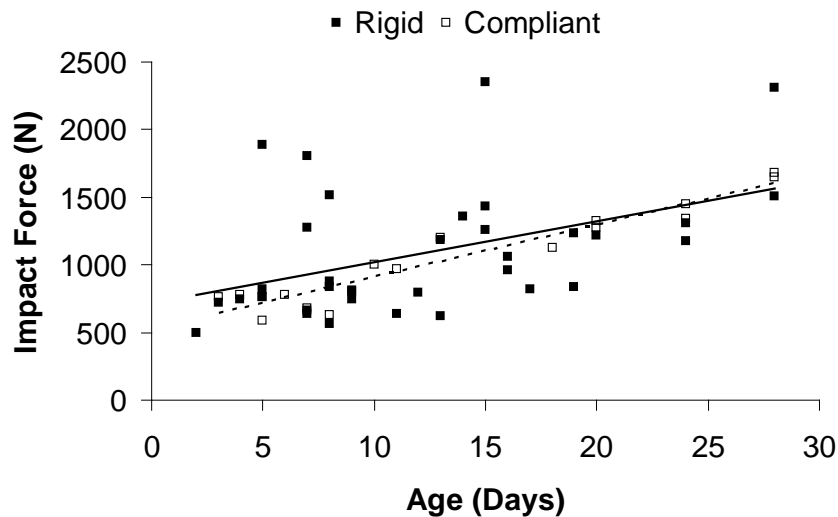


Figure 30. Peak impact force versus age for both the rigid and compliant interfaces.

The contact areas generated during impact were found to significantly increase ($p=0.003$) with age at a similar rate for both interfaces (Figure 31). A two-factor ANOVA (age, interface) for the contact area showed a significantly larger area of contact generated with the compliant than rigid interface.

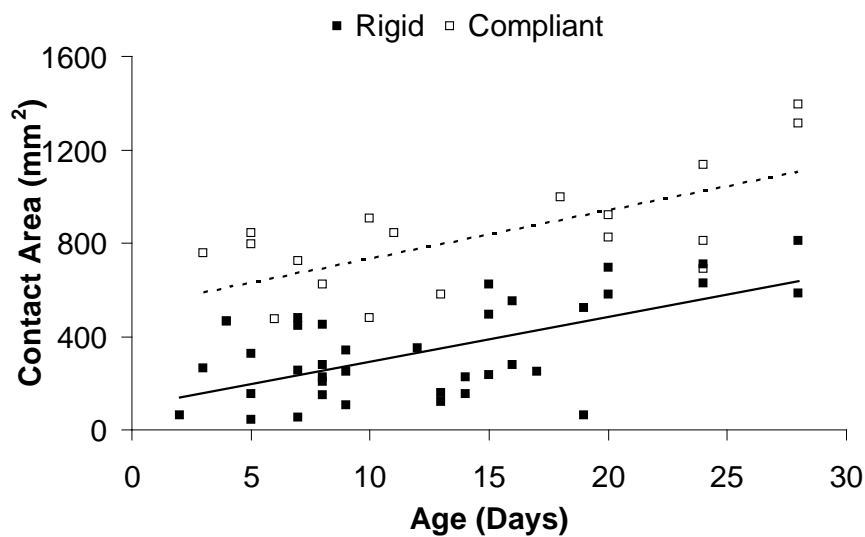


Figure 31. Contact area as a function of age for both rigid and compliant interfaces.

The length of fracturing (in bone and along sutures) versus age plot showed, on average, a significantly larger ($p=0.034$) amount of fracturing for the rigid than the compliant interfaces (Figure 32).

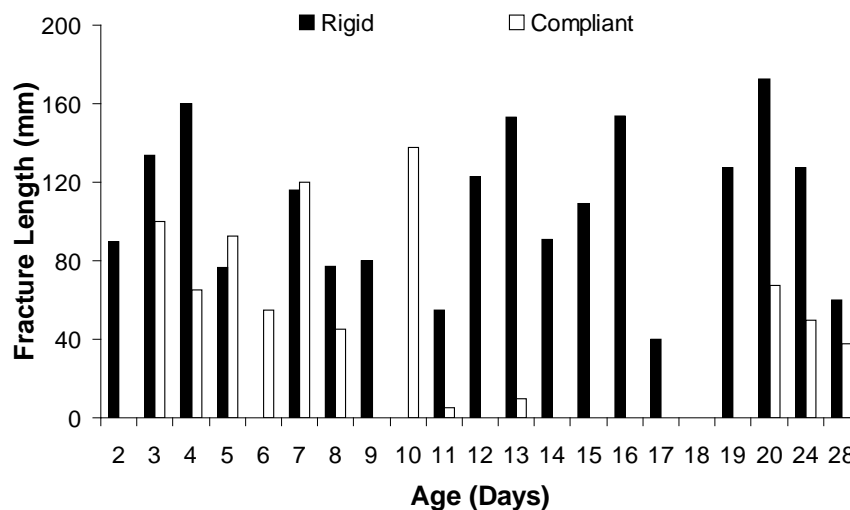


Figure 32. The average length of skull fractures as a function of age.

The GIS fracture maps confirmed that the length of fractures was greater for rigid than compliant interface impacts for the younger age group in the current study (Figure 33a and 33b). For the compliant interface experiments the pattern maps showed fractures primarily appearing to initiate at 4 sites adjacent to sutures along the perimeter of the parietal bone. However, for the rigid, there appeared to be numerous initiation sites. There was also significantly more diastatic fracturing in the rigid than compliant interface experiments, specifically along the coronal suture.

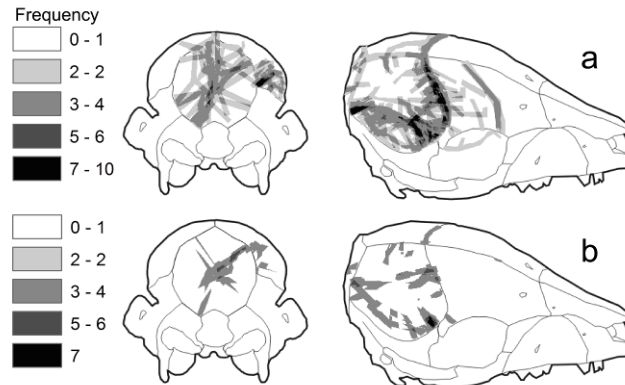


Figure 33. GIS map of 2-9 day old rigid (a) and compliant (b) impacts at high energy.

In the older group of specimens (19-28 days) more fracturing was again confirmed for the rigid than compliant interface experiments (Figure 34a and 34b). Yet, in these experiments, no diastatic fractures were noted. Sites of fracture initiation were evident in the parietal bone along the coronal and lambdoid sutures for the compliant interface experiments. Two of these sites were similar to those documented in the younger age group. These sites were also noted in the rigid interface impacts, however there were more propagated fractures with the rigid interface. Interestingly, in the current study using high energy impacts to the parietal bone, significant fracturing was also documented in the occipital bone for both age groups and interfaces.



Figure 34. GIS map of the 19-28 day old rigid (a) and compliant (b) impacts at high energy.

The GIS maps of the revisited Baumer et al. (In press) data showed three primary areas of fracture initiation, regardless of interface. For the younger age group (2-9 days old), the compliant interface produced more fracture of the skull than the rigid at the same impact energy level (Figure 35a and 35b).

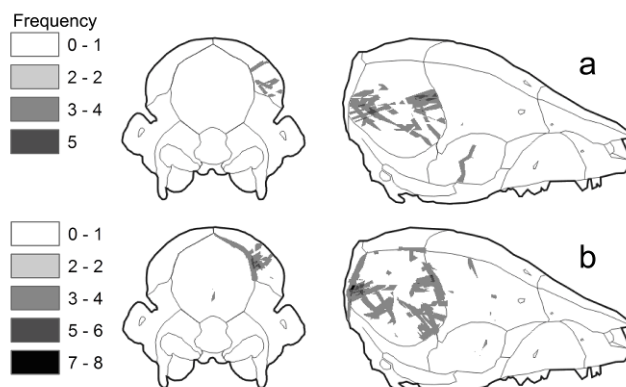


Figure 35. GIS map of the 2-9 day old rigid (a) and compliant (b) impacts at low energy.

For a low energy of impact there was little to no skull fracture with the compliant interface for the older age group (Figure 36b). Two fracture initiation sites were noted along the coronal and lambdoid sutures. The rigid impacts produced more propagated fractures initiating at approximately the same locations as in the compliant interface experiments (Figure 36a).

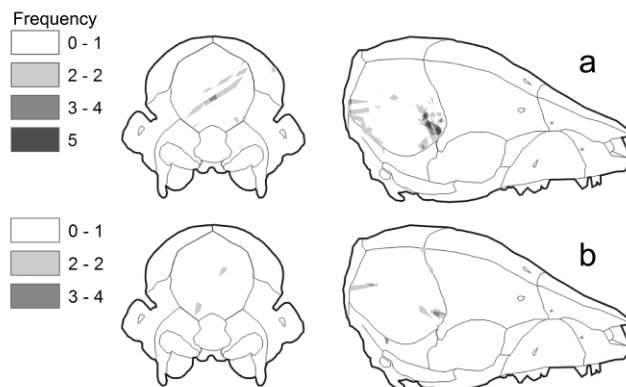


Figure 36. GIS map of the 19-28 day old rigid (a) and compliant (b) impacts at low energy.

There were many specimens in both high energy age groups where fractures appeared in the occipital region. These fractures were not present in the revisited Baumer et al. (In press) data.

Results: Porcine Material Property Study

There was no difference in average thickness measurements between the bone and bone-suture-bone specimens for any age. Linear regression analyses also showed a significant increase in thickness with age ($p < 0.001$ for each specimen type).

For each orientation of parietal bone specimen, there was a significant increase in bending stiffness with age (Figure 37a). The slopes were not statistically dependent on orientation. Interestingly, there was no significant change in bending stiffness in the bone-suture-bone specimens up to fourteen days, but between fourteen and eighteen days there was a significant increase (Figure 37b). The stiffness of the suture was lower than that of the bone up to fourteen days, but it became statistically greater than the parallel bone specimens at eighteen days (suture 1197 ± 246 N/m; parallel 864 ± 367 N/m).

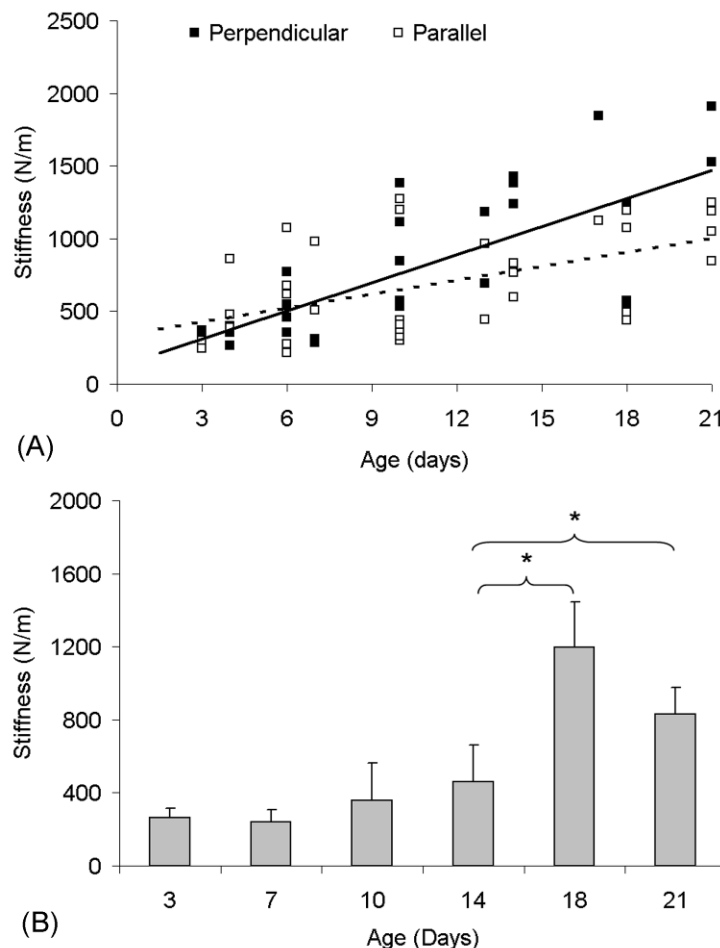


Figure 37. Recorded values of stiffness for (a) both orientations of bone and (b) bone-suture-bone specimens from 3 to 21 days. *Significantly different means.

All bone specimens failed at a thinned area and all bone-suture-bone specimens failed in the suture. Linear regression analyses showed significant decreases in ultimate stress for both orientations of bone ($p < 0.05$) and for the bone-suture-bone specimens ($p < 0.01$) with age (Figure 38). The slopes were not different.

There was no change with age in ultimate strain in the bone (0.0163 ± 0.0053 mm/mm) and bone-suture-bone (0.0313 ± 0.0072 mm/mm) specimens (Figure 39). The ultimate strain for the bone-suture-bone specimens was significantly higher than that for the bone specimens up to fourteen days.

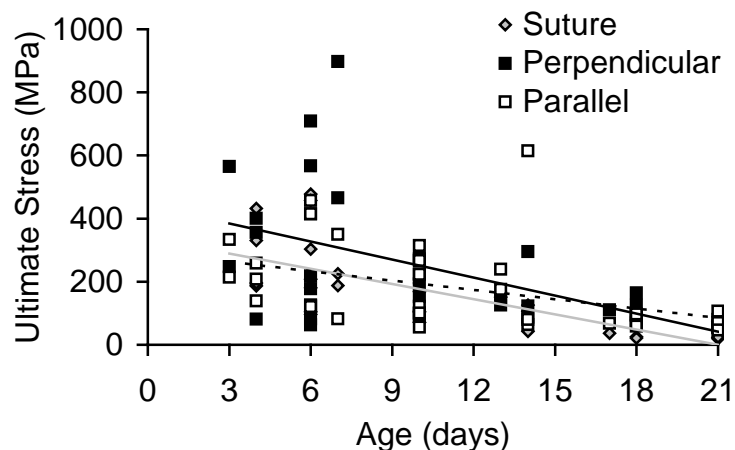


Figure 38. Linear regressions of ultimate stress for bone and bone-suture-bone specimens against age.

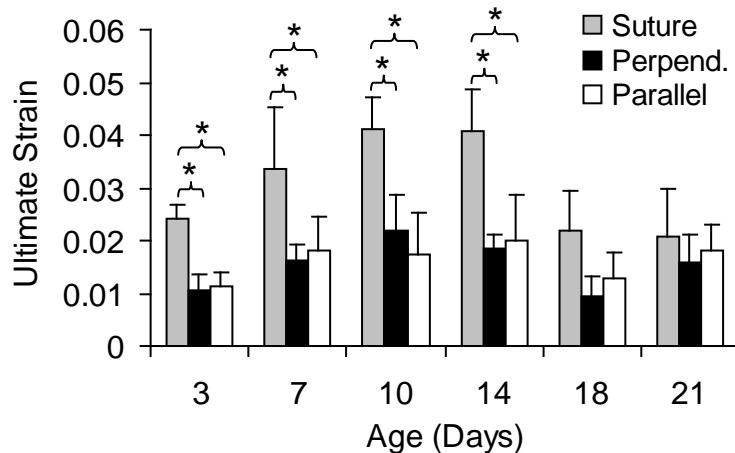


Figure 39. Ultimate strain for bone and bone-suture-bone specimens. *Significantly different means.

There was no change with age in the bending modulus of the bone (6.01 ± 1.73 GPa) and bone-suture-bone (2.73 ± 0.84 GPa) specimens (Figure 40). The bending modulus of the bone-suture-bone specimens was significantly lower than that of the bone specimens up to fourteen days.

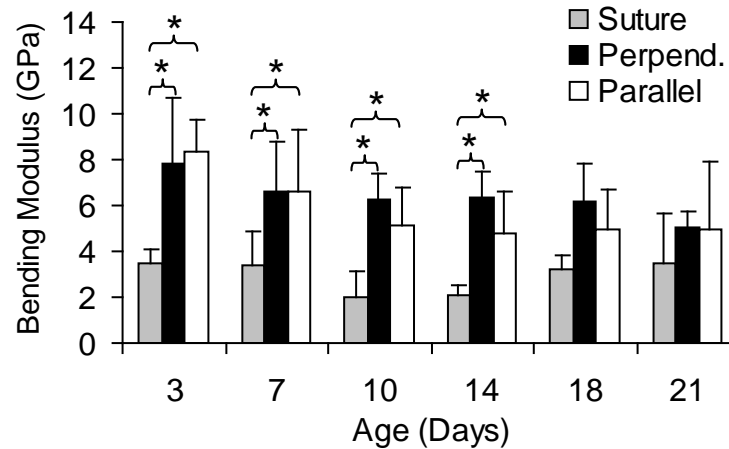


Figure 40. Bending modulus for bone and bone-suture-bone specimens versus age. *Significantly different means.

There was also no change with age in the strain energy to failure for the bone specimens, being 0.03 ± 0.03 J and 0.03 ± 0.04 J for perpendicular and parallel orientations, respectively (Figure 41). The bone-suture-bone specimens showed no change up to fourteen days (0.23 ± 0.13 J). For ages up to fourteen days, the strain energy to failure of the bone-suture-bone specimens was significantly higher than that of the bone specimens. From fourteen to eighteen days, however, there was a significant decrease in the strain energy of the bone-suture-bone specimens. Therefore, the strain energy to failure was no longer different for the bone (0.01 ± 0.00 J) versus bone-suture-bone specimens (0.01 ± 0.00 J).

The morphological characteristics of the skull bone from the infant porcine specimens changed during the aging process. It was found that two distinct layers, one that was visually quite compact and another more porous layer, were present as early as three days. The porous layer appeared as pockets beneath the compact layer which developed through ten days, and by fourteen days there was a clear separation of zones along the entire specimen.

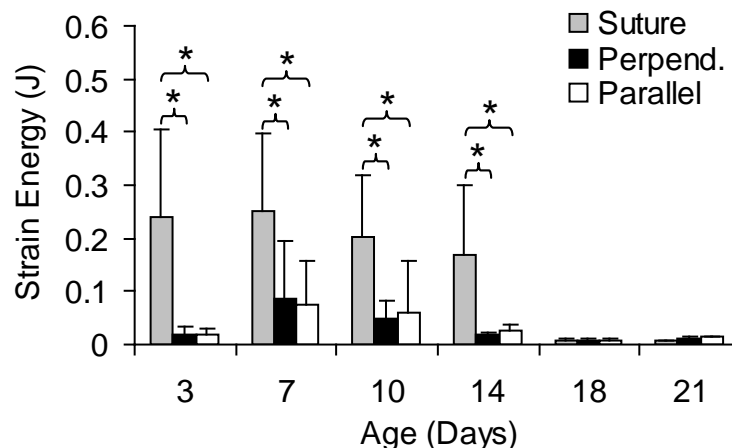


Figure 41. Strain energy of bone and bone-suture bone specimens versus age. *Significantly different means.

Analysis of both orientations of bone specimens revealed an increase in porosity with age ($p < 0.001$) (Figure 42). Correlation analysis of the combined data revealed a weak (-0.391), but significant ($p < 0.01$), negative correlation between ultimate stress and porosity. No other mechanical property had a significant correlation with porosity.

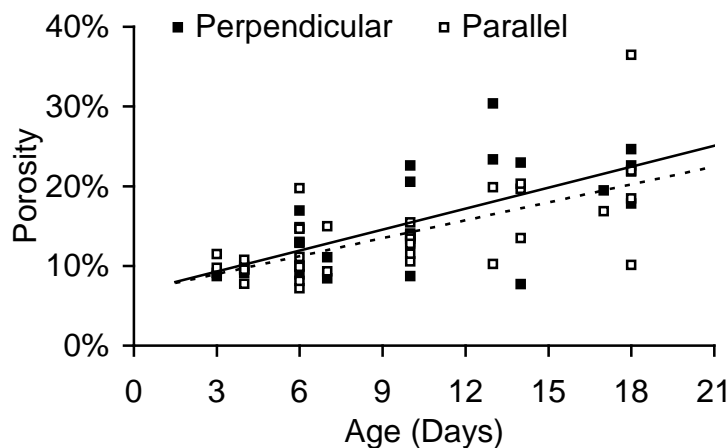


Figure 42. Linear regression analyses of both orientations of infant porcine bone specimens against age. Both orientations displayed significant dependencies on age.

The bending modulus data from the human parietal bone of Coats and Margulies, 2006 have also been compared to the bending modulus of the porcine parietal bone. It was clear that the porcine parietal bone bending modulus was significantly higher than that of the human parietal bone. However, this is a material rather than a structural parameter of comparison. Since the current thought was to use the porcine model to study issues of potential childhood abuse, a structural comparison may be more appropriate. In this effort we were able to obtain unpublished human infant parietal bone thickness data for ages 2 to 24 months, $n=314$, from a recent study by Li et al, 2007. While the human skull was significantly thicker than the porcine skull over the ages studied here, a linear regression of parietal bone thickness versus age indicated growth rates of parietal bone thickness for humans to be 0.0487 mm/month and that of pigs to be 0.0492 mm/day. Using bending modulus data from Coats and Margulies, 2006 and thickness values obtained during the Li et al, 2007 study, the bending rigidity of human infant parietal bone versus age in months was compared to that of the porcine specimens versus age in days (Figure 43). The slopes of parietal bone bending rigidity versus age for humans of 0.505 ± 0.812 GPa*m⁴/month and 0.596 ± 0.499 GPa*m⁴/day for the porcine specimens were not significantly different ($p > .05$, using Student's T-test).



Figure 43. Bending rigidity of human and porcine specimens versus age (Human – months; porcine – days).

Results: Free Fall Head Drops

The aim of the current study was to assess the impact characteristics of a porcine head dropped in a free fall scenario. There was a characteristic rapid drop in force documented in the force-time plots, which was associated with skull fracture (Figure 44). A more pronounced peak was noted if no fracture was present.

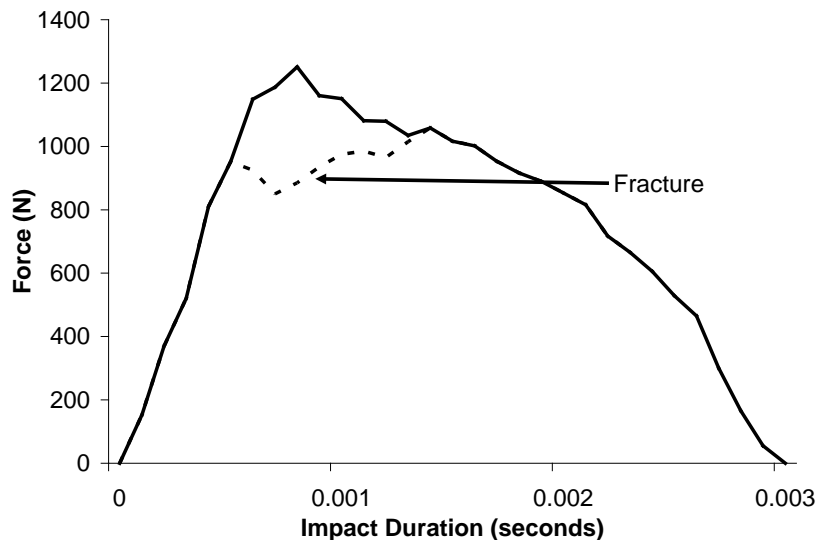


Figure 44. An overlay of force-time plots showing the characteristic rapid drop in force associated with skull fracture.

Peak impact force significantly increased with age at a rate of 40.9 N/day of age ($p < 0.001$) (Figure 45). Also, impact energy significantly increased with age at a rate of 0.19 J/day ($p = 0.009$).

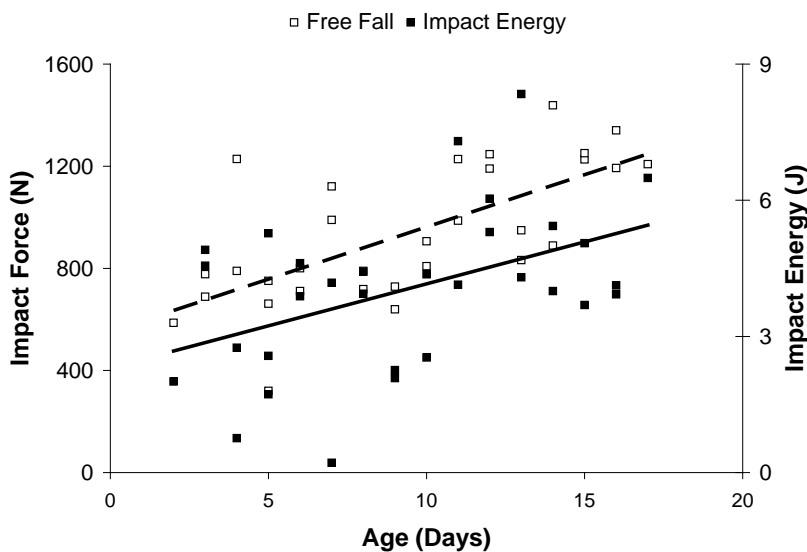


Figure 45. Peak impact force with respect to age.

Total fracture length (bone and diastatic) was found to significantly decrease with age at a rate of -1.83 mm/day ($p < 0.001$) (Figure 46). In 5 of the 31 specimens, no skull fracture (bone or diastatic) was documented.

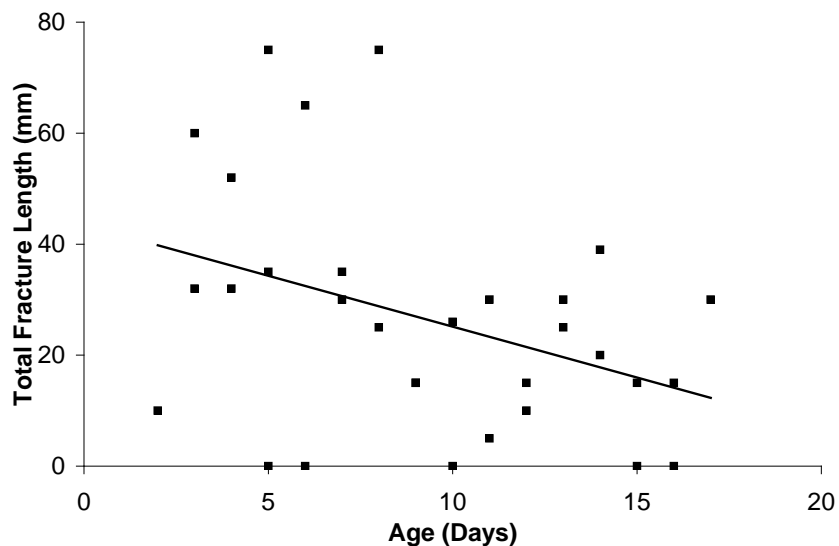


Figure 46. Total fracture length with respect to age for free fall and entrapped impacts.

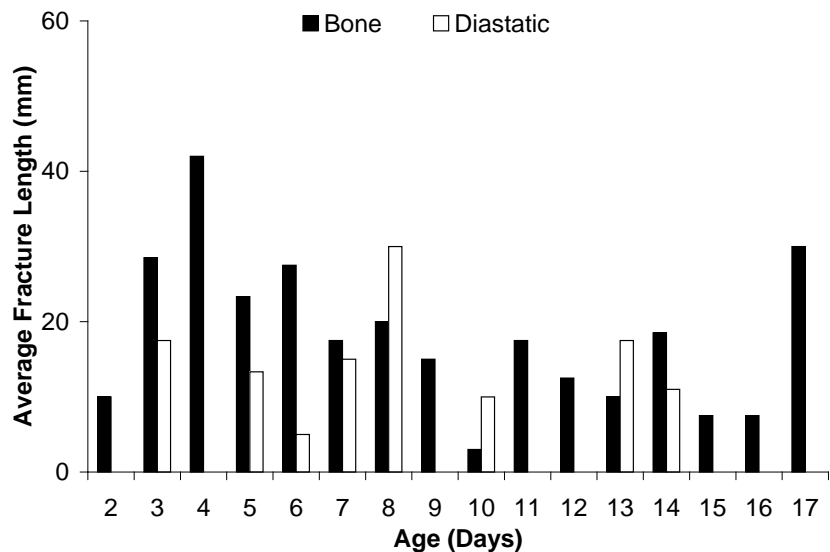


Figure 47. The average total fracture length versus age.

Average diastatic and bone fracture were compared at each age (Figure 47). Diastatic fracture was documented as early as 3 days of age. However, no diastatic fracture was noted in specimens older than 14 days of age.

In the younger age group (2-9 days old), extensive diastatic fracture was documented along the coronal suture in the free fall impacts (Figure 48a). Additionally, several bi-lateral bone fractures extended across the coronal suture into the frontal and parietal bones. Bone fracture tended to initiate at the coronal suture. There were no documented initiation sites along the posterior or superior edges of the parietal bone. Also, there was no documented occipital fracture in the free fall head impacts contrasting the extensive occipital fracture noted in the high energy, entrapped, rigid impacts (Figure 48b).

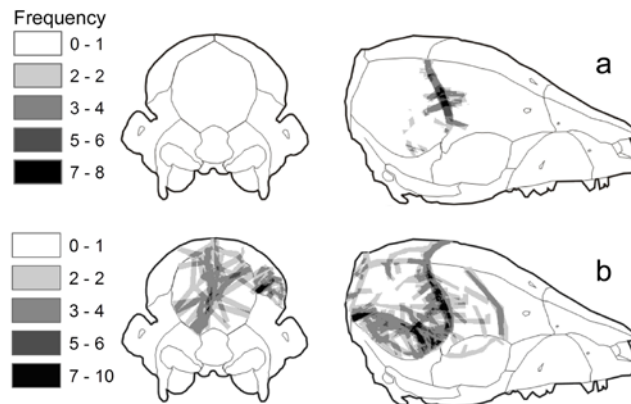


Figure 48. GIS map of the 2-9 day old age group for the free fall (a) and entrapped (b) impacts.

In the older age group (10-17 days old), several fracture initiations were documented at the lamdoidal and squamosal suture intersection (Figure 49a). However, fracture initiation was documented more frequently along the anterior parietal bone as in the younger age group. In the high energy, entrapped, rigid impacts, the sites of fracture initiation were frequent and numerous along the perimeter of the parietal bones (Figure 49b).



Figure 49. GIS map of the 10-17 day old age group for the free fall (a) and entrapped (b) impacts.

As with the young age group, no occipital fracture was documented in the 10-17 day old age group when dropped in free fall. This again contrasted with the extensive occipital fracturing documented for the entrapped head impacts. Diastatic fracture in the coronal suture was again recorded in the older age group. However, the degree of diastatic fracture was significantly less in the older age group than in the younger.

Several of the older specimens had fracture initiation on either side of the parietal bone at locations remote from the point of impact (Figure 50). This was also documented in the high and low energy entrapped impacts.

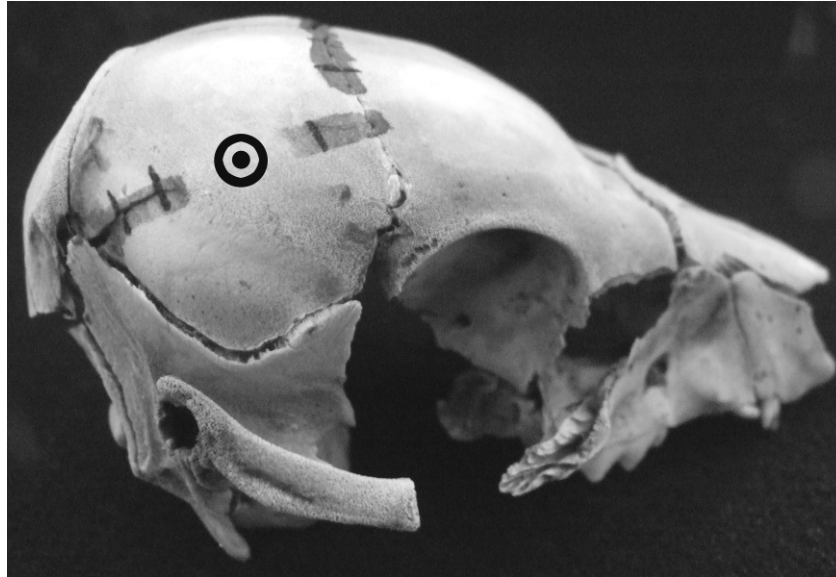


Figure 50. Fracture initiation sites located remote of the point of impact (represented by the bull's-eye). Shaded areas represent fractures and each mark represents 5 mm of fracture length.

Results: Porcine Head Model Computational Modeling (MSU)

An overlay of maximum principal tensile stress directions revealed a concentration at the impact site for all age-interface combinations (Figure 51). The length of the arrow at each location represents the relative magnitude of stress at that location. Comparison of these overlays revealed distinct lines of expected fracture between suture boundaries and the impact point, regardless of age or interface. However, the proximity of the stress field to the boundary varied by interface. Specifically, larger regions of high tensile stresses were located nearer the suture-bone boundary for compliant interface impacts than for rigid interface impacts. Furthermore, tensile stresses developed in the sutures of the young specimens were significantly greater for compliant interface impacts than for rigid interface impacts. The old specimens had similar levels of stress in the sutures for both interfaces.

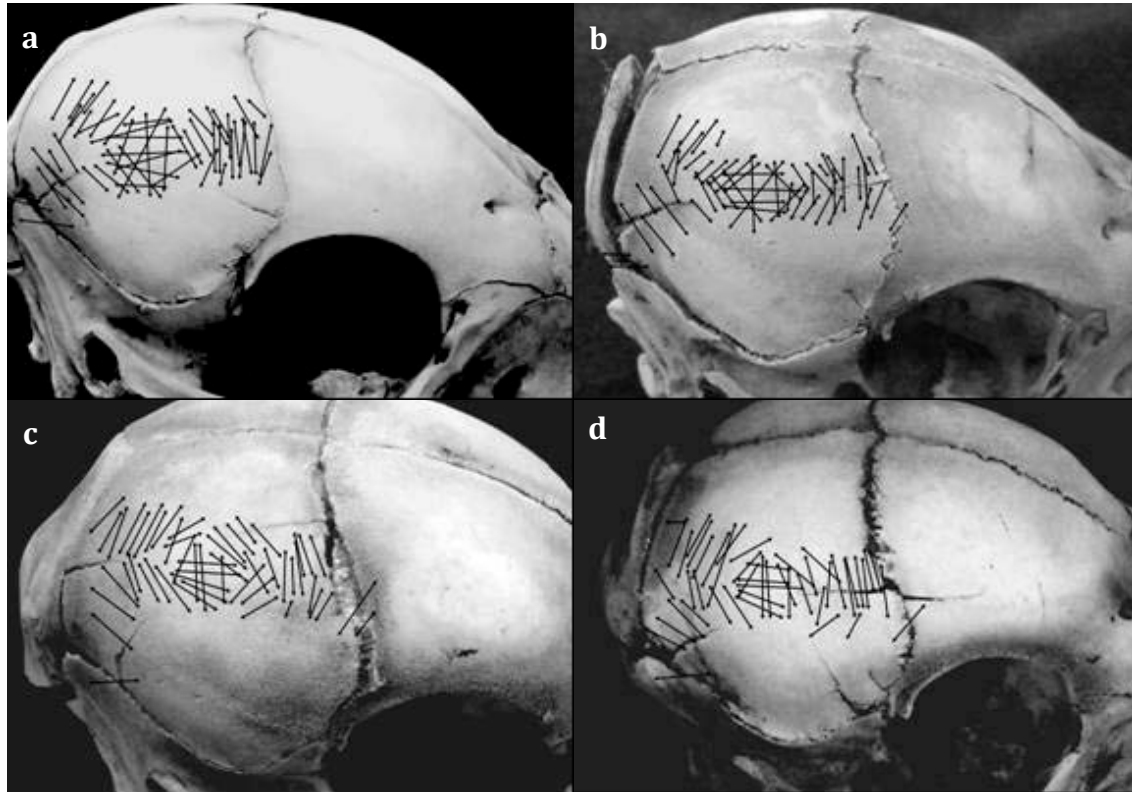


Figure 51. Overlay of maximum principal tensile stresses from FE models on representative experimental cranial fractures for (a) rigid interface impact to a young specimen, (b) rigid interface impact to an old specimen, (c) compliant interface impact to a young specimen, and (d) compliant interface impact to an old specimen. Longer lines represent higher stresses.

An overlay of the directions of maximum principal tensile strain revealed high strains at or near bone-suture boundaries, with lower levels of strain at the impact site for all age-interface combinations (Figure 52). The rigid interface impacts produced higher levels of strain closer to the impact site than the compliant interface impacts, however, the highest strains were still located away from the impact site. Furthermore, the magnitude of the tensile strains developed in the sutures of the young specimens from compliant interface impacts was considerably greater than those from rigid interface impacts. The old specimens had similar levels of strain in the sutures for both interfaces. Comparison of these overlays revealed some possible paths of expected fracture between bone-suture boundaries and the impact point.

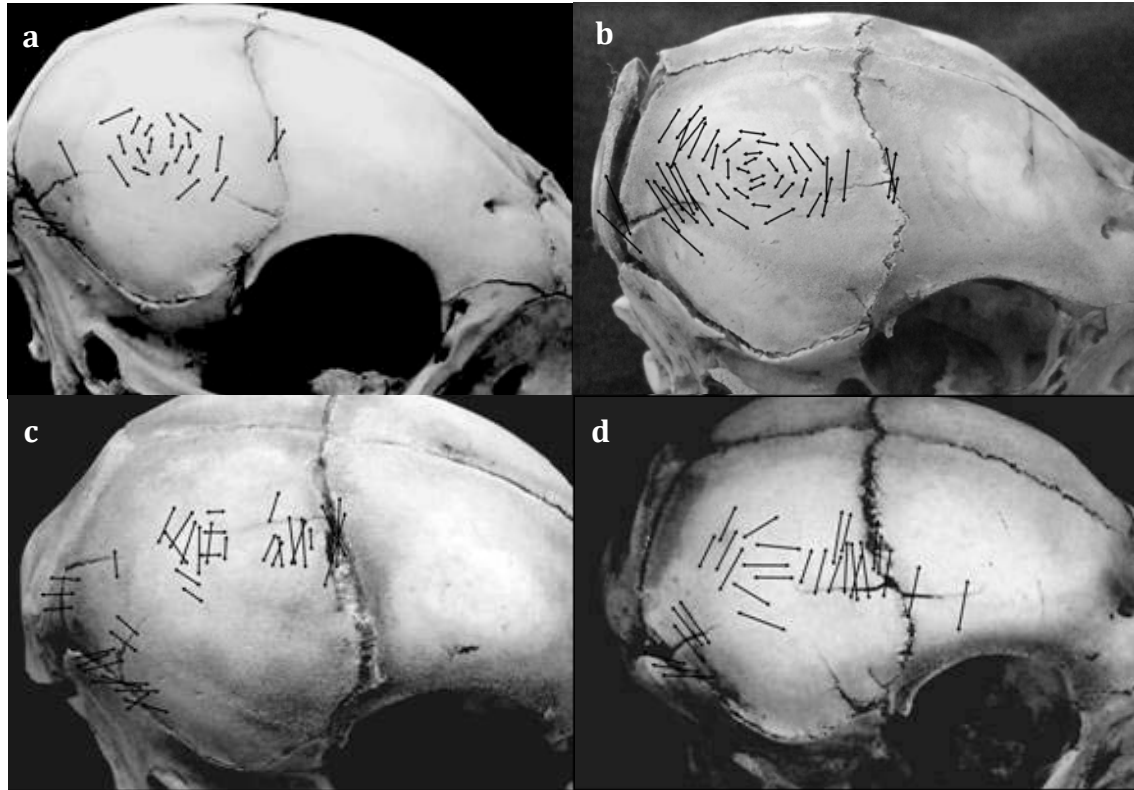


Figure 52. Overlay of maximum principal tensile strains from FE models on representative experimental cranial fractures for (a) rigid interface impact to a young specimen, (b) rigid interface impact to an old specimen, (c) compliant interface impact to a young specimen, and (d) compliant interface impact to an old specimen. Longer lines represent higher strains.

Results: Porcine Computational Modeling: Sensitivity of FE model parameters to proposed injury mechanism (Wayne State University)

After the determination that MAT124 would be utilized, geometrically simplified models were used to exercise the sensitivity of the fracture pattern to certain parameters. Two geometries are presented here: a curved square plate and a dome. The angles of curvature were similar to a single 21-day-old piglet parietal bone. These model geometries were assigned similar properties to the baseline piglet skull model, and the same mesh size (0.5 x 0.5 mm, with thickness = 2 mm) was used unless otherwise noted. An inertial impactor load of proportional impact energy to the piglet drop tests was applied and allowed to rebound.

The first sensitivity issue is smoothness, as it relates to anatomic accuracy in the geometrically complex piglet skull. The two models in Figure 53 show that, for the same mesh density, differing fracture patterns (shown in dark blue) occur based on very small changes in geometry. The smooth model on the right has nodal coordinate changes of less than 0.5 mm compared to the model on the left. It is also interesting to note that, although the geometry, mesh, and loading are all symmetric, the fracture lines are not.

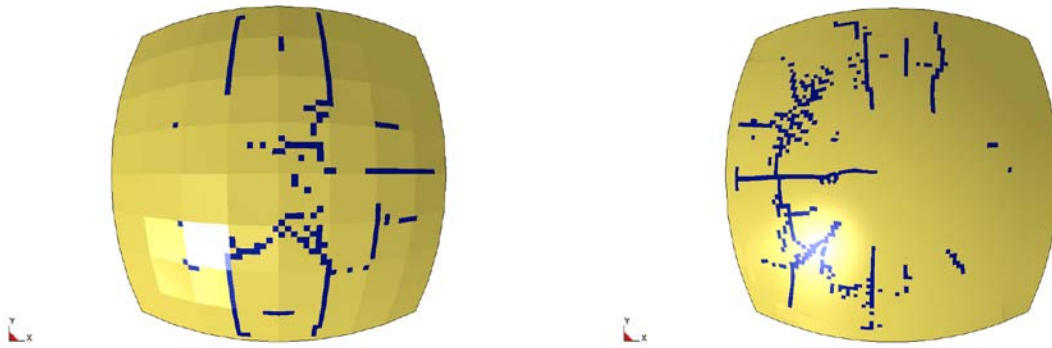


Figure 53. Sensitivity of failure pattern to geometry- smoothed model on right

To remove any effects related to the corners of the curved plate, a dome was also considered. In Figure 54 on the left is the fracture initiation point, and on the right is the fracture pattern at rebound. A layer of elements representing the suture (shown in green) has been incorporated. At this impact energy, the fracture line propagates to the center of the dome, but mostly, periphery fracture is seen.

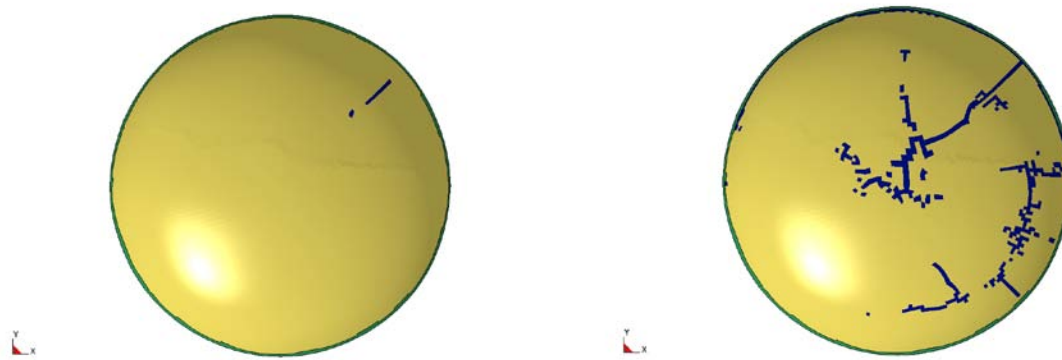


Figure 54. Sensitivity of fracture pattern and initiation location to shape change- initiation point shown on left, fracture pattern after rebound shown on right

The role of the immature suture in skull deformation biomechanics has not been well-quantified in published literature studies. The fracture patterns in Figure 55 show that the softer suture properties (on the left) lead to a more symmetric fracture pattern, while the four times stiffer suture (on the right) yields a much different fracture pattern. In both cases, fracture initiation occurs closer to the periphery and propagates either towards the center or radially.

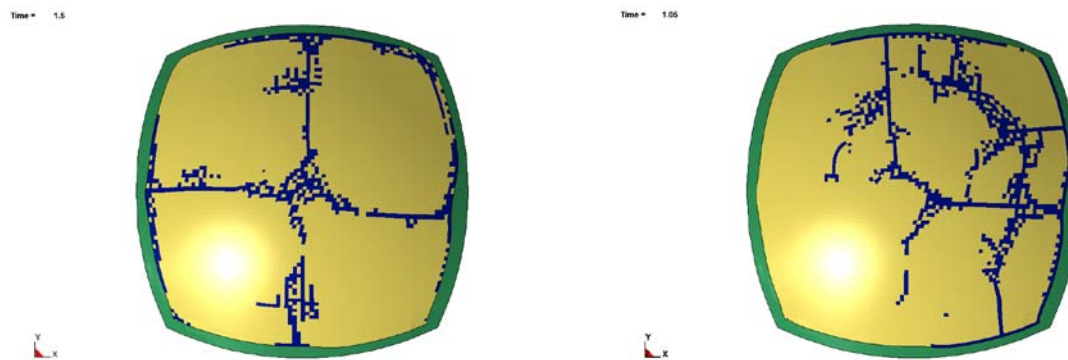


Figure 55. Suture strength- softer suture on left, 400% stronger on right

The shape of the suture boundary also has a noticeable effect as illustrated by Figure 56. The top and bottom rows show models with two slightly different sutural geometries, though the average suture width remains relatively constant. The leftmost models are fully constrained at the edges,

while the rightmost models are simply supported, allowing in-plane translation. It can be seen that the fracture pattern changes with suture geometry change, but this effect is much more significant for the fully constrained case. Neither of these boundary conditions is completely representative of the parietal bone borders, but the importance of modeling boundary conditions appropriately is certainly indicated. For the parietal bone, it is assumed that the behavior of the sutures dictating motion at the boundary of bone plate is more significant to accurate fracture pattern predictions than the precise suture shape.

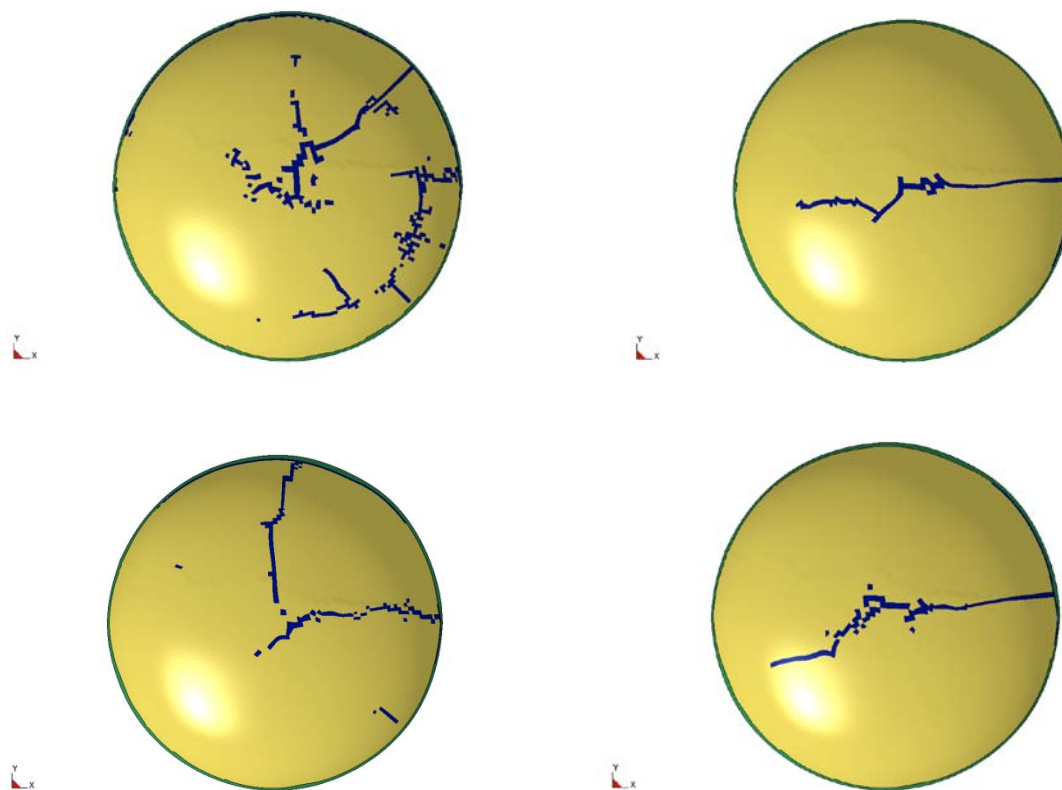


Figure 56. Suture geometry changes alter fracture patterns more in fully constrained case (left) than in simply supported case (right)

Compared with the models from Figure 56, Figure 57 has the same two boundary conditions, but the mesh density was increased by a factor of four. Mesh size is well-known to affect both

model convergence and element elimination, but while the smallest elements yield the best results (so long as the shell thickness to length ratio is appropriate), computational time increases dramatically. Comparing the two figures, it is noteworthy that the fracture location can change dramatically with element refinement. This will be discussed further in the Conclusions section.

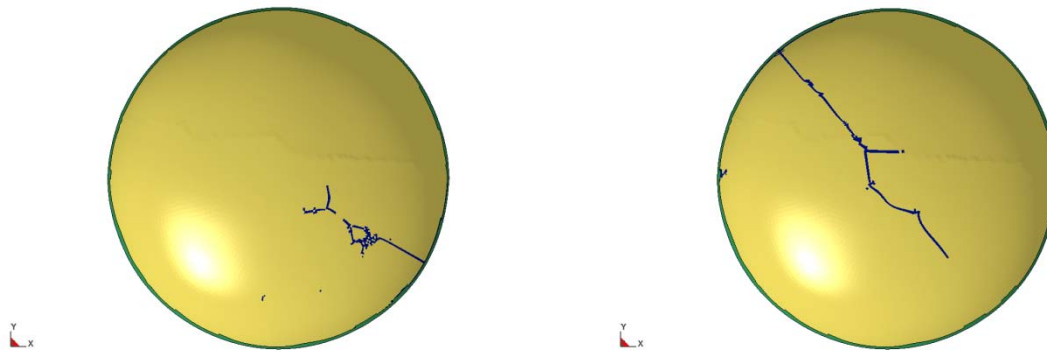


Figure 57 Dome at higher mesh density- fully constrained left, simply support right

Lastly, sensitivity to impactor position and orientation is expected. Graphically, this can be seen in Figure 58. Although centering the impactor between the bone margins is fairly straightforward, the angle at which the flat impactor plate strikes the bone is more difficult to determine. The normal to a curved surface changes instantaneously. In the hemi-spherical domed surface, the fracture pattern occurs off-center from the impactor edge, which may be related to suture geometry or mesh quality. This finding indicates that slight adjustments to impactor orientation allow for tuning of fracture location in the FE model, in the absence of precise impactor position recording.

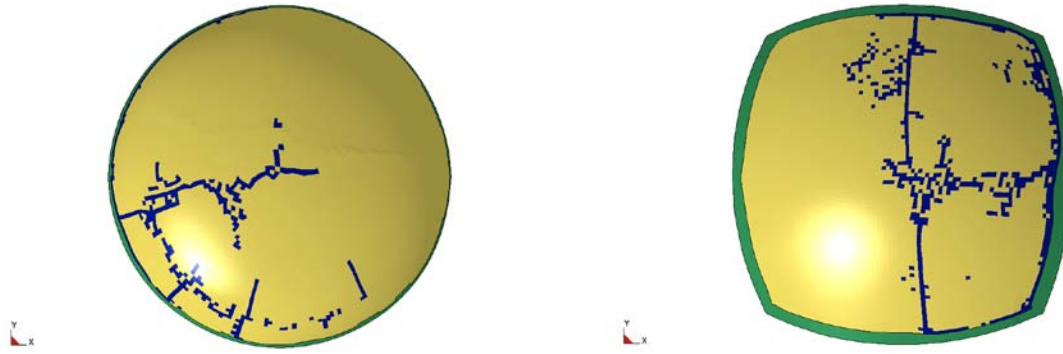


Figure 58. *Impactor orientation rotated five degrees from center- failure occurs in areas impactor is tilted towards*

The results from these sensitivity studies were used in development of the piglet skull models, as related to anatomical accuracy, mesh generation, manual definition of suture boundaries, and positioning of the impactor above the mid-parietal area.

Results: Piglet skull fracture pattern

The results in this section pertain to a 60 cm drop height and a 1.919 kg rigid impactor, unless otherwise stated. Because of the sensitivity of the model and the wide range of data values in the experimental results despite remarkably similar fracture patterns, modeling efforts focused on a single impact event in order to more fully understand the biomechanics of this skull fracture type. These findings will guide future work to be discussed in the Conclusion section.

A purely elastic model (which could not support element deletion due to LS-DYNA v971 limitations) indicated the highest strains occurred at the impact center, as well, and developed before high strains remote from the impact location. However, the elastic modulus was the only age-dependent data point available for direct implementation into the FE model generated in this study. Literature sources mentioned previously had investigated the plasticity of both long bones

and skull bones, so a relationship could be drawn between the modulus reported by MSU and other necessary material properties.

The pilot 21-day-old piglet head FE model, employing isotropic elastic-plastic MAT24, yielded poor results, as seen in Figure 59. Fracture initiation beneath the impactor, as well as along the margins of the parietal, frontal, and occipital bones. However, the direction of fracture propagation at the periphery was along the suture boundaries, as opposed to perpendicularly. While sensitive to yield stress, the tangent modulus had only small effect.

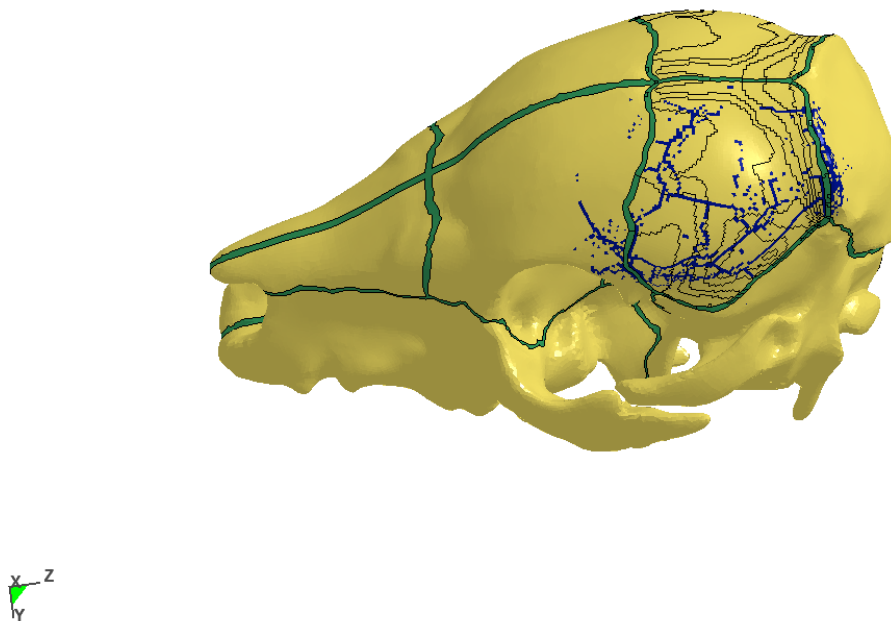


Figure 59. Pilot 21-day-old model, utilizing elastic-plastic MAT24

Several solutions for the fracture predictions under the impactor were considered, including growth-related material changes radially from the ossification center, the possible effects of the incompressible intracranial contents on bending stresses, and other techniques for suture

representation. However, given the large parietal deformations and the overall compliance of the skull, it was determined that bending effects were clearly a factor. In bending, the structure experiences both tension and compression throughout the loading event in different areas. Given published data showing long bones are more susceptible to tensile failure than compressive failure, an FE model that could reflect that phenomenon from the parietal bone would be expected to predict fracture remote from the contact area. The direction of fracture propagation is thought to be more related to global shape or local curvatures, though this needs to be investigated further.

If it is assumed that only yield stress and strain are affected by tensile weakness, then the tangent modulus remains the same (Figure 60). In this way, compressed elements would need to experience higher stress before element elimination can occur. However, the peak compressive stress before failure is still too low to prevent failure under the impactor, as shown in Figure 61. However, the fracture lines propagate cleanly in a direction perpendicular to the sutures, indicating that this method may still be appropriate.

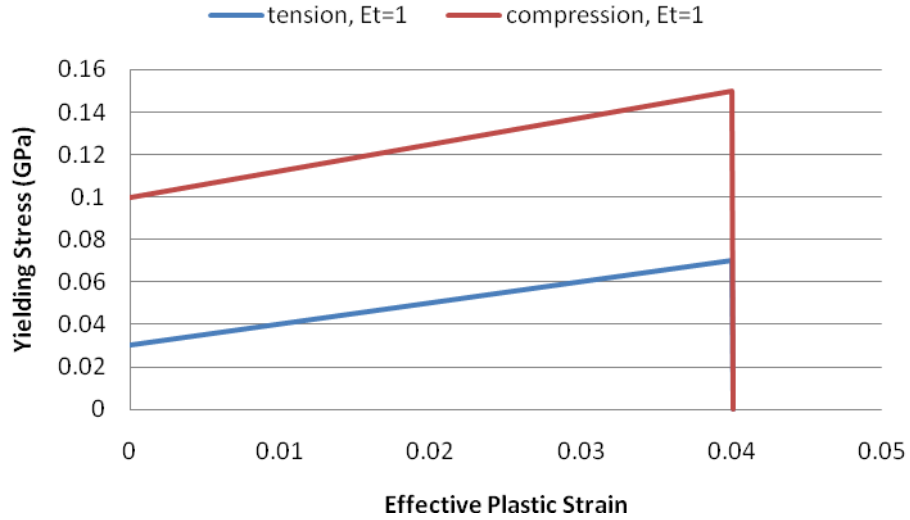


Figure 60. Plasticity curves with equal tangent modulus

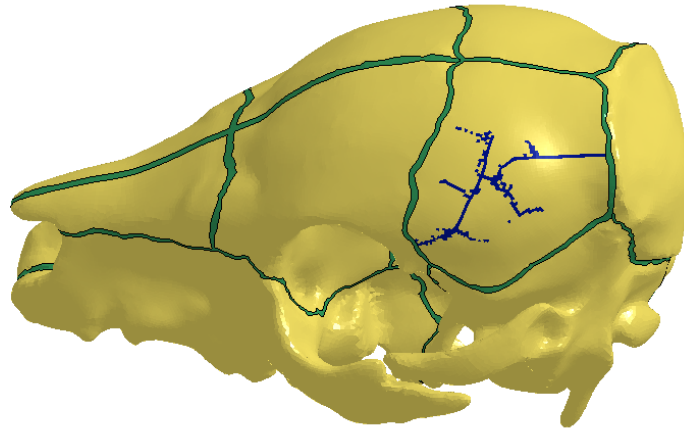


Figure 61. Fracture pattern for parallel MAT124 plasticity curves at 4% failure strain

To disallow the elements under the impactor to fail, the tangent modulus is increased by a factor of ten, as shown in Figure 62. The fracture pattern in this case is limited to the periphery, but it

is more diffuse and somewhat indicative of suture separation. (See Figure 63) This is somewhat consistent with suture involvement seen in the experimental tests. The diffuse pattern may be numerical artifact. Further investigation is warranted.

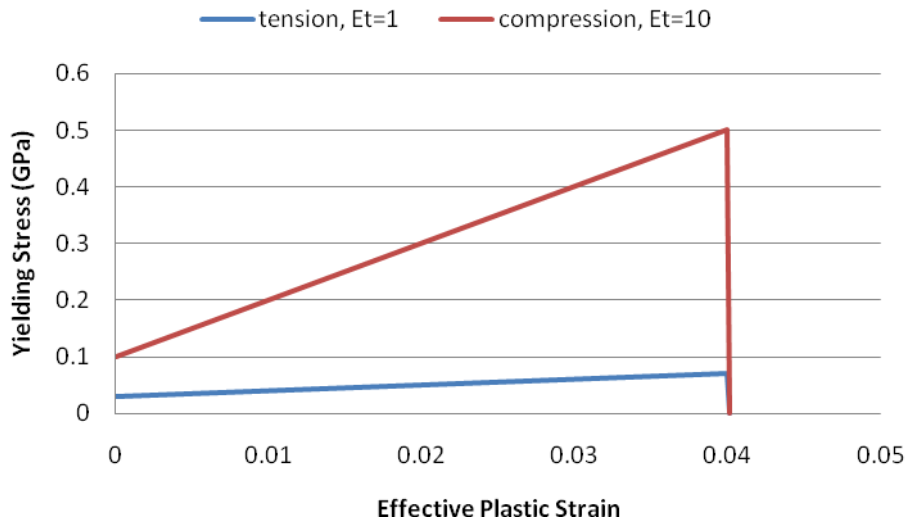


Figure 62. Plasticity curves where compression has ten times the tangent modulus

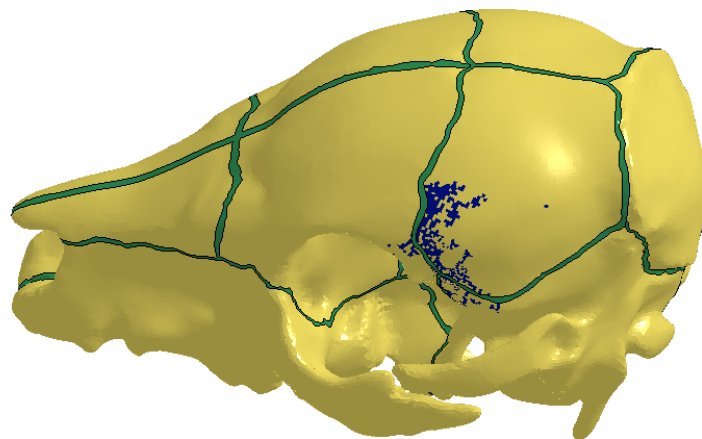


Figure 63. *Fracture pattern for high compressive tangent modulus (4% failure strain)*

Figures 64 and 65 show two different strain contours for this model. First is effective plastic strain, the failure criterion. Although the elements deleted are somewhat diffuse, clear strain contours are evident. The maximum principal strain contours are similar, except that high strain also develops in the sutures. These elements are not assigned a failure constitutive model, which facilitates the bending of the parietal bone plate within the model.

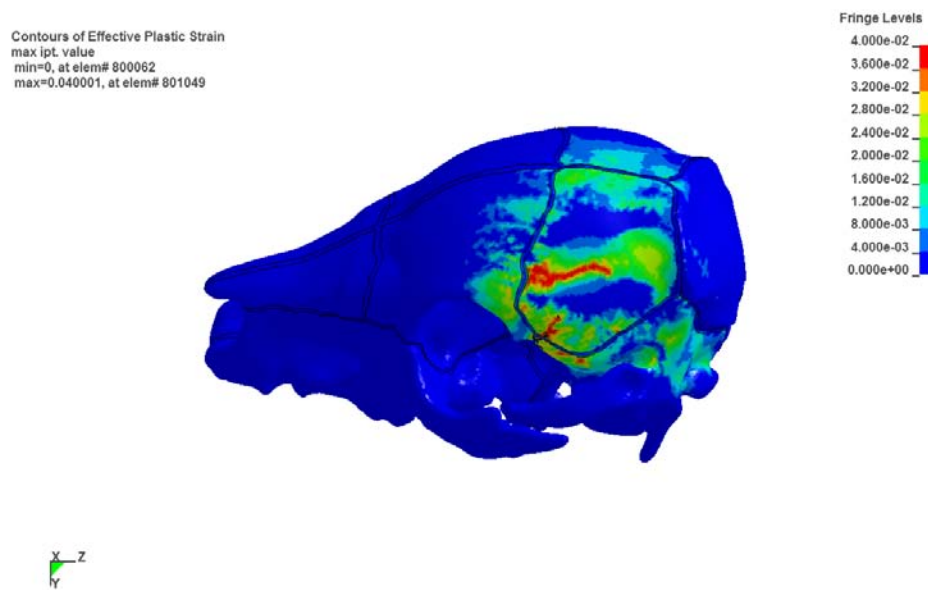


Figure 64. Effective plastic strain development in the 21-day-old piglet model

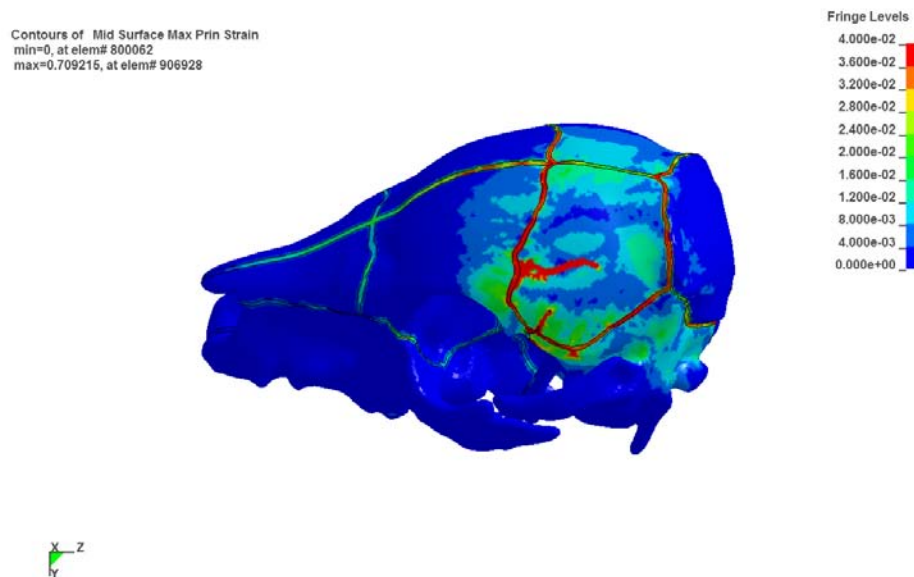


Figure 65. Maximum principal strain for comparison with effective plastic strain

Selection of an appropriate effective plastic failure strain criterion is best done parametrically. Figure 66 illustrates how the fracture lines change for different threshold values, although the locations remain consistent. These predictions are reasonably consistent with the findings of the

experimental study, but further validation and statistical analysis needs to be performed before translation to a human model, especially since the material properties are not well-defined.

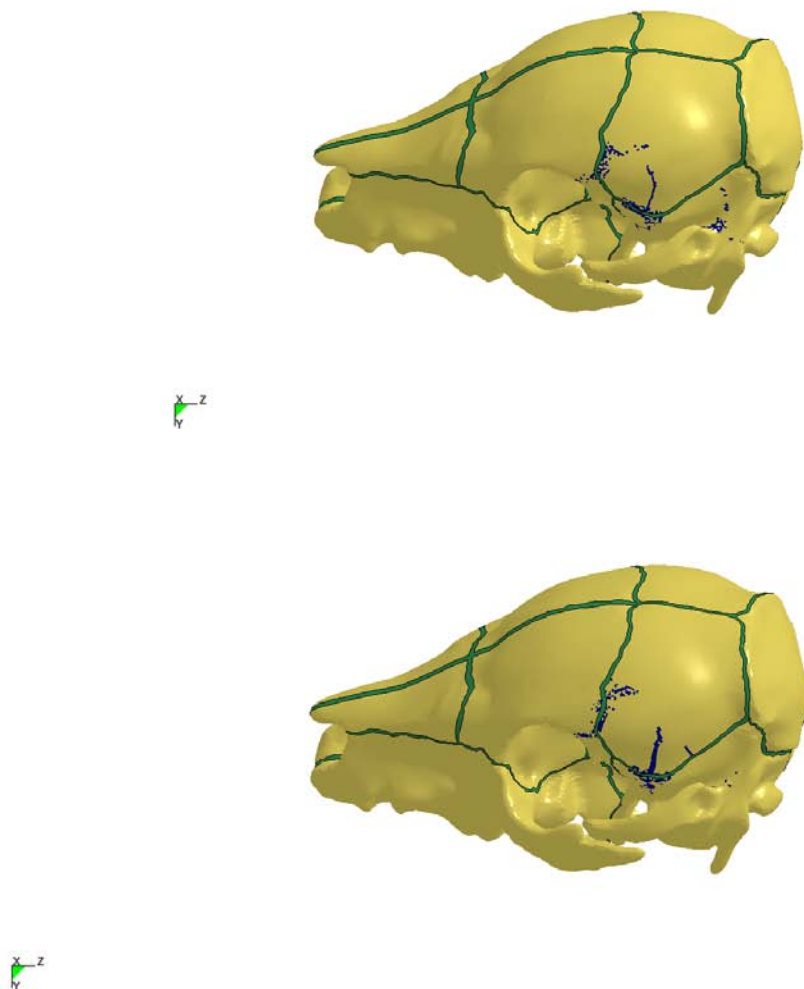


Figure 66. Fracture pattern for same high compressive tangent modulus but with lower strain thresholds (3% failure strain above, 2% below)

Validation of this model is not possible at this time. The peak deflection, contact area, and impact duration all fall within the lower range of the data reported for subject above 14 days of

age. However, the contact force predicted by LS-DYNA is approximately six times higher than the average value recorded. This is clearly a numerical artifact. In Figure 67, a 21-day-old piglet head model is shown, but the sutures have been strengthened to reduce compliance. Although all other outputs are affected, such as peak displacement, the calculated contact force remains the same. This is a known issue to LSTC that has yet to be resolved.

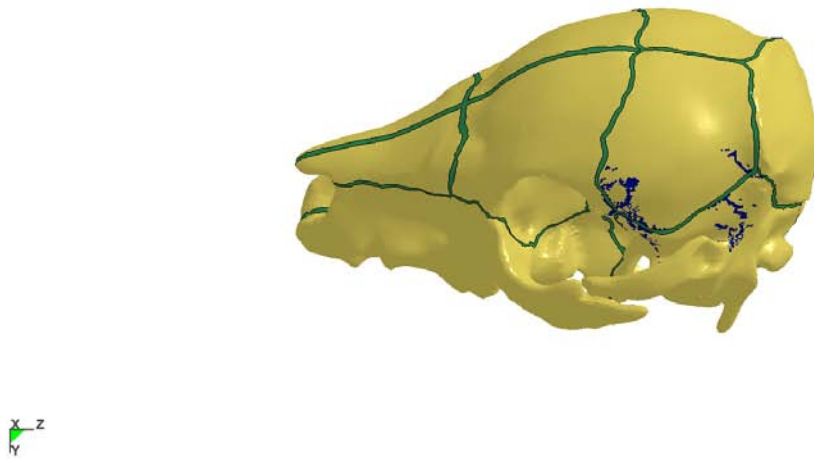


Figure 67. *Strengthening the sutures yields slightly different fracture pattern for 2% failure strain*

As presented in the sensitivity study, small changes to the model development or input can have large effects on the predicted fracture pattern. An input condition parametric study is currently underway with both the 21-day and 7-day piglet head FE models to better quantify the sensitivity to impactor orientation around the parietal bone midpoint. It is anticipated that several common fracture patterns will emerge, similar to what was seen in the experimental study.

Results: Human Pediatric Crush Scenario Computational Modeling (MSU)

CASE REPORTS

Case 1

A 5-year-old female child was struck by her family's sedan when she fell in an attempt to stop the vehicle after her brother accidentally engaged the transmission. Her head was run over by the right front tire of the car. The autopsy revealed an intact cranial vault with a cranial base fracture that traversed the lateral right anterior cranial fossa, the midline of the middle cranial fossa, and the left lateral aspect of the posterior cranial fossa. This fracture bridged the blunt impact sites on the right anterior and left posterior aspects of the head.

Case 2

An unhelmeted 6 year-old male was struck by a car while riding his bike. His head was run over by the vehicle's left rear tire. Autopsy revealed an intact cranial vault. The cranial base, however, was bisected by a gaping X-shaped fracture centered in the midline of the middle cranial fossa. There were two adjacent arms of the fracture in the right middle cranial fossa. The other two adjacent arms were in the posterior aspect of the left middle cranial fossa and the anterior aspect of the left posterior cranial fossa. This fracture bridged the blunt impact sites on the right anterior and lateral aspects of the head and the left lateral and posterolateral aspects of the head.

Case 3

A 3-year-old male was run over attempting to run away from a farm grain wagon that had begun to roll. His head was run over by one of the wheels of the wagon. Autopsy revealed gaping linear fractures that traversed the parietal bones and the right and left sides of the frontal bone. One end of each fracture intersected the widely gaping right side of the coronal suture,

other ends were continuous with fractures of the cranial base. A dominant cranial base fracture traversed the left petrous bone, the midline of the middle cranial fossa, the anterior aspect of the right middle cranial fossa and the posterolateral aspect of the right anterior cranial fossa. Additional intersecting fractures were centered in the left middle and posterior cranial fossae.

Case 4

A 1.5-year-old female was entrapped under a small moving van and her head was run over by the right rear wheel. Autopsy revealed an intact cranial vault but extensive intersecting fractures of the cranial base that predominately traversed the middle and posterior cranial fossae from side to side. A large fracture also bisected the anterior cranial fossae.

Fracture Pattern Similarities

Each of the cases presented fracture patterns that bridge the impact sites and traversed the middle cranial fossa in the area of the spheno-occipital synchondrosis. Additionally, the damage was concentrated in the basicranium leaving the cranial vault intact in all cases except the 3-year-old boy impacted by the farm grain wagon. Furthermore, general amounts of fracture increased with inferred increase in magnitude of applied force (grain-wagon vs. car) or decrease in age.

The four cases presented three contact scenarios with four different fracture patterns. Specifically, the contact forces in Case 1 were applied primarily to the frontal and occipital bones in a direction between anterior-posterior and lateral (Figure 68a), the contact forces in Cases 2 and 3 were also applied to the frontal and occipital bones but had an additional lateral component (Figure 68b, c), and the contact forces in Case 4 were applied to the lateral surfaces of the cranial model (Figure 68d).

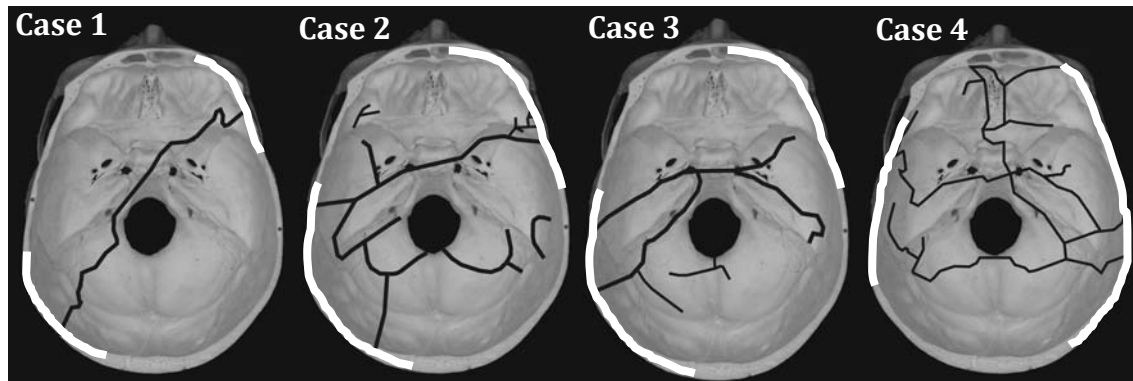


Figure 68. Diagrams of fractures due to quasi-static crushing forces to skulls aged (a) 5 years – Case 1, (b) 6 years – Case 2, (c) 3 years – Case 3, and (d) 1.5 years – Case 4. White cranial margins represent contact of applied forces (ground and tire).

FE Analysis

Modeling of all four cases revealed that locations of high tensile stress and high tensile strain were located on the basicranium. There were some areas of lower tensile stress at the sites of the applied load and in a few areas on the cranial vault, but due to the assumption that failure would occur at locations of high stress, these areas were ignored for this analysis. The maximum tensile stresses for all models were similar (standard deviation of $\pm 5\%$). The tensile stresses developed on the skull were filtered to display only the highest 20% for correlation to fracture patterns. The length of the arrow at each location represented the relative magnitude of stress at that location.

Case 1 presented the simplest fracture pattern as a single linear fracture traversing the basicranium from the right greater wing of the sphenoid across the spheno-occipital synchondrosis to the left lateral portion of the occipital, connecting the loading sites (Figure 69a). An overlay of the directions of maximum principal tensile stresses revealed a linear concentration on the right side of sphenoid and in the area of the spheno-occipital synchondrosis, which correlated well with sections of the observed fracture (Figure 69b).

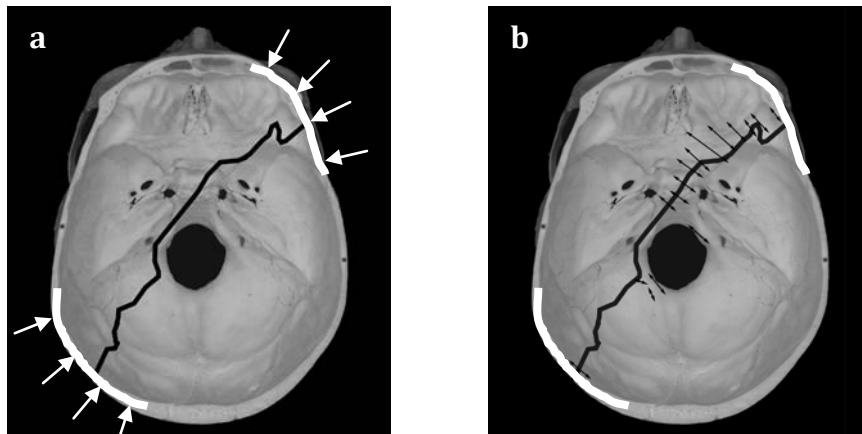


Figure 69. (Case 1) Crushing injury to the skull of a 5-year-old. Diagrams of (a) clinically observed fractures and (b) an overlay of the highest 20% of principal tensile stresses produced from a FE model. White cranial margins represent contact of applied forces (ground and tire).

Cases 2 and 3 presented slightly more complex fracture patterns. In part, the complexity was increased due to the similarities in loading but dissimilarities in fracture (Figure 70a and Figure 71a, respectively). A similar fracture in both cases stretched from the right aspect of the sphenoid through the sella turcica and along the superior aspect of the petrous portion of the temporal. The overlay of the directions of maximum principal tensile stresses was identical in both cases due to the similarity of loading patterns. There was correlation between the stress and the fracture for both cases, especially along the line of similar fracture, although each had areas of high stress where fracture did not occur (Figure 70b and Figure 71b).

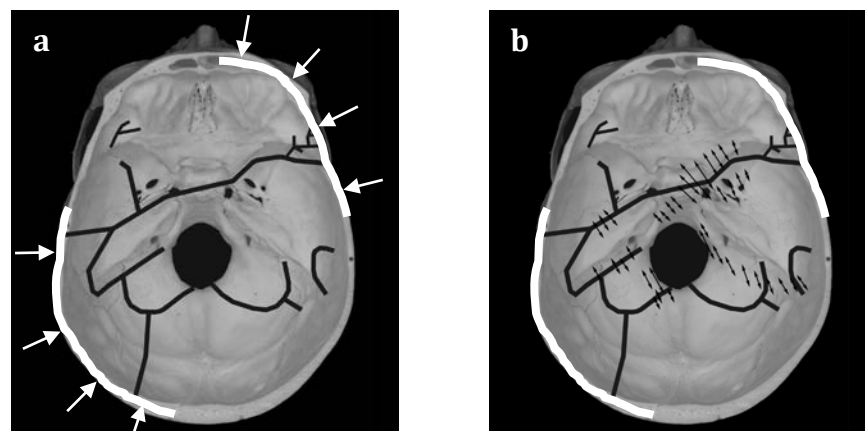


Figure 70. (Case 2) Crushing injury to the skull of a 6-year-old. Diagrams of (a) clinically observed fractures and (b) an overlay of the highest 20% of principal tensile stresses produced from a FE model. White cranial margins represent contact of applied forces (ground and tire).

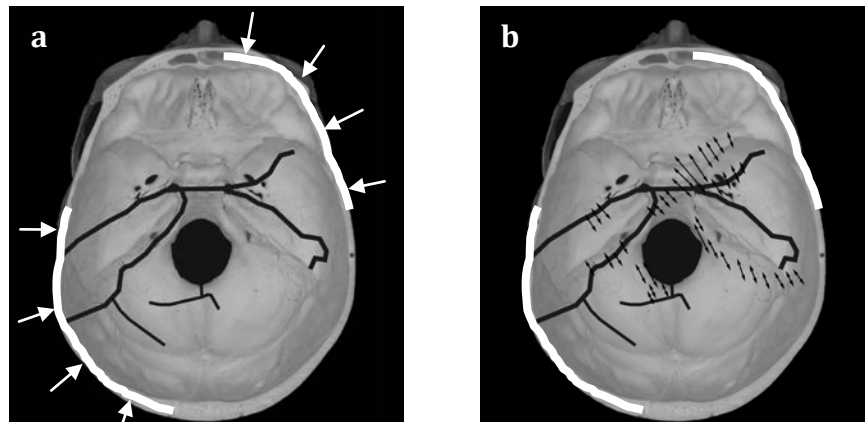


Figure 71. (Case 3) Crushing injury to the skull of a 3-year-old. Diagrams of (a) clinically observed fractures and (b) an overlay of the highest 20% of principal tensile stresses produced from a FE model. White cranial margins represent contact of applied forces (ground and tire).

Case 4 presented the most complex fracture pattern extending both longitudinally and transversely through the basicranium (Figure 72a). Fractures ran longitudinally across the midline of the anterior cranial fossa, and horizontally through the middle and posterior cranial fossa with various areas of comminution. The overlay of the directions of maximum principal tensile stresses revealed an area of complex stress in the same area as the highly comminuted fracture of the right side of the cranial base. Additionally, a more linear pattern of stresses occurred near the fractures on the left side of the skull (Figure 72b).

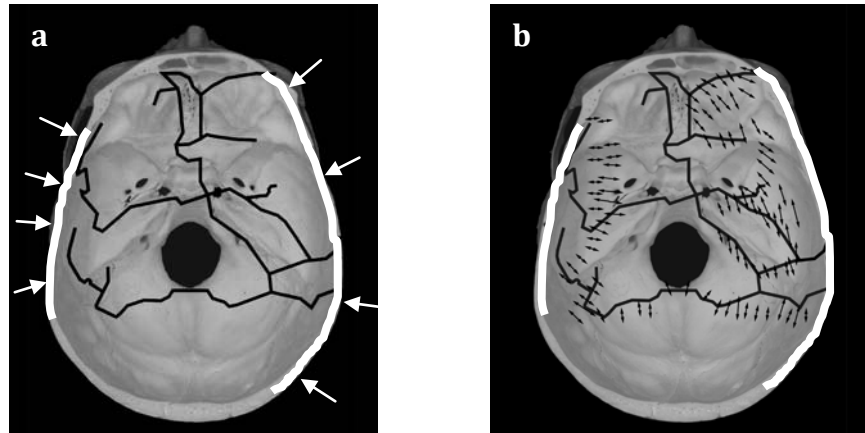


Figure 72. (Case 4) Crushing injury to the skull of a 1.5 year old. Diagrams of (a) clinically observed fractures and (b) an overlay of the highest 20% of principal tensile stresses produced from a FE model. White cranial margins represent contact of applied forces (ground and tire).

CONCLUSIONS

Discussion of Findings: Michigan State University team

A number of conclusions can be drawn from the results that have been generated in the current research proposal. A goal of the study was to document the patterns of fracture from blunt impacts to the skull, and changes that might occur with skeletal development, using the porcine model. The study generally showed that for the very young porcine head (less than 18 months human and 18 days of pig age) impact to a constrained skull by a deformable (compliant) object that distributes impact loads will cause relatively more fracturing than an impact at the same energy with a rigid object. In contrast, impacts with rigid objects cause relatively more fracture than with deformable objects in the more mature porcine head. The studies conducted with beam specimens of bone and bone-suture from the developing porcine skull had a two-fold objective. Firstly, to help explain the potential mechanism of diffuse fracturing in the very young porcine skull versus the more localized fracture pattern for the older porcine skull. The studies on individualized sections of bone, as well as bone-suture, showed that while sutures

were quite compliant in the very young porcine specimen, in older specimens the suture rigidity and strength approached that of skull bone itself. This result helps to explain the nature of diastatic (suture) fracturing in the very young porcine specimen, versus more bone fracture in the more matured porcine specimen. Secondly, the results of the study showed a parallel pattern of bone stiffness (rigidity) change with age between the porcine skull and human data from a recent reference in the literature. This result helps to validate the developing porcine model as a surrogate of the human pediatric skull.

An interesting result from the current study was that porcine cranial fractures typically initiate near suture boundaries and propagate towards the site of impact trauma. This means that cranial fractures can, and do, occur away from the site of impact on the skull, and especially in cases of the young porcine specimen. In the studies presented here relating to impact energy effects, we have been able to show under controlled experimental conditions that with increasing energy of impact, fractures begin to cross sutures and propagation into adjacent bones of the skull. Thus, a single impact can cause multiple cranial fractures in the impacted and adjacent bones of the skull. This result can have critical implications in abuse cases where multiple sites of cranial fracture are often associated with multiple sites of blunt force trauma to the porcine victim.

Another important aspect of the current study was the development of a computational tool that could be used to help determine the forces needed to generate various patterns of cranial fracture in the porcine model and then in the human pediatric victim. A study was conducted to model the porcine cranium and use the computational model to predict fracture patterns based on the assumption that these defects would be created along the lines of the largest developed stresses and strains in the skull during impact. While the first study utilized a rather simplified

anatomical model of the impacted parietal bone, the results showed strain patterns in the cranium that generally paralleled with the fracture lines generated by impacts using rigid and deformable interfaces. The results showed large strains in and adjacent to sutures, and smaller ones in the impact area, especially for the younger porcine model. As the cranial model was set up to simulate the more mature cranial vault, the largest strains appeared closer to the impact site. The importance of these data is to show that a simplified computational model can be developed to show the general fracture patterns observed in experimental studies with the porcine model, yet some aspects deviated from the observed experimental results.

In order to accurately predict the mechanisms of cranial fracture and their corresponding patterns, a more detailed modeling effort was performed under subcontract with Wayne State University. Their studies provided a detailed look at the various factors of the cranial vault that determine the onset and propagation of bone fractures. The complexity of the porcine cranial vault was examined with micro-CT and modeled, and various theoretical considerations were parametrically studied in the effort to simulate the porcine fracture patterns. The study largely showed that to more accurately predict fracture characteristics of the pediatric, porcine skull, the computational model has to be made quite complex. This resulted in another problem in that due to its complexity and the lack of some critical information on individualized cranial properties, such as the mechanism of the fracture propagation in a mathematical sense and detailed thickness patterns of the cranial vault, the suitability of this approach for a variety of impact conditions and victim characteristics was brought to question by the research team. In order to validate the general concept of the proposed approach, and to initially avoid some of the complexities, a simple anatomical model was constructed, using the originally proposed ideas, to model 4 cases of crash injuries to the human pediatric skull. The results of the study showed that the general

pattern of high strains in the basicranium paralleled well with the pattern of cranial fracture in the human, pediatric victim. The importance of this study is to show that detailed computational modeling is capable of predicting the general pattern of cranial fracturing from blunt impact.

Discussion of Findings: Application of FE model to forensic tool (Wayne State University Team)

The results of this study illustrate that FE models can assist researchers in determining injury mechanism due to local effects. FE models allow scientists to look at many aspects of biomechanical response that are not always practical to measure or even considered prior to experimental testing.

From this model, it appears that skull bones behave differently in tension and compression, which is a reasonable conclusion to draw as other similar biological materials display the same characteristics. This highlights the need for more comprehensive material testing related to this work in the future.

The sensitivity of the model to even very small changes in curvature and other geometry shows that more biomechanical FE models need to be developed from high-resolution medical imaging and meshed finely in order to facilitate adequate numerical approximation. Although, as any probabilistic FE model, only one solution exists for a set of inputs, comparison with experimentally-produced fracture patterns suggest that local geometry anomalies may play a large role in fracture initiation and propagation. This knowledge can help guide future research, especially in the field of subject-specific modeling and stochastics.

In order to apply this technique to a practicable forensic tool, several further steps must be undertaken. Firstly, a complete material property dataset across the continuum of pediatric ages required by the forensics community would be needed. Secondly, automated meshing

methods that provide a fairly uniform, smooth mesh without sacrificing anatomic accuracy would be needed. For this project, manual techniques were used to ensure that the mesh quality did not affect the overall study, but this is not time-efficient for multiple geometries. Thirdly, an algorithm to link the mesh density with age-specific strain tolerances would allow convergent and accurate model predictions. Lastly, a quantified method for determining statistical likelihoods for clouds of model-generated outcomes would be useful for the practitioner and minimize subjective error or bias.

For this study, it was originally proposed to apply the techniques developed using the piglet surrogate to real-world cases of child injury. Given that much of the FE model development involved material property estimation and other simplifications, the addition of further variables would not yield good results. Further work on the piglet FE model should be carried out before translation into human subjects.

Implications for Policy and Practice

This research sought to establish a computational-based tool that could be used to determine the input required to generate a specific pattern of fracture on the human pediatric victim. While this goal was not attained in the current studies, a number of important findings on the characteristics of fracture patterns in controlled impacts to the infant porcine cranium will help towards this end. The work, importantly, showed that the response of an infant head to impact is quite variable during its developmental stages. The fracture patterns can be altered by impact interface, impact energy and the degree of head constraint. Most importantly, fractures can often occur away from the site of impact and a single impact can generate multiple fractures. These are important concepts that can help determine many cases of infant abuse and separate

them from accidental injury, such as falls from short heights. The work lays the groundwork for helping to understand and substantiate data in current forensic files and may ultimately play an important role in future litigation.

While the studies on a computational-based modeling effort showed that some of the general characteristics of cranial fracturing can be predicted with rather simplified models, the advanced studies that sought to better understand the physics of cranial fracture showed that these mathematical-predicted fractures are quite dependent on local geometry and material properties of the cranial vault, making them very subject specific. Currently, there are insufficient methods available that could precisely determine these properties for each case to make the modeling efficient enough for current forensic practice.

Implications for Further Research: Michigan State University Team

Based on the results of the current study and the limitations realized during the course of this research, the Michigan State University research team has developed the following plan for future research. In the medicolegal death investigation, current techniques for interpreting pediatric cranial trauma are of questionable reliability due to a lack of baseline data that matches pediatric skull fracture patterns with known impact scenarios. We have therefore proposed future research that will address this significant gap in best practice through a multidisciplinary effort that: (1) collects the defining data on pediatric deaths involving cranial fracture and known impact scenarios from forensic case files at medical examiner offices across the country; (2) continues the development and validation of an experimental animal model to help correlate input forces and fracture patterns based on the physics of the problem; and (3) develops a pattern recognition method for “fracture-printing” to be used in the identification of injury causation.

The proposed research would utilize automated pattern recognition methods to classify pediatric skull fracture patterns by contact interface and impact energy based on the subject's age. This predictive analysis would use classification models that are generated using data (e.g. digital images of skull fracture and diagrams) that are accompanied with the ground truth data (i.e. contact interface and impact energy). For a given cranial fracture pattern on a pediatric victim of a specific age, we would be able to compute a statistical probability that 'there was a particular impact condition of causation'. Future studies would then develop a computer-based program that would take fracture pattern inputs and automatically generate a fracture feature set that could be compared to a known database to help predict the most likely causation of a particular fracture print. This research would bring together a team of investigators from established laboratories in forensic anthropology, orthopaedic biomechanics (www.obl.msu.edu), and pattern recognition and image processing (<http://biometrics,cse.msu.edu>) at Michigan State University to work on this significant gap in best practice. This research plan would then build on studies that have been performed in the currently funded NIJ research project titled "A Forensic Pathology Tool to Predict Pediatric Skull Fracture Patterns" (Award No. 2007-DN-BX-K196).

Implications for further research: Wayne State University Team

In this study, the injury mechanism was hypothesized to be related to differences in strain tolerance between tension and compression. One limitation of this study is that only one strain threshold was used. The FE solver used for this model, LS-DYNA, has hundreds of constitutive material models that have been developed and tested, but none have the option to choose dissimilar tension and compression failure criteria. Because of this, an artificial means of preventing the compressed elements under the impactor from going into a plastic failure mode

was employed by increasing the tangent modulus of the compressive plasticity curve. This may have had an adverse effect on global skull deformation, although the experimental data was insufficient to confirm this. Although the option exists to create user-defined subroutines to control the failure algorithm, these may incite model instabilities as they have not necessarily been thoroughly exercised and validated during development. For this study, a user-defined subroutine may have been able to provide a more appropriate dual failure threshold or improve upon crack propagation by including strain energy density considerations (not incorporated into any current LS-DYNA failure material) but a much more comprehensive material behavior study would have been necessary. This should be considered for further model development.

Due to the high degree of geometric effect, the data available for model validation had a very large spread. A large age range of piglets was tested in order to see what age-related changes in biomechanical response could be observed. For validation purposes, it may have been more beneficial to focus on one or two precise ages or develop a subject-specific model of a particular piglet whose pre-impact CT would be used to create model geometry. While the impact event itself was well-controlled, anatomic variability is a limitation of any biological study.

A final limitation was the exclusion of the intracranial contents. While it was considered, the model response without this component was acceptable and saved computational time. With the goal of developing a technique that could be put into practice as a numerical tool, the more simplified the formulation, the better. In future work, if the head is dropped onto a surface as opposed to an impactor being dropped onto a head, then the brain will have to be incorporated to account for inertial effects.

REFERENCES

- Atkinson PJ, Newberry WN, Atkinson TS, Haut RC, 1998, "A method to increase the sensitive range of pressure sensitive film," Journal of Biomechanics, **31**(9), pp. 855-859.
- Baumer TG, Passalacqua NV, Powell BJ, Newberry WN, Fenton TW, Haut RC, In Press, "Age-Dependent Fracture Characteristics of Rigid and Compliant Surface Impacts on the Infant Skull – A Porcine Model," Journal of Forensic Science.
- Baumer TG, Powell BJ, Fenton TW, Haut RC, 2009, "Age Dependent Mechanical Properties of the Infant Porcine Parietal Bone and a Correlation to the Human," Journal of Biomechanical Engineering, **131**(11), pp. 1-6.
- Belechri M, Petridou E, Trichopoulos D, 2002, "Bunk versus conventional beds: a comparative assessment of fall injury risk," Journal of Epidemiology and Community Health, **56**, pp. 413-417.
- Belfer R, Klein B, and Orr L, 2001, "Use of the Skeletal Survey in the Evaluation of Child Maltreatment," American Journal of Emergency Medicine, **19**, pp. 122-4.
- Bertocci G and Pierce M, 2006, "Applications of Biomechanics Aiding in the Diagnosis of Child Abuse," Clinical Pediatric Emergency Medicine, **7**, pp. 194-9.
- Bertocci GE, Pierce MC, Deemer E, Aguel F, Janosky JE, Vogeley E, 2003, "Using Test Dummy Experiments to Investigate Pediatric Injury Risk in Simulated Short-Distance Falls," Archives of Pediatrics and Adolescent Medicine, **157**(5), pp. 480-486.
- Billmire ME and Myers PA, 1985, "Serious head injury in infants: accident or abuse?" Pediatrics, **75**, pp. 340-342.
- Bozic KJ, Keyak JH, Skinner HB, Bueff UH, Bradford DS, 1994, "Three-Dimensional Finite Element Modeling of a Cervical Vertebra: An Investigation of Burst Fracture Mechanism," Journal of Spinal Disorders & Techniques, **7**(2), pp. 102-110.
- Burstein AH, Zika JM, et al., 1975, "Contribution of collagen and mineral to the elastic-plastic properties of bone." Journal of Bone and Joint Surgery-American Volume **57**, pp. 956-961.
- Bylski D, Kriewall TJ, et al., 1986, "Mechanical behavior of fetal dura mater under large deformation biaxial tension." Journal of Biomechanics **19**(1), pp. 19-26.
- Chalmers D, Marshall S, Langley J, Evans M, Brunton C, Kelly A, et al., 1996, "Height and surfacing as risk factors for injury in falls from playground equipment: a case- control study," Injury Prevention, **2**, pp. 98-104.

- Coats B and Margulies SS, 2006, "Material properties of human infant skull and suture at high rates." Journal of Neurotrauma **23**(8), pp. 1222-32.
- Coats B, Margulies SS, et al., 2007, "Parametric study of head impact in the infant." Stapp Car Crash Journal **51**, pp. 1-15.
- Cooperman DR and Merten DF, 2001, "Skeletal Manifestation of Child Abuse," In: RM Reece & S Ludwig, editors. Child Abuse: Medical Diagnosis and Management. Philadelphia: Lippincott, Williams, and Wilkins.
- Currey JD, 1969, "The mechanical consequences of variation in the mineral content of bone." Journal of Biomechanics **2**, pp. 1-11.
- Currey JD, 1999, "What determines the bending strength of compact bone?" Journal of Experimental Biology **202**, pp. 2495-2503.
- Desantis Klinich K, Hulbert GM, et al, 2002, "Estimating infant head injury criteria and impact response using crash reconstruction and finite element modeling." Stapp Car Crash Journal **46**, pp. 165-94.
- Dickerson J and Dobbing J, 1966, "Some Peculiarities of Cerebellar Growth in Pigs," Proceedings of the Royal Society of Medicine, **59**, pp. 1088.
- Frank F and Lawn B, 1967, "On the Theory of Hertzian Fracture," Proceedings of the Royal Society of London, **299**(1458), pp. 291-306.
- Franklyn M, Peiris S, et al, 2007, "Pediatric material properties: a review of human child and animal surrogates." Critical Reviews in Biomedical Engineering **35**(3-4), pp. 197-342.
- Gruskin KD and Schutzman SA, 1999, "Head Trauma in Children Younger Than 2 Years," Archives of Pediatrics and Adolescent Medicine, **153**, pp. 15-20.
- Hall J, Reyes H, Horvat M, Meller J, Stein R, 1989, "The Mortality of Childhood Falls," The Journal of Trauma, **29**(9), pp. 1273-1275.
- Herring S and Teng S, 2000, "Strain in the Braincase and Its Sutures During Function," American Journal of Physical Anthropology, **112**, pp. 575-93.
- Hobb CJ, 1984, "Skull Fracture and the Diagnosis of Abuse," Archives of Disease in Childhood, **59**, pp. 246-252.
- Holck P, 2005, "What Can a Baby's Skull Withstand? Testing the Skull's Resistance on an Anatomical Preparation," Forensic Science International, **151**, pp. 187-91.
- Knight B, 1991, Forensic Pathology. London: Edward Arnold.

- Kriewall TJ, 1982, "Structural, mechanical, and material properties of fetal cranial bone," American Journal of Obstetrics and Gynecology **143**(6), pp. 707-14.
- Kriewall TJ, McPherson GK, et al., 1981, "Bending properties and ash content of fetal cranial bone." Journal of Biomechanics **14**(2), pp. 73-9.
- Kurtz SM, Thibault KL, et al, 1998, "Finite element analysis of the deformation of the human infant head under impact conditions," 8th Injury Prevention Through Biomechanics Symposium, Detroit, Michigan.
- Lallier M, Bouchard S, St-Vil D, Dupont J, Tucci M, 1999, "Falls From Heights Among Children: A Retrospective Review," Journal of Pediatric Surgery, **34**(7), pp. 1060-1063.
- Lapeer RJ and Prager RW, 2000, "3D shape recovery of a newborn skull using thin-plate splines," Computerized Medical Imaging and Graphics **24**(3), pp. 193-204.
- Lapeer RJ and Prager RW, 2001, "Fetal head moulding: finite element analysis of a fetal skull subjected to uterine pressures during the first stage of labour." Journal of Biomechanics **34**(9), pp. 1125-33.
- Lee MC and Haut RC, 1989, "Insensitivity of tensile failure properties of human bridging veins to strain rate: implications in biomechanics of subdural hematoma." Journal of Biomechanics **22**(6-7), pp. 537-42.
- Leventhal JM, Thomas SA, Rosenfield NS, Markowitz RI, 1993, "Fractures in young children: distinguishing child abuse from unintentional injuries," American Journal of Diseases of Children, **147**, pp. 87-92.
- Li H, Ruan J, Xie Z, Wang H, and Liu W., 2007, "Investigation of the Critical Geometric Characteristics of Living Human Skulls Utilising Medical Image Analysis Techniques," Int. J. Vehicle Safety, **2**(4), pp. 345-361.
- Marean CW, Abe Y, Nilssen PJ, Stone EC, 2001, "Estimating the Minimum Number of Skeletal Elements (MNE) in Zooarchaeology: A Review and a New Image-Analysis GIS Approach," American Antiquity, **66**(2), pp. 333-348.
- Margulies SS and Thibault KL, 2000, "Infant Skull and Suture Properties: Measurements and Implications for Mechanisms of Pediatric Brain Injury," Journal of Biomechanical Engineering, **122**(4), pp. 364-371.
- Margulies SS and Thibault KL, 2000, "Infant skull and suture properties: measurements and implications for mechanisms of pediatric brain injury," Journal of Biomechanical Engineering **122**(4), pp. 364-71.

- McPherson GK and Kriewall TJ, 1980, "The elastic modulus of fetal cranial bone: a first step towards an understanding of the biomechanics of fetal head molding," Journal of Biomechanics **13**(1), pp. 9-16.
- McPherson GK and Kriewall TJ, 1980, "Fetal head molding: an investigation utilizing a finite element model of the fetal parietal bone," Journal of Biomechanics **13**(1), pp. 17-26.
- Melvin J, McElhaney J, et al., 1970, "Development of a mechanical model of the human head-determination of tissue properties and synthetic substitute materials," Proceedings of the 14th Stapp Car Crash Conference, New York, SAE.
- Mertz H, 1984, "A Procedure for Normalizing Impact Response Data," SAE #840884, 29th Stapp Car Crash Conference, Chicago, IL.
- Meservy CJ, Towbin R, McLaurin RL, Myers PA, Ball W, 1987, "Radiographic characteristics of skull fractures resulting from child abuse," American Journal of Roentgenology, **149**, pp. 173-175.
- Pierce M, Valdevit A, Anderson L, Inoue N, and Hauser D, 2000, "Biomechanical Evaluation of Dual-Energy X-Ray Absorptiometry for Predicting Fracture Loads of the Infant Femur for Injury Investigation: An In Vitro Porcine Model," Journal of Orthopaedic Trauma, **14**(8), pp. 571-6.
- Prange M and Margulies S, 2002, "Regional, Directional, and Age-Dependant Properties of the Brain Undergoing Large Deformations," Journal of Biomechanical Engineering, **124**(2), pp. 244-52.
- Prange M, Luck J, Dibb A, Van Ee C, Nightingale R, Myers B, 2004, "Mechanical Properties and Anthropometry of the Human Infant Head," Stapp Car Crash Journal, **48**, pp. 279-99.
- Prange M, Meaney D, Margulies S, 2000, "Defining brain mechanical properties: Effects of region, direction, and species," Stapp Car Crash Journal, **44**, pp. 205-13.
- Prange MT, Kiralyfalvi G, et al., 1999, "Pediatric rotational inertial brain injury: the relative influence of brain size and mechanical properties," Stapp Car Crash Conference.
- Reece RM and Sege R, 2000, "Childhood Head Injuries: Accidental or Inflicted?" Archives of Pediatric and Adolescent Medicine, **154**, pp. 11-15.
- Reiber GD, 1993, "Fatal falls in childhood: How Far Much Children Fall to Sustain Fatal Head Injury?" American Journal of Forensic Medicine and Pathology, **14**, pp. 201-207.
- Roth S, Raul JS, et al., 2007, "Finite element analysis of impact and shaking inflicted to a child," International Journal of Legal Medicine **121**(3), pp. 223-8.

- Runge CF, Youssef A, Thibault KL, Kurtz SM, Magram G, Thibault LE, 1998, "Material properties of human infant skull and suture: experiment and numerical analysis," 9th Injury Prevention through Biomechanics Symposium, Detroit, Michigan.
- Schneider L, Lehman R, Pflug M, Owings C., 1986, "Size and Shape of the Head and Neck From Birth to Four Years," Washington, D.C. The Consumer Product Safety Commission, Report No.: UMTRI-86-2.
- Silva MJ, Keaveny TM, Hayes WC, 1998, "Computed Tomography-Based Finite Element Analysis Predicts Failure Loads and Fracture Patterns for Vertebral Sections," Journal of Orthopaedic Research, **16**(3), pp. 300-8.
- Soni B, Littlefield D, Wagner C, Yang K, "Pediatric Computational Models," in Myers B, Meaney D, Crandall C (editors), Pediatric Injury Biomechanics Data Archive & Textbook (in pre-publication revision).
- Thibault K and Margulies S, 1998, "Age-Dependant Material Properties of the Porcine Cerebrum: Effect on Pediatric Head Injury Criteria," Journal of Biomechanics, **31**(12), pp. 1119-26.
- Thibault KL and Margulies SS, 1998, "Age-dependent material properties of the porcine cerebrum: effect on pediatric inertial head injury criteria." Journal of Biomechanics **31**(12), pp. 1119-26.
- Weber W, 1984. "[Experimental studies of skull fractures in infants]," Zeitschrift Fur Rechtsmedizin-Journal of Legal Medicine **92**(2), pp. 87-94.
- Weber W, 1985, "[Biomechanical fragility of the infant skull]," Zeitschrift Fur Rechtsmedizin-Journal of Legal Medicine, **94**(2), pp. 93-101.
- Wheeler DS and Shope TR, 1997, "Depressed skull fracture in a 7-month old who fell from bed," Pediatrics, **100**, pp. 1033-1034.
- Yang K, Mao H, Wagner C, Zhu F, Chou CC, King AI, "Modeling of the Brain for Injury Prevention," in Bilston L (editor) Studies in Mechanobiology, Tissue Engineering and Biomaterials: Neural Tissue Biomechanics Springer Publisher.
- Zimmerman R and Bilaniuk L, 1994, "Pediatric Head Trauma," Neuroimaging Clinics of North America, **4**(2), pp. 349-366.

DISSEMINATION OF FINDINGS: PUBLICATIONS, PRESENTATIONS AND AWARDS

Peer Reviewed Publications

Powell B, Passalacqua N, Baumer T, Fenton T, and Haut R. Fracture Patterns On the Infant Porcine Skull Following Severe Blunt Impact. *J. Forensic Sciences*. (in review)

Baumer T, Nashelsky M, Hurst C, Passalacqua N, Fenton T, Haut R. Characteristics and Prediction of Cranial Crush Injuries in Children. *Journal of Forensic Sciences*. 2010 (in press)

Baumer T, Passalacqua N, Powell B, Newberry W, Smith W, Fenton T, and Haut R. Age-Dependent Fracture Characteristics of Rigid and Compliant Surface Impacts on the Infant Skull – A Porcine Model. *Journal of Forensic Sciences*. 2010 (in press)

Baumer T, Powell B, Fenton T, and Haut R. Age Dependent Mechanical Properties of the Infant Porcine Skull and a Correlation to the Human. *Journal of Biomechanical Engineering*. Nov 2009, 131(11), pp. 111006-1/6.

Conference Presentations

Powell BJ, Passalacqua NV, Baumer TG, Fenton TW, Haut RC. Fracture Patterns on the Infant Porcine Skull Following Severe Blunt Impact. American Society of Mechanical Engineering, Naples, FL, 2010.

Passalacqua NV, Fenton TW, Baumer TG, Powell BJ, Newberry WN, Haut RC. A Forensic Pathology Tool to Predict Pediatric Skull Fracture Patterns, Part 2: Fracture quantification and further investigations on infant cranial bone fracture properties. American Academy of Forensic Sciences (AAFS), Seattle, Washington, 2010.

Fenton TW. A Forensic Pathology Tool to Predict Pediatric Skull Fracture Patterns. 2010 NIJ General Forensics R & D Grantees Meeting, Aspen Room, Sheraton Seattle, Seattle, WA. February 23, 2010.

Baumer TG, Powell BJ, Fenton TW, Haut RC. Age Dependent Mechanical Properties of the Infant Porcine Skull and a Correlation to the Human. American Society of Mechanical Engineering, Lake Tahoe, CA, 2009.

Fenton TW, Passalacqua NV, Baumer TG, Powell BJ, Haut RC. A Forensic Pathology Tool to Predict Pediatric Skull Fracture Patterns - Part 1: Investigations on Infant Cranial Bone Fracture Initiation and Interface Dependent Fracture Patterns. American Academy of Forensic Sciences (AAFS), Denver, Colorado, 2009. [*Winner of the Ellis R. Kerley Award*]

Baumer TG, Nashelsky M, Hurst CV, Passalacqua NV, Fenton TW, Haut RC. Characteristics and Prediction of Cranial Crush Injuries in Children. American Academy of Forensic Sciences (AAFS), Denver, Colorado, 2009.

Masters Theses

Baumer, TG. Material Property Documentation and Fracture Analyses of the Developing Skull. East Lansing, MI: Michigan State University, 2009.

Powell, BJ. Fracture Patterns of the Developing Skull Attributable to Different Impact Scenarios. East Lansing, MI: Michigan State University, 2010.

Doctoral Dissertations

Wagner, Christina (Ph.D. candidate in the Biomedical Engineering Department at Wayne State University). The working title of her dissertation is "Computational Simulation of Skull Fracture Patterns in Pediatric Subjects Using a Porcine Model".